# Impedances Studies of Transport Phenomena in Supramolecular Polymer Assemblies

**Dissertation presented to the Department of Mining and Metallurgical Engineering and Materials Science (E.T.S.I. Bilbao / UPV-EHU) for the degree of International Doctor in Materials Science and Engineering by**

**TEODORO ALONSO GARCIA**

**Thesis advisor: Dr. Sergio E. Moya**
**University Tutor: Dr. Emiliano Meaurio**

Bilbao ,June of **2014**

This PhD thesis has been performed at:

**CICbiomaGUNE**

Biosurfaces Unit

Donostia-San Sebastian (SPAIN)

**Zhejiang University**

Department of Polymer Science and Engineering

Hangzhou (CHINA)

**Instituto de Investigaciones Fisicoquímicas Teóricas y Aplicadas (INIFTA)**

Fac. de Cs. Exactas. Universidad Nacional de La Plata & CONICET

La Plata, Bs. As. (ARGENTINA)

## Acknowledgements:

I would like to acknowledge my supervisor Dr. Sergio Moya for giving me the chance to start this doctorate. I would alsolike to thank all the people that made me feel like at home when I was far away. I neither cant forget to thank the persons that offered me their support in difficult times .

And in the end I want to express my gratitude for the unconditional help in science and in life that Professor Claudio Gervasi offered me.

Y por supuesto a mi familia que siempre siempre está ahí.

## OUTLINE

# LIST OF FIGURES

## Chapter 1 GENERAL BACKGROUND



## Chapter 2 MATERIALS AND METHODS

**Chapter 3 Mathematical modeling of the Faradaic impedance of a redox probe inside grafted polymer brushes**



**Chapter 4 Molecular Transport in Thin Thermo-responsive Poly (N-isopropylacrylamide) Brushes with Varying Grafting Density**

**Chapter 7 Separate Assessment of Permeation and Electron Transfer of Charged Redox Probes at Gold Electrodes Modified with Cationic Polyelectrolyte Brushes.**

# RESUMEN

Esta tesis tiene como objetivo primario el obtener una caracterización, en términos de variables microscópicas, de los procesos de transporte de materia y carga en sistemas de "materia blanda", en particular en cepillos poliméricos (polymer brushes), utilizando para ello nuevas aplicaciones de técnicas electroquímicas, como la voltamperometría cíclica (CV) y la Espectroscopia de Impedancia Electroquímica (EIS), complementadas con técnicas de caracterización superficial como la microbalanza de cristal de cuarzo con disipación (QCM-D) o el microscopio de fuerza atómica (AFM). Intenta además, responder cuestiones fundamentales de relevancia en los sistemas estudiados usando principios electroanalíticos. Tales cuestiones en general no son susceptibles de ser respondidas eficientemente por otras técnicas experimentales. Un análisis tanto cualitativo como cuantitativo ha sido utilizado en el modelado y en la simulación de los datos que se presentan. Más aún, se han hecho esfuerzos para proporcionar una descripción de amplio alcance en las discusiones referidas a nano-estructuras poliméricas en forma de cepillos adheridos a una superficie y cuyo estado conformacional responde a diferentes estímulos externos.

La medición de las propiedades de transporte a nanoescala exige nuevos enfoques experimentales y teóricos. Se necesita una perspectiva multidisciplinaria, que abarque desde la síntesis, hasta el auto-ensamblaje, correlacionando principios básicos de la química física y a la física teórica.

El uso combinado de diferentes técnicas experimentales como la Espectroscopia de Impedancia Electroquímica (EIS), voltamperometría cíclica (CV), microbalanza de cristal de cuarzo con disipación (QCM-D) o microscopía de fuerza atómica (AFM) permite obtener una mejor comprensión de fenómenos dinámicos relevantes, tales como los procesos de transporte molecular y transferencia de electrones que tienen lugar en estas interfaces.

Estructuras macromoleculares como las descritas juegan un papel importante en el diseño racional de sistemas de liberación controlada de fármacos o sensores materiales a base de polímeros con respuesta transitoria, por nombrar sólo unas pocas aplicaciones relevantes. En este contexto, el presente trabajo tiene como objetivo proporcionar nuevas herramientas y metodologías para modificar superficies con películas poliméricas delgadas y de carácter responsivo que generen un deseado comportamiento interfacial "inteligente".

El comportamiento responsivo de cepillos poliméricos confinados en superficie exhibe bajo diferentes condiciones de temperatura y fuerza iónica, efectos importantes en transporte molecular en electrodos modificados. La técnica polimerización radicalaría por transferencia de atomos (Atom Transfer Radical Polymerization (ATRP)) se utilizó para la síntesis de cepillos adheridos covalentemente a una superficie a partir de monocopas de iniciadores previamente ensambladas.

En el **Capítulo 4** de este trabajo se estudia el efecto de la densidad superficial de las cadenas poliméricas en el transporte molecular a través de un cepillo

termorresponsivo de poli(N-isopropilacrilamida) (PNIPAM) soportado en sustratos de oro. Para ello se obtuvieron cuatro densidades superficiales a partir del proceso de ATRP iniciado en superficie (SI-ATRP) partiendo de una monocapa inicial autoensamblada resultante de la mezcla de dos tioles (ω-mercaptoundecil bromoisobutirato y undecanotiol). Los tioles forman enlaces de tipo coordinación con el oro quedando adsorbidos sobre su superficie. Aquí como en el resto de las secciones, el análisis de los resultados de la impedancia electroquímica requirió del desarrollo de un modelo matemático de la impedancia faradaica, expresado en función de parámetros fisicoquímicos del sistema. Posteriormente se llevó a cabo un ajuste paramétrico de los datos experimentales mediante un programa computacional basado en algoritmos de cuadrados mínimos no-lineales y complejos.

Los cepillos de PNIPAM con densidades de empaquetamiento de cadenas (grafting densities) menores al 25 % de tiol iniciador en la monocapa inicial exhiben las mismas propiedades de transporte que la monocapa autoensamblada sin posterior crecimiento del cepillo. Para mayores grafting densities, los coeficientes de difusión, D, de la sonda redox $K_3[Fe(CN)_6]/K_4[Fe(CN)_6]$ son siete órdenes de magnitud más pequeños que aquellos en soluciones acuosas, independientemente de si el estado conformacional del cepillo es colapsado o extendido. El colapso de un cepillo de PNIPAM conduce a una transición hidrofílica/hidrofóbica que sumado a las transiciones estructurales / conformacionales, genera valores menores del coeficiente de difusión D. Sin embargo, estos cambios no conducen a un efecto de bloqueo del área activa de la superficie del sustrato de oro, la cual está determinada solo por defectos o discontinuidades de la monocapa inicial

autoensamblada. Estos resultados corresponden solo a películas delgadas de cepillos de PNIPAM.

El desarrollo de estrategias para evaluar la temperatura de transición vítrea (Tg) en films de polielectrolitos confinados en superficie es muy importante para comprender y racionalizar el comportamiento dependiente de la temperatura de tales películas en una amplia gama de condiciones. A pesar de la percepción predominante de la importancia de la medición de la Tg en condiciones acuosas, para configuraciones de películas delgadas su medición directa plantea un desafío experimental que todavía sigue siendo difícil de superar en el área de polímeros y ciencia de los materiales. En consecuencia, en la siguiente sección se describe un nuevo método basado en la espectroscopía de impedancia electroquímica (EIS) para estimar la temperatura de transición vítrea de los cepillos de polielectrolitos confinados en interfases sólido-líquido. Para medir la Tg, se obtuvo la resistencia de transferencia de carga ($R_{ct}$) de una sonda redox que difunde a través del cepillo de polielectrolito en un rango de temperaturas. La fuerte discontinuidad observada en la variación de la $R_{ct}$ con la temperatura a un temperatura bien definida puede ser correlacionado a la Tg. Además, se demuestra que las mediciones de impedancia permiten una evaluación fiable de los coeficientes de difusión, cerca de la temperatura de transición vítrea. Consideramos que este enfoque tiende un puente entre la electroquímica y las herramientas tradicionales que se utilizan en la ciencia de los polímeros y ofrece nuevas oportunidades para caracterizar el comportamiento térmico de estructuras poliméricas en interfaces complejas y en estructuras macromoleculares.

Los **Capítulos 5 y 6** se centran en la explicación del uso combinado de técnicas electroquímicas (EIS y CV) y QCM-D para resolver por separado los efectos que los cambios de temperatura ejercen sobre la difusión y la transferencia de electrones de la reacción electroquímica de la cupla redox $[Fe(CN)_6]^{3-/4-}$ en un electrodo de Au modificado con cepillos de PMETAC. Se observaron dependencias de tipo Arrhenius para la constante cinética y el coeficiente de difusión en diferentes electrolitos. El colapso por formación de pares iónicos de cepillos de PMETAC en contacto con solución de $NaClO_4$ resulta en estructuras rígidas y compactas, que retienen menor cantidad de agua en la estructura y que resulta ser muy diferente de los mismos cepillos que sufren un colapso generado solamente por apantallamiento culómbico de cargas en el cepillo por parte de los aniones de una solución de NaCl. Una diferencia notable relacionada con el tipo de contraión es la ocurrencia de una transición térmica para el cepillo de polielectrolito en la presencia de iones $ClO_4^-$ a temperatura cercana a la ambiente (~ 17 ° C). Las energías de activación para la transferencia de electrones y los procesos de difusión se duplican frente a las que se presentan para temperaturas por encima de la transición térmica. Estos estudios electroquímicos no sólo demuestran el papel fundamental de las interacciones basadas en un apareamiento iónico en la determinación de las propiedades físico-químicas del sistema macromolecular, sino también proporcionan evidencia experimental del transporte termo-controlado inducido funcionalmente por la presencia de un dado contraión en la capa de cepillo-polielectrolito.

Finalmente, en el **Capítulo 7** y basado en el enfoque experimental ya presentado se muestra una caracterización cuantitativa de la resistencia de transferencia de

carga y coeficientes de difusión asociados con las reacciones electroquímicas de las cuplas redox $Ru(NH_3)_6^{3+/2+}$ y $Fe(CN)_6^{3-/4-}$ sobre electrodos de oro modificados con cepillos de PMETAC catiónicos. Cepillos de PMETAC se crecieron con diferente densidad de cadenas y se ensayaron en solución 50 mM de NaCl, que corresponde a una relativamente baja concentración de contraión, con el fin de evitar fuertes efectos de apantallamiento de la carga en las cadenas del polímero por los iones cloruro. Los cambios en los parámetros de QCM-D, en particular la disminución de la disipación después de la inmersión del cepillo en la solución salina, se corresponden con una disminución de la viscosidad de la muestra o estado menos rígido asociado a la liberación de agua. Este efecto es muy marcado para 100% de densidad de incrustación del cepillo y casi imperceptible a 5%. En consecuencia resulta un coeficiente de difusión de la sonda mayor en esta solución soporte dentro del cepillo a mayor densidad de cadenas. La resistencia de transferencia de carga ($R_{tc}$) es considerablemente mayor para la reacción con la sonda de Ru que para la sonda de Fe. El paso de adsorción previo a la transferencia de electrones es más favorable (mayor acercamiento entre la sonda y la superficie) para la sonda $Fe(CN)_6^{3-/4-}$ cargada negativamente debido a la interacción con la carga positiva en las unidades de la cadena del cepillo en el entorno cercano a la zona de reacción. Por otra parte, esta situación da lugar a una transferencia de electrones con mayor impedimento para la cupla $Ru(NH3)_6^{2+/3+}$ cargada positivamente y en consecuencia un aumento de $R_{tc}$.

Se obtuvieron valores similares del coeficiente de difusión D independientemente del signo de la carga de la sonda. En estos sistemas D apenas se ve afectado por la interacción electrostática entre grupos cargados de las cadenas de polielectrolito

y las sondas redox. Sin embargo, cambios en las propiedades viscoelásticas después de la inmersión del cepillo en la solución que contiene el contraion, provoca un efecto común para ambas especies redox con la disminución de la grafting density de cepillo, vinculado a una caída en los coeficientes de difusión. Un gran aumento relativo en los valores de la resistencia del camino electrolítico dentro del cepillo ($R_l$) se midió en presencia de la sonda de Ru en comparación con la sonda de Fe. Se cree que esto es resultado de cambios de composicion y / o cambios en la movilidad iónica de los iones con mayor número de transporte en cada medio.

En consecuencia, entre las numerosas conclusiones que se pueden extraer de este trabajo nos centraremos sólo en las contribuciones innovadoras relacionadas con las aplicaciones de EIS mostradas en el **Capítulo 8**:

- ✓ La estrategia electroquímica desarrollada en el presente trabajo de tesis para caracterizar cepillos poliméricos confinados en superficie, en particular en lo que se refiere a la forma en que se utilizó la espectroscopia de impedancia (EIS), ha ganado recientemente el reconocimiento por carácter novedoso, así como por ser la única alternativa establecida a técnicas basadas en fluorescencia para el estudio de aspectos críticos como lo es la difusión de moléculas dentro de los cepillos [1].

- ✓ Para usos específicos en dispositivos electroquímicos, presentamos una metodología basada en el estudio de la impedancia electroquímica como la mejor opción disponible para caracterizar la actividad de un electrodo

modificado de acuerdo al comportamiento responsivo del cepillo (es decir, la caracterización independiente de transporte de masa *normal* a la superficie más la transferencia de electrones en el sustrato).

- ✓ Se demuestra por primera vez el uso potencial de la EIS para medir la Tg de películas poliméricas confinadas en una superficie.

- ✓ Los datos de impedancia a bajas frecuencias, como se miden en este trabajo, son una prueba concluyente de que: i) los cepillos colapsados retienen suficiente cantidad de agua como para permitir el transporte de masa de la sonda redox dentro del cepillo; ii) los cepillos parcialmente colapsados representan una barrera difusional de espesor finito para las sondas moleculares electroactivas, y iii) la difusión en el interior del cepillo seguido por la transferencia de electrones en la superficie es el mecanismo de conducción predominante en vez del "hopping" de electrones (saltos cuánticos) entre moléculas vecinas de la sonda coordinadas en posiciones fijas en las cadenas del polímero.

- ✓ Por otra parte, la combinación de impedancia, voltamperometría cíclica y estudios de QCM-D para indagar la difusión de iones, las barreras de energía de transferencia de electrones, y la hidratación de cepillos, todo de modo unificado, representa un logro importante y proporciona un nivel de conocimiento sin precedentes en su propia área temática.

## REFERENCES

(1). Wang, S.; Jing, B.; Zhu, Y., *J. Polym. Sci. Part B: Polym. Phys.* **2014** - DOI: 10.1002/polb.23414.

# Chapter 1

# GENERAL BACKGROUND

## 1.1 POLYMER BRUSHES

The assembly of polymers attached by one end to the solid/solvent interface started to be a topic of interest both experimentally and theoretically along the 1980s [1-5]. This interest stems from their utility for a wide range of technological applications which include photolithography, liquid crystal displays, sensors or antireflection coatings, among others.

The term “polymer brush” refers to the case where long chain polymer molecules attached by one end to a surface or interface have a density of attachment points high enough, so that steric repulsions between neighboring chains force them to stretch away from the interface, sometimes much farther than the typical un-stretched size of a chain .[6]

In recent years, the synthesis of polymer brushes is following the techniques which are based in surface-initiated polymerization reactions. However, this is not the single approach to attach the polymer chains to the solid substrate. Many examples can be provided that show up some recent developments aimed at strategies for the functionalization of surfaces with polymer brushes, in the way of realizing smart surfaces with switchable properties, and at the production of micro- and nanostructured polymer monolayers.

Thin coatings applied to the surface of materials can improve the properties of objects considerably as they permit control of the interaction of a material with its environment. This has been known more or less empirically to humanity for several thousand years. Varnish generated from tree sap was used in China in the past as

a protective coating for wooden objects. Cold process coatings were also used by Egyptian ship builders used beeswax, gelatin and clay to produce varnishes to waterproof their ships. The early Greeks and Romans, as well as the ancient Asian cultures in China, Japan and Korea, used lacquers and varnishes applied to homes and ships for decoration and as protective measures against adverse environmental conditions. In modern times, the coatings industry is a multi-billion dollar business where the application range of surfaces modified with thin polymer films is targeted to tailor surface properties such as wettability, biocompatibility, corrosion resistance and friction [7,8]. Thus, the challenge is produce modifying surfaces with thin polymeric films that display responsive behaviour renders a surface with "smart" function, for different applications. A particularly useful application in the field of polymer nanotechnology results when the responsive surface builds a barrier that restricts transport of water-soluble molecules or ions in a reversible fashion at nanoscale dimensions [9] .

## 1.2 SURFACE-INITIATED ATOM TRANSFER RADICAL POLYMERIZATION (ATRP)

The anchorage of the polymer chains to build a brush is generally based on two methods called "*grafting to*" (to the surface) and "*grafting from*" (from surface). In the “grafting to” method, the pre-formed polyelectrolyte chains are endowed with a terminal functional group in its structure which after reacting with the surface generates the desired layer. Normally the density of the coating obtained by this method is low and the film thickness is little [10,11]. In general polymer chains are voluminous and therefore grafting one polymer molecule by a single covalent

binding hinders the access of other chains to the area where the chain has been attached. The “grafting from” approach is a potent tool to produce polymer tethered layers in which all polymer chains are attached covalently with one of their chain ends to the substrate. This densely packed arrangement of surface grafted polymer chains is refer to as polymer brush [12] . In a polymer brush the grafting density is such that steric repulsions force the chains to stretch out from the surface in order to avoid overlapping.

Polymer brushes are grown from a surface via a two steps surface-initiated polymerization. First, the substrate is modified with a polymerization initiator (or a polymerization active molecule).The use of small molecules with a reactive head group that is amenable to form a covalent bond with the surface of the substrate, which is to be modified represents the initial layer in the form of a self-assembled monolayer (SAM) [13]. The second is the direct surface-initiated polymerization of the monomer. The polyelectrolyte film on the surface is consequently grown from a previously bound SAM incorporating an appropriate polymerization initiator [14-16]. Examples of initial SAMs are silanes on non-metallic oxide surfaces, phosphates or phosphonate on metal(oxide)s, and thiols or disulfides on noble metal surfaces Fig1.1 .

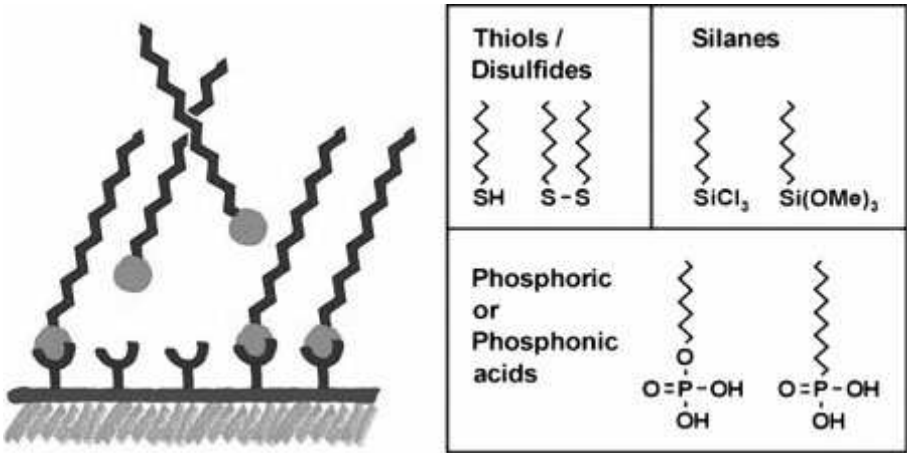


**Figure 1.1** Schematic of the self-assembly process and examples of anchor groups used for the modification of surfaces with selfassembled monolayers (SAMs) of organic molecules.

Silanes or thiols initiators molecules used in the grafting from approach are on the rule small and display surface areas of ca. 20 $Å^2$, this value is much smaller than the average cross sectional area of a polymer chain grafted to the surface (~180-200 $Å^2$) what in turn can result in denser layers for the grafting to methodology [17]. Hence, monomers migrate to these active sites of initiation and polymerize, forming a polymer layer of higher density and thickness as the film obtained by the procedure of grafting to.

The features of the surface to be modified often define the best approach to follow for the brush synthesis. For solid substrates, the “grafting from” protocol usually proves to be the most attractive way to prepare thick, covalently tethered polymer brushes, with a high grafting density. The immobilization of initiators onto the substrate, forming a 2-D SAM, is followed by in situ surface-initiated polymerization to generate the tethered polymer brush. In this regard, different polymerization

strategies, such as free-radical, cationic, anionic, or ring opening metathesis polymerization (ROMP), have been applied to form brush-like structures on surfaces [18]. Among these types of polymerization methods, atom transfer radical polymerization (ATRP) has attracted significant interest for its living/controlled character that provides a control over molecular weight and polydispersity, for its tolerance of functional groups, and the soft experimental conditions involved.[19,20]

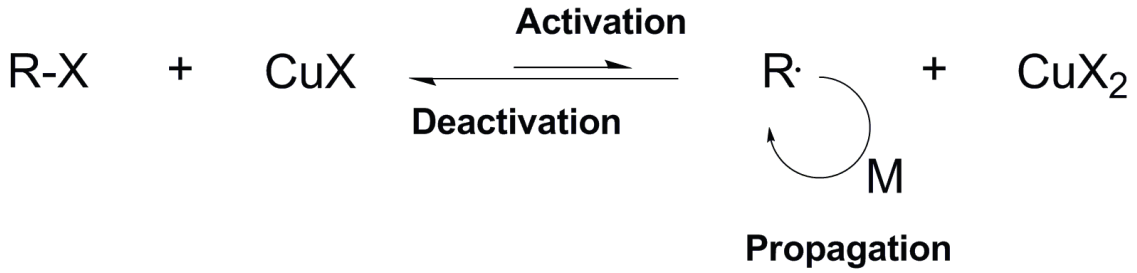


**Scheme 1.1** Schematic representation of the mechanism for atom transfer radical polymerization.

As the chains grow from the surface, the only limits to propagation are the diffusion of monomer to the polymerization-active chain ends, or the blockage of the active radical. This results in thick tethered polymer brushes with high grafting density.

The first highly successful demonstration of the grafting from technique for the synthesis of brush layers was reported by Rühe and co-workers who succeeded in preparing various polyelectrolyte brushes from planar surfaces with high grafting densities and high molecular weight [21,22].Since then, polymer brushes have become a central model in many important problems in polymer science, and are relevant even in biophysics and surfactant science.

## 1.3 GRAFTING DENSITY IMPACT ON CHAIN CONFORMATION

As mentioned briefly above, the term “polymer brush” refers to a system in which chains of polymer molecules are attached with one or with a few anchor points to a surface in such a way that the graft density of the polymers is high enough that the surface-attached chains become crowded and are stretched away from the surface (Figure 1.2).


**Figure 1.2** Artist’s perception of the terms (a) “mushroom”,(b) “pancake” and (c) “brush” used for the different possible conformations of surface attached polymers.

When polymer molecules are tethered to a surface, two basic cases must be distinguished depending on the grafting density of the attached chains [23–25]:

**1.-**If the distance between two anchoring sites is larger than the size of the surface-attached polymers, the segments of the individual chains do not “feel” each other and behave more or less like single chains “fixed” down onto the surface by one end. Depending on the strength of interaction of the polymer segments with the surface, again two cases must be distinguished [25]. If the interaction between the polymer and the surface is weak (or even repulsive), the chains form a typical random coil that is linked to the surface through a “stem” of varying size. For such a

situation, the term “mushroom” conformation has been coined (Figure 1.2a). However, if the segments of the surface attached chains adsorb strongly to the underlying surface, the polymer molecules obtain a flat, “pancake”-like conformation (Figure 1.2b).

**2.-** A completely different picture is obtained if the chains are attached to the surface at such short distances between the anchor points that the polymer molecules overlap. In this case, the segments of the chains try to avoid each other as much as possible and minimize segment–segment interactions by stretching away from the surface (Figure 1.2c). This chain stretching, however, reduces the number of possible polymer conformations, which is equivalent to a reduction in the entropy of the chains. This loss of entropy gives rise to a retracting force trying to keep the chains coiled, as occurs in a stretched piece of rubber. Thus, a new equilibrium at a higher energy level is obtained in which the chains are stretched perpendicular to the surface.

## 1.4 RESPONSIVE BEHAVIOUR

Interestingly, polymer brushes that exhibit responsive behavior towards external stimuli are characterized by two limiting polymer molecule conformations, namely, a fully-stretched state and a collapsed state, being a reversible rearrangement between both states possible [26].

The external stimuli that provoke the responsive behaviour could be temperature, in which case the system is called thermoresponsive. Most of the thermoresponsive

brushes that have been reported show a lower critical solution temperature (LCST) behavior. At temperatures below the LCST, these brushes are hydrophilic, while raising the temperature above the LCST leads to a collapse of the brushes when they are exposed to water what in turn renders the surface hydrophobic. PNIPAM is one of the most studied thermoresponsive polymers and surface-tethered PNIPAM brushes have attracted much attention in the past two decades [27].Whereas in solution PNIPAM shows a sharp LCST at 32 °C,[28] the LCST transitions observed for surface-confined PNIPAM brushes are broader, starting at lower temperature while the transition takes place over a wider temperature range (from 29 °C to 40 °C).[29-32] Polyelectrolyte brushes consist of polymer chains that contain charged repeating units. Depending on the nature of the charged groups polyelectrolyte brushes are classified as strong or weak polyelectrolyte brushes [33]. In strong polyelectrolyte brushes, the number and position of charges along the chain is fixed. In this case, variation of pH or ionic strength will not influence the number of charges. For example, weak polyelectrolyte brushes display significant reorganization processes at interfaces upon protonation/dissociation of their acidic/basic groups and they have influence of pH or ionic strength [34,35].

Genzer, Szleifer and coworkers carried out theoretical and experimental studies to investigate the behavior of surface-attached polyelectrolytes.[36,37] Theoretical considerations predicted a different behavior for strong and weak polyelectrolyte brushes.For strong polyelectrolytes, the electrostatic interactions are largely screened at high salt concentrations, and the brush behaves as a neutral, *i.e.* collapsed, brush. Decreasing the salt concentration generates an unbalance

between the ion concentration inside and outside the brush what results in electrostatic interactions that lead to swelling of the brush.

For weak polyelectrolyte brushes the scenario is different. In the neutral and salted brush regimes, the salt concentration inside and outside the brush is approximately equal and the internal degree of dissociation is the same as in bulk solution. A significant electric potential difference is developed between the brush and the bulk solution and, in addition, the salt concentration inside the brush is considerably higher. These unfavorable electrostatic conditions result in a discharge of the electrolyte groups and a collapse of the layer thickness.

Ayres et al. reported the effects of mono- and divalent salts on the behavior of PMAA brushes [38,39] .Upon decreasing the salt concentration, it was found that the threshold concentration that marks the onset of brush expansion was higher for the monovalent salt.

Huck and coworkers have extensively studied the influence of the counterion on the structure and properties of PMETAC brushes [40-42].In contrast to many other studies that use highly hydrated and mobile counterions, these authors investigated scarcely hydrated anions, which can undergo ion-pairing interactions with the quaternary ammonium groups in the brush [43-45]. The characteristics of the brush (e.g. wettability) were found to be very sensitive to the nature of the counterion. Upon exchanging the original chloride counterion with a variety of other counterions it was found that the wettability of the counterion-modified brushes increased from

ClO4- > SCN- > I- > Br- > Cl-> $PO4^{3-}$, which correlates with the Hofmeister classification of the hydrophobicity of these anions.[46]

## 1.5 ELECTROCHEMICAL APPROACH TO STUDY POLYMER BRUSHES

Characterization of nanoscale polymer films has attracted strong widespread interest, both as fundamental intellectual and technological challenges, to chemists, materials scientists, physicists and engineers. This interest stems from their usefulness for the wide range of technological applications as already mentioned. A more detailed knowledge of the characteristics of polymers deposited on solid substrates is critical for understanding and improving the performance of polymers in numerous applications and is also necessary for further molecular design of soft surfaces. It is well known that in surface science and technology, unravelling and quantifying the physicochemical details of processes occurring within a thin polymer layer often poses a challenge.

The responsive behavior of polymer brushes is normally investigated electrochemically in aqueous environments in the presence of one of the following soluble redox probes: $[Fe(CN)_6]^{4-}$ and $[Ru(NH_3)_6]^{3+}$. So far, the greatest experimental challenge has been the determination of individual mass transport parameters independently from kinetic parameters associated with charge transfer at the surface. Both processes taking place during the electrochemical reaction of the redox probe are thermally activated and related to the conformational state of the polymer brush at the surface. The strategy chosen to graft the polymer brush at

the electrode surface determines the electroactive area available for the electrochemical reaction and must be evaluated first in order to obtain reliable kinetic and diffusion data. Furthermore, the conformational state, either fully extended or collapsed, is expected to have a different impact on both processes. Grafting density of the polymer as well as size and charge of the diffusing species may have an impact that, in a desirable way, results measurable through application of electrochemical experiments.

A final complexity regarding temperature-responsive brushes results from the fact that the working temperature plays two simultaneous roles regarding the diffusion reaction step, i.e. thermal activation and conformational change of the structure. Consequently, proper selection of the electrochemical technique to use is required according with the expected characterization goals. In other words, even when certain electrochemical experiments can yield relevant information frequently this information is of a qualitative character and an alternative complementary approach must be selected.

The concept of surface fractional coverage is essential for the interpretation of electrochemical data recorded with electrodes modified with polymer brushes that were grown from an initial self-assembled monolayer (SAM), for example a long-chain initiator thiol on a Au surface. Thus, the initial SAM behaves like a hydrophobic barrier to electroactive ions in the aqueous electrolyte attempting to reach the electrode surface [47]. Most SAMs contain a certain density of defects or pinholes, at which electron transfer reactions between electroactive molecules and the electrode surface may take place. Under these conditions the electrochemically active area of the substrate ($A_e$) corresponds to the fractional area determined

solely by pinhole sites and other defects in the initial SAM [48,49]. Moreover, the fractional area of pinholes may be affected by the collapse of the brush structure blocking the surface.

Cyclic voltammetry (CV) is the most widely used technique to gain qualitative information from the study of electrochemical reactions [50]. CV has been used to probe electronic properties such as the resistance, capacitance, charge as well as the redox properties of polymer brushes. It was demonstrated that this method can be used to monitor the swelling/collapse of polymer brushes upon ion exchange or ionic strength variations. [51-54]

Electrochemical Impedance spectroscopy (EIS) is increasingly recognized as a very powerful technique for studying and characterizing thin polymer films deposited on solid supports and additionally to study molecular transport and charge transfer processes related to electrochemical reactions of the redox probe inside the polymer brush. In this way information can be gained about processes such as the charging of the interface and conduction of electrical carriers (electrons and ions). Moreover, the use of EIS allows to uncouple elementary phenomena that constitute global charge transfer processes [55]. However, if a large number of elementary phenomena are involved in the process under study, data analysis can become rather difficult [56].

Electrochemical impedance measurements disclose information on the dielectric properties of materials [57]. Thus, capacitance and conductance measurements are routinely performed in order to reveal basic structural features of polymer brushes

[58]. Characterization studies from the literature performed with EIS are primarily focused on kinetics of formation, degree of coverage of the metal substrate and responsive switch between conformational states. [59]

The use of impedance techniques requires that a particular emphasis be placed on complex least squares fitting of small-signal frequency response data. Most such data are normally fitted to an equivalent electrical circuit since derivation of a detailed microscopic model of the response is usually cumbersome. However, obtaining a proper transfer function in terms of microscopic parameters together with identification procedures must be performed in order to gain valuable quantitative information.

Based on electrochemical impedance spectroscopy measurements, Jennings and coworkers developed an equivalent circuit model for polymer brush coated substrates [60,61].Reversible conformational changes of surface-tethered polymer brushes were analyzed qualitatively in terms of the voltammetric response and impedance data of the bare electrode relative to the response of the film-covered electrode in both conformational states [62].

Impedance results were interpreted in terms of an equivalent circuit of the Randle's type. In principle, since water is released from the brush during collapse [63] consequent changes are expected in the values of the film capacitance. Salt-induced collapse of polyelectrolyte brushes exhibit intrinsically different impedance magnitude as probed with EIS. Charged screened brushes retain good permeability

to electroactive probes. On the other hand, strongly coordinating hydrophobic anions lead to insoluble brushes, normally related to higher impedance values [59].

EIS and CV were used together with different spectroscopic techniques to study counterions exchange in poly(methacryloyloxy)-ethyl-trimethyl-ammonium chloride (PMETAC) brushes [64] .This work revealed that ferrocyanide and ferricyanide species form stable ion pairs with the quaternary ammonium groups of the polymer brush while chloride counterions are partially replaced by electroactive ions.
It has been claimed that collapse of grafted polymer brushes does not necessarily lead to complete blocking of transport, since the electrolyte and redox probes can be incorporated into the collapsed brushes, which remain sufficiently hydrated to allow mobility of ions [59]. There are several arguments that indicate that ion diffusion rather than electron hopping is the charge transport mechanism in PMETAC brushes. Deviations from the straight line in a Cottrell representation at large times were interpreted in terms of the confinement of the electroactive species in a finite layer [40]. Typical values of the diffusion coefficient D as calculated from chronoamperometric data were informed in the $10^{-12}$ — $10^{-10}$ $cm^2s^{-1}$ range and they result dependent on the supporting electrolyte concentration and independent of the brush thickness [42].

In order to estimate the permeability of a p-NIPAM brush CV experiments were performed with the film in its collapsed state while potassium ferricyanide was added to the solution [65]. Diffusion of ions through the gel layer takes some time. Measuring the time of voltammetric cycling necessary to observe a characteristic

redox peak after the addition of potassium ferricyanide to the solution allowed to calculate a diffusion coefficient in the range of $10^{-12}$ $cm^2s^{-1}$.

Surface-tethered PMETAC brushes in $ClO_4^-$-containing solutions of varying concentration were studied with EIS measurements [66]. In the presence of the ion–paired $ClO_4^-$ species the brush experiences not only an electrostatic change but also a drastic (hydrophilic–to-hydrophobic) chemical change. Consequently, the brush suffers a “hydrophobic collapse” instead of the traditional “electrostatic–driven collapse”. EIS experimental spectra exhibit a high-frequency capacitive contribution associated with the interfacial charge transfer reaction and a distinctive contribution at low frequencies related to finite-length diffusion. Regarding the second time constant at low frequencies, it corresponds to an electrode uniformly accessible to mass transfer through a polyelectrolyte brush of finite thickness. Noteworthy, in this work the lowest measurement frequency was set at a lower value than that regularly used in comparable experiments from the literature [59] .Complete theoretical equations for CV experiments are required, describing finite diffusion with a permeable boundary located at a distance from the electrode equal to the brush thickness are not readily available [67].

Although, at present, much has been done in terms of characterizing these systems significant nanoscale polymer film challenges/opportunities still remain to be addressed. This will certainly prove useful to engineer new surfaces with valuable applications. Consequently, this served as a motivation to performed the present PhD thesis. For that reason, the following objectives were initially set.

## 1.6 OVERALL GOALS

One purpose of this thesis is to succeed in explaining mass transport within grafted polymer brushes in terms of a plausible model with predictive capability, which can be characterized independently of the electron transfer step. A second expected contribution aims at getting a detailed insight into the effect of varying brush grafting density or the size and charge of the redox probe molecule on molecular transport through polyelectrolyte brushes. This work also has the objective of revealing the exact degree of impact on surface blocking of hydrophobic collapse and electrostatic–driven collapse of polyelectrolyte brushes and how the presence of an initial SAM determines the electroactive area of the modified electrode. A relevant additional double aim of this work is: firstly, to show the applicability of EIS to the measurement of the glass transition temperature Tg of surface confined polyelectrolyte brushes and secondly, to show the influence on the Tg of the type of counter-ion in the electrolyte. Furthermore, this work was performed with the goal of showing that electron transfer at metal substrate surface can be studied in detail according to the influence of conformational and thermal transitions of the polymeric structures.

Finally,this works serves the valuable purpose of discussing critical advantages and drawbacks of the different approaches to apply electrochemical impedance spectroscopy.

Achieving these goals represents a significant contribution to the engineering of new smart surfaces based on polymer assemblies or to a deeper understanding of the operating principles of already established designs.

## 1.7 REFERENCES


(1). Cosgrove, T.; Heath, T.; van Lent, B.; Leermakers, F.; Scheutjens, J. Macromolecules **1987**, 20, 1692.

(2). Milner, S. T.; Witten, T. A.; Cates, M. E. Macromolecules **1988**, 21, 2610.

(3). Milner, S. T.; Witten, T. A.; Cates, M. E. Macromolecules **1989**, 22, 853.

(4). Misra, S.; Varanasi, S.; Varanasi, P.P. Macromolecules **1989**, 22, 4173.

(5). Murat, M.; Grest, G. S. Macromolecules **1989**, 22,4054.

(6). Milner, S. T. Science, **1991**, 251, 905.

(7). I. Luzinov, S. Minko, Vladimir V. Tsukruk, Prog. Polym. Sci. 29 **2004** 635–698.

(8). Steve Edmondson, Vicky L. Osborne and Wilhelm T. S. Huck, Chem. Soc. Rev., **2004**, 33, 14–22.

(9). Yameen, B.; Ali, M.; Neumann, R.; Ensinger, W.; Knoll, W.; Azzaroni, O. *Small* **2009**, *5,* 1287–1291.

(10). Brittain, W. J.; Minko, S. *Journal of Polymer Science Part a-Polymer Chemistry* **2007**, *45*, 3505-3512.

(11). Zhao, B.; Brittain, W. J. *Progress in Polymer Science* **2000**, *25*, 677-710

(12). Milner, S. T. *Science* **1991**, *251*, 905-914.

(13). A. Ulman, An Introduction to Ultrathin Organic Films, Academic Press, New York,**1991** .

(14). Advincula, R.; Zhou, Q.; Park, M.; Wang, S.; Mays, J.; Sakellariou, G.; Pispas, S.;Hadjichristidis, N. Langmuir **2002**, 18, 8672.

(15). Jordan, R.; Ulman, A. J. Am. Chem. Soc. **1998**, 120, 243.

(16). Ingall, M. D. K.; Honeyman, C. H.; Mercure, J. V.; Bianconi, P. A.; Kunz, R. R. J. Am. Chem. Soc. **1999**, 121, 3607.

(17). Jones, D. M.; Brown, A. A.; Huck W. T. S.. Langmuir **2002**, 18, 1265

(18). Steenackers, M.; Küller, A.; Ballav, N.; Zharnikov, M.; Grunze, M.; Jordan, R. Small **2007**, 10, 1764.

(19). Matyjaszewski, K.; Xia, J. Chem. Rev. **2001**, 101, 2921 .

(20). Pyun, J.; Kowalewski, T.; Matyjaszewski, K. Macromol. Rapid Commun. **2003**, 24, 1043.

(21). Prucker, O.; Rühe, J. Macromolecules **1998**, 31,592 .

(22). Prucker, O.; Rühe, J. Macromolecules **1998**; 31, 602.

(23). R. A. L. Jones, R. W. Richards, Polymers at Surfaces and Interfaces, Cambridge University Press, Cambridge, **1999**.

(24). G. J. Fleer, M. A. Cohen Stuart, J. M. H. M. Scheutjens, T. Cosgrove, B. Vincent, Polymers at Interfaces, Chapman & Hall, London, **1993**.

(25). P. G. deGennes, J. Physique **1976**, 37, 1445.

(26). S. Minko *Journal of Macromolecular Science, Part C: Polymer Reviews*, 46:397–420, **2006**.

(27). Schild, H. G. *Progress in Polymer Science* **1992**, *17*, 163-249.

(28). Mark, J. E., *Polymer Data Handbook*. Oxford University Press Inc.**1999**.

(29). Sun, T. L.; Wang, G. J.; Feng, L.; Liu, B. Q.; Ma, Y. M.; Jiang, L.; Zhu, D. B.*Angewandte Chemie-International Edition* **2004**, *43*, 357-360.

(30). Wei, Q. S.; Ji, J.; Shen, J. C. *Macromolecular Rapid Communications* **2008**, *29*, 645-650.

(31). He, Q.; Kuller, A.; Grunze, M.; Li, J. B. *Langmuir* **200**7, *23*, 3981-3987. (32). Raula, J.; Shan, J.; Nuopponen, M.; Niskanen, A.; Jiang, H.; Kauppinen, E. I.; Tenhu, H. *Langmuir* **2003**, *19*, 3499-3504.

(33). Rühe,J.;Ballauff, M.; Biesalski, M.; Dziezok, P.; Grohn, F.; Johannsmann, D.;Houbenov, N.; Hugenberg, N.; Konradi, R.; Minko, S.; Motornov, M.; Netz, R.R.;

Schmidt, M.; Seidel, C.; Stamm, M.; Stephan, T.; Usov, D.; Zhang, H. N. *Polyelectrolytes with Defined Molecular Architecture I* **2004**, *165*, 79-150

(34). Zhang, N.H; Ruhe, J. *Macromolecules* **2005**, *38*, 4855-4860.

(35) Konradi, R.; Ruhe, J. Macromolecules **2005**, *38*, 4345-4354

(36). Wu, T.; Gong, P.; Szleifer, I.; Vlcek, P.; Subr, V.; Genzer, J. *Macromolecules* **2007**, *40*, 8756-8764. 79.

(37). Gong, P.; Wu, T.; Genzer, J.; Szleifer, I. *Macromolecules* **2007**, *40*, 8765-8773

(38). Treat, N. D.; Ayres, N.; Boyes, S. G.; Brittain, W. J. *Macromolecules* **2006**,*39*, 26-29.,

(39). Ayres, N.; Boyes, S. G.; Brittain, W. J. *Langmuir* **2007**, *23*, 182-189

(40). Choi, E. Y.; Azzaroni, O.; Cheng, N.; Zhou, F.; Kelby, T.; Huck, W. T. S.*Langmuir* **2007**, *23*, 10389-10394.

(41). Zhou, F.; Biesheuvel, P. M.; Chol, E. Y.; Shu, W.; Poetes, R.; Steiner, U.; Huck,W. T. S. *Nano Letters* **2008**, *8*, 725-730.

(42). Spruijt, E.; Choi, E. Y.; Huck, W. T. S. *Langmuir* **2008**, *24*, 11253-11260

(43). Azzaroni, O.; Moya, S.; Farhan, T.; Brown, A. A.; Huck, W. T. S.*Macromolecules* **2005**, *38*, 10192-10199.

(44). Moya, S.; Azzaroni, O.; Farhan, T.; Osborne, V. L.; Huck, W. T. S. *Angewandte Chemie-International Edition* **2005**, *44*, 4578-4581.

(45). Moya, S. E.; Azzaroni, O.; Kelby, T.; Donath, E.; Huck, W. T. S. *Journal of Physical Chemistry B* **2007**, *111*, 7034-7040

(46). Azzaroni, O.; Brown, A. A.; Huck, W. T. S. *Advanced Materials* **2007**, *19*, 151-154.

(47). Liu, X.; Ye, Q.; Yu, B.; Liang, Y.; Liu, W.; Zhou, F. *Langmuir* **2010**, *26,* 12377–12382.

(48). Finklea, H.O., *Electroanalytical Chemistry* Vol. 19,

(49). Bard, A. J.; Rubinstein I. Eds., Marcel Dekker Inc.: New York, **1996**; pp 160-239.

(50). J. Wang in Analytical Electrochemistry, 3rd edition, Chapter 2, Wiley-VCH New Jersey **2006**

(51). Raphaël Barbey, Laurent Lavanant, Dusko Paripovic, Nicolas Schüwer, Caroline Sugnaux, Stefano Tugulu, Harm-Anton Klok, *Chem. Rev.* **2009**, *109,* 5437–5527.

(52). T. Kin Tam, M. Ornatska, M. Pita, S. Minko, E. Katz, *J. Phys. Chem. C* **2008**, *112,* 8438–8445.

(53). T. Kin Tam, M. Pita, O. Trotsenko, M. Motornov, I. Tokarev, J. Halámek, S. Minko, E. Katz, Langmuir **2010**, 26(6), 4506–4513.

(54). J. Zhou, G. Wang, J. Hu, X. Lu, J. Li, Chem. Commun., **2006**, 4820–4822.

(55).M. Rueda, Applications of the impedance method in organic electrode kinetics, in: R.G. Compton and G. Hancock (Eds.), Research in Chemical Kinetics, Vol. 4, Blackwell Science Ltd., New York, **1997**, pp. 31-95.

(56). A. Lasia, Electrochemical impedance spectroscopy and its applications, in: B.E. Conway, J. O'M. Bockris and R.E. White (Eds.) Modern Aspects of Electrochemistry, Vol.32, chapter 2, Kluwer Academic / Plenum, New York, **1999**, pp. 143-248.

(57). J.R. Macdonald, Fundamentals of impedance spectroscopy, in: J.R. Macdonald (Ed.), Impedance Spectroscopy, emphasizing solid materials and systems, Wiley, New York, **1987**, p 13.

(58). Y. Pei, J. Travas-Sejdic, D.E. Williams, Langmuir **2012**, 28, 8072-8083

(59). F. Zhou, H. Hu, B. Yu, V.L. Osborne, W.T.S. Huck, W. Liu, Anal. Chem. **2007**, 79, 176-182.

(60). Brantley, E. L.; Jennings, G. K. *Macromolecules* **2004**, *37*, 1476-1483. (61). Bantz, M. R.; Brantley, E. L.; Weinstein, R. D.; Moriarty, J.; Jennings, G. K. *Journal of Physical Chemistry B* 2004, *108*, 9787-9794.

(62). B. Yu, F. Zhou, H. Hu, C. Wang, W. Liu, Electrochimica Acta 53 **2007** 487–494.

(63). J.J. Iturri Ramos, S.E. Moya, *Macromol. Rapid Commun.* **2011***, 32,* 1972−1978.

(64). C. Combellas, F. Kanoufi, S. Sanjuan, C. Slim, Y. Tran, *Langmuir* **2009**, 25(9), 5360–5370.].

(65). Johanna Reuber, Helke Reinhardt, and Diethelm Johannsmann, *Langmuir* **2006**, *22,* 3362-3367.

(66). M.J. Rodríguez Presa, L. M. Gassa, O. Azzaroni, C.A. Gervasi, *Anal. Chem.* **2009**, *81,* 7936–7943

(67). V. Mirčeski, Ž. Tomovski, *J. Solid State Electrochem.* **2011**, 15, 197–204.

# Chapter 2

# MATERIALS AND METHODS

## 2.1. MATERIALS

Methacryloyloxy ethyl trimethylammonium chloride (METAC, Mw=207.5, d25=1.105), N-isopropyl acrylamide (NIPAAm, Mw=113), N, N-dimethylformamide 99.85% (DMF), copper (I) chloride, copper (II) chloride, and 2,2-bipyridyl were purchased from Aldrich. LiClO4, NaCl and KCl were purchased from Fluka. Ethanol, 96% was purchased from Scharlau S.A. Water was purified using a Nanopure purification system (Thermo Scientific Barnstead)

The inhibitor undecanethiol were purchased from Sigma-Aldrich (Spain) and used without further purification. Thiol initiator ω-Mercaptoundecyl bromoisobutyrate was synthesized following the protocol described by Huck et. al. [1].

Redox probes: $K_4[Fe(CN)_6]$ Potassium hexacyanoferrate (II) trihydrate and $K_3[Fe(CN)_6]$ Potassium hexacyanoferrate (III) ;also $K_3$ $[Ru(NH_3)_6]$ Potassium hexaaminruthenium(III) were purchased from Sigma-Aldrich (Spain)

## 2.2. METHODS

### 2.2.1.Working electrode synthesis

Au substrates were prepared by sputtering deposition over glass, cleaned by sonication, followed by water rinsing while the final cleaning step comprised exposure to UV radiation in a Bioforce Nanosciences chamber for 30 minutes just before modification step. Modification of Au surfaces was carried out by immersion in 10 mM thiol solutions in ethanol for 16 hours in order allow the spontaneous formation of the initial assembled monolayer (SAM). In other to obtain brushes with four different grafting densities, four different thiol solutions were prepared mixing

initiator and inhibitor thiols with the following content of the initiator: 100%; 50%; 25% and 5%.

Polymer brushes were grown from the different mixed self-assembled monolayers constituted of ω-mercaptoundecyl bromoisobutyrate (thiol initiator) and 1-undecanethiol (blank thiol) chemisorbed on gold, which ultimately defines the grafting density of the polymer chains. Polymer synthesis was accomplished by surface-initiated aqueous atom transfer radical polymerization (SI-ATRP) [2,3] . Polymer brushes were prepared as follows: thiol functionalized surfaces were immersed in a mix of CuCl/ Bipyridine/ monomer in a ratio of 1:2:10 in DMF/water (3:2) as solvent, at 40 ºC in an inert atmosphere of $N_2$.The polymerization was left to proceed for 5 hours. At the end the subtrates were rinsed with water, acetone, ethanol and water.

## 2.3. TECHNIQUES

In the development of this thesis, and in order to achieve the objectives established, some of the techniques already mentioned, as well as some other different although complementary ones have been applied. A brief theoretical description of the most relevant features of the techniques employed becomes necessary for a better understanding of the results discussed in this work

### 2.3.1 Quartz Crystal Microbalance with Dissipation (QCM-D)

The quartz crystal microbalance (QCM) is a simple, cost effective, high-resolution mass sensing technique. The signal transduction mechanism of the QCM technique

is based on the piezoelectric consequence in quartz crystals. Due to the piezoelectric effect, a mechanical oscillation of characteristic frequency, $f_0$, is produced in the quartz crystal by applying an alternating electric field across the crystal through upper and lower metal electrodes covering the quartz surface. The frequency of such oscillation is determined by the thickness of the crystal (d) and the speed of shear waves in quartz (vQ) [4]. When a mass is loaded on top of the quartz crystal the mobility of the sensor becomes more limited and the oscillation frequency decays. A schematic view of the different frequency responses obtained from a single quartz sensor when sandwiched between a pair of electrodes is shown in Figure 2.1.

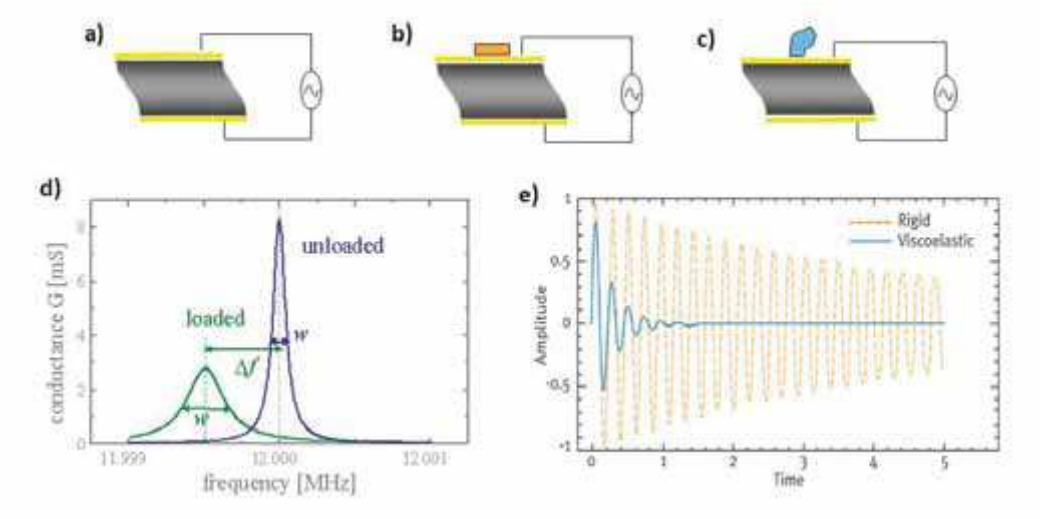


**Figure 2.1** Scheme of an electric circuit applied onto **(a)** a bare quartz sensor, **(b)** a quartz sensor with a rigid mass deposited on top and **(c)** a sensor with a viscoelastic mass. The frequency decrease observed **(d)** when passing from (a) to any of the other systems will depend on the viscoelastic character of the mass being adsorbed **(e)**, from www.qsense.com).

The derived relationship between the frequency decrease of the oscillating quartz crystal and the bound mass was reported in 1959 by Günter Sauerbrey. [5] Since then, QCM technique has been extensively used in order to detect thin film deposition on the surface of the crystal with a resolution down to ng/cm2 because it can be operated in vacuum, in gaseous environment or in liquid and its applicability has been shown for a wide range of systems. The ability of QCM to sensitively measure mass changes associated with liquid-solid interfacial phenomena, as well as to characterize energy dissipative or viscoelastic behavior of the mass deposited upon the metal electrode surface of the quartz crystal have turn this technique into a very useful tool in surface science.

**2.3.1.1 Quantitative evaluation of QCM-D data.**

The Sauerbrey equation [5] links frequency shifts and adsorbed masses per unit area in a very simple way:

$$m_{\mathrm{QCM}} = -C\frac{\Delta f_i}{i}, \quad (2.1)$$

with the mass sensitivity constant, $C$ = 18.06 ± 0.15 ng·cm$^{-2}$·Hz$^{-1}$ for sensors with a resonance frequency of 4.95 ± 0.02 MHz, and the overtone number $i$. The normalized frequency shifts, $\Delta f = \Delta f_i/i$, for the 3$^{rd}$ overtone were employed to determine $m_{\mathrm{QCM}}$. This acoustic mass comprises the mass of the adsorbed polymer and the mass of the solvent that is trapped inside or hydrodynamically coupled to the polymer film. The applicability of Eq. 2.1 is limited to sufficiently rigid films. For soft and dissipative films, more complex models would be required that account for the viscoelastic properties of the film [6] .

For the supramolecular assemblies investigated here, we found the ratio of dissipation and normalized frequency shifts, $\Delta D/-\Delta f$, to be smaller than 0.2×10$^{-6}$/Hz,

indicating that Eq. 2.1 is a good approximation. The application of the viscoelastic models to selected datasets corroborated that the Sauerbrey equation is indeed a good approximation for the films presented here, with an error below 5%. The experimental noise was typically below 2 ng/cm2

The brush thickness was further determined by

$$d_{\mathrm{QCM}} = m_{\mathrm{QCM}} / \rho_{\mathrm{Brush}} \quad (2.2)$$

where $\rho_{\mathrm{Brush}}$ = 1.0 g/cm$^3$ being the density of the solvated polymer film. In the pure form, the employed polymer exhibit densities between 1.0 and 1.1 g/cm$^3$, while the density of water or salt solutions is 1.0 g/cm$^3$. Equation (2.2) hence could overstimate the thickness by at most 10%.

In addition to measuring the frequency, the dissipation is often measured to help analysis. The dissipation is a parameter quantifying the damping in the system, and is related to the sample's viscoelastic properties. The dissipation is equal to the ratio of bandwidth, w, and frequency, f.

The viscoelastic data allows broader characterization of systems that fall outside of the scope of the linear Sauerbrey relationship between Δ*f* and Δ*m* and makes QCM-D more than a simple mass balance. Additionally, associated solvent or water content of adsorbed films can be measured by comparing the mass measured using QCM-D with that of complementary techniques such as ellipsometry or surface plasmon resonance [7].

### 2.3.2 Spectroscopic Ellipsometry

Ellipsometry is a optical techniques which is appropriate for the study of optical properties in thin films. It relies on the fact that the state of polarization of a light wave is altered upon reflection at an interface [8-10]. Ellipsometry experiment consist in that elliptically polarized light can be produced through reflection of linearly polarized from a flat surface. Reflection associates to a change of phase of the components of E parallel (Ep) and perpendicular (Es) to the plane of incidence of light. The two components of E, which were in phase (for linearly polarized light), appear from the phase of the surface (for elliptically polarized light). Figure 2.2 illustrates how a beam of linearly polarized light incident on a bare surface and a film-covered surface is reflected.

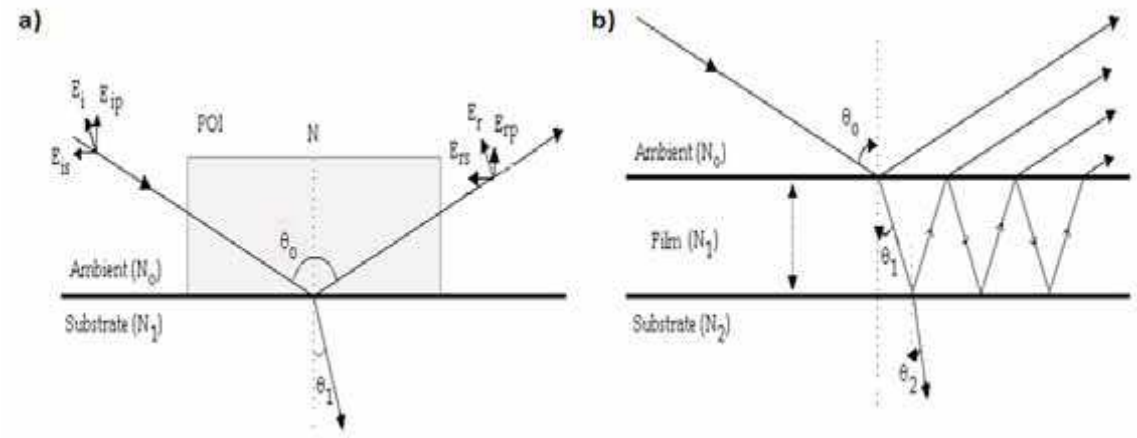


**Figure 2.2.** Reflection of polarized light on: **(a)** bare surface **(b)** film-covered surface

The plane of incidence (POI) includes the incident beam and the sample surface normal N, which is in the plane of the paper. The components parallel (Ep) and perpendicular (Es) to the POI are out of phase after reflection, and both phase and amplitude of the reflected light changes in a distinct way depending on the optical

properties of the surface [11]. Thus, an ellipsometric measurement allows one to quantify the phase difference between Ep and Es, Δ, and the change in the ratio of their amplitudes given by tan Ψ. For a bare reflecting surface, the forms for Δ and Ψ are:

Δ = δrp - δrs and tang Ψ=| *r p⁄ r s*|

where rp and rs are the Fresnel coefficients for the components p and s of light. Therefore, the resulting change in polarization after reflection from a surface can be measured through a complex reflection coefficient:

$$\rho = \frac{r_p}{r_s} = \tan(\Psi) e^{i\Delta}$$

which for a model substrate/film/ambient is obtained as a function of $N_0$, $N_1$, $N_2$, λ, $L_1$, $\theta_0$ where $N_0$, $N_1$ and $N_2$ are the indexes of refraction for the ambient, film and substrate, respectively (Fig. 2.2). Usually, $N_0$, λ and $\theta_0$ are known, $N_2$ can be independently obtained, and $N_1$ and $L_1$ (film thickness) can be obtained.
Thus, ellipsometry can be used to study growth or adsorption of very thin films (< 1 nm) on solid surfaces [12] . Although most of the work has so far concerned measurements at the air/solid interface, it is also possible to do measurements in water solution to study, for example, adsorption of surfactants, proteins, and polymers at the liquid/solid interface. [13-17]

### 2.3.2.1 Quantitative evaluation of ellipsometric data

Bound masses were determined by numerical fitting of the ellipsometric data to a multilayer model. Data were fitted over the accessible wavelength spectrum, using the software CompleteEASE (Woollam). The model relates the measured ellipsometric responses, Δ and Ψ as a function of λ, to the optical properties of the sensor surface, the adsorbed film and the surrounding solution. The glass windows

in the fluid cell were verified not to perturb the polarization of the probing light beam, and the optical properties of the sensor coating were calibrated prior to each measurement.

To extract the properties of the growing polymer chains from the ellipsometric response, a three-layer model was used. The layers represented the bulk solution, the polymer film and the gold coating of the sensor that interact with the light beam. The polyelectrolyte brush was treated as a single layer, which we assumed to be transparent and homogeneous (Cauchy medium), with a given thickness, $d_{opt}$, a wavelength-dependent refractive index, $n_{Brush}(\lambda) = A_{Brush} + B_{Brush} / (\lambda/\mu m)^2$, and a negligible extinction coefficient ($k_{Brush} = 0$). $A_{Brush}$ , $B_{Brush}$ and $d_{opt}$ were fitted simultaneously. The semi-infinite bulk solution was also treated as a transparent Cauchy medium, with a refractive index of $n_{sol}(\lambda) = A_{sol} + B_{sol} / (\lambda/\mu m)^2$. For water, $A_{sol} = 1.323$ and $B_{sol} = 0.00322$ were estimated from the literature [18] .The optical properties of the sensor's coating gold layer were fixed to the values established during calibration.

The adsorbed mass per unit area was determined from de Fejter's equation [19] .

$$m_{opt} = \frac{d_{opt}\left(n_{Brush} - n_{sol}\right)}{\mathrm{d}n/\mathrm{d}c}. \qquad (2.3)$$

To calculate $m_{opt}$, we employed the refractive indices at $\lambda = 632.5$ nm, and used a refractive index increment of $dn/dc = 0.150$ cm$^3$/g [20].We note that the errors associated with $d_{opt}$ and $n_{Brush}$-$n_{solvent}$ can be rather high for films that exhibit only a few nanometers in thickness. We observed also that the absolute values for $d_{opt}$ and $n_{Brush}$-$n_{solvent}$ are quite sensitive to minor variations in the optical properties of

the solid support. When discussing our results in terms of thickness, we will therefore consider $d_{QCM}$ rather than $d_{opt}$. The errors in $d_{opt}$ and $n_{Brush}$-$n_{solvent}$ are though covariant, i.e., the product $d_{opt} \times (n_{Brush}-n_{solvent})$ and $m_{opt}$ can be determined with good accuracy [21].

### 2.3.3 In situ combination of QCM-D and ellipsometry

Both the formation of polyelectrolyte multilayers and the synthesis of the polyelectrolyte brushes were monitored simultaneously, by QCM-D and ellipsometry, in liquid environment. Measurements were performed using a purpose designed flow cell (Q-Sense AB, Västra Frölunda, Sweden) with a total volume of ~300 µL. The flow cell was attached to a Q-Sense E1 setup, providing access to QCM-D data, and mounted on a spectroscopic rotating compensator ellipsometer (M2000V, Woollam, NE, USA), providing access to ellipsometric data. QCM-D data, $\Delta f$ and $\Delta D$, were acquired at 6 overtones ($i$ = 3, 5 … 13, corresponding to resonance frequencies of $fi \approx$15, 25 … 65 MHz) simultaneously, with sub-second time resolution. Ellipsometric data, $\Delta$ and $\Psi$, were acquired over a wavelength range from $\lambda$ = 380 to 1000 nm, simultaneously, at 65º angle of incidence, and with a time resolution of ~5 s. The working temperature was 23ºC.

### 2.3.4 QCM-D synthesis of Polymer brushes

Brushes were synthesized from a monolayer of thiol initiator ω-mercaptoundecyl bromo isobutyrate and mixture of the thiol initiator and thiol inhibitor undecanethiol, bound to gold coated quartz sensors (QSX 301, 4.95 MHz, Q-Sense AB). The sensors were pretreated with UV/ozone for 30 min and then exposed overnight to a 10-2 M thiol solution in EtOH.

Finally, the quartz sensor was rinsed with EtOH and water, and immediately taken to the next step. Both the thiol solutions and the washing EtOH and milli-Q water were passed through the flow cell with a peristaltic pump (ISM935C, Ismatec, Zürich, Switzerland). For brush polymerization the gold surface coated with the thiol initiator was incubated for 5 h in a N,N-dimethylformamide (DMF)/water (3:2) ,solution of monomer /2,2-bipyridine/ CuCl (molar ratio 10:2:1). Then, the gold surfaces were consecutively rinsed in DMF/water (3:2) and water [22] . Polymerization was also kept for 5 hours in this case.

### 2.3.5 Atomic Force Microscopy

Atomic force microscopy (AFM) or scanning force microscopy (SFM) is a very high-resolution type of scanning probe microscopy, with demonstrated resolution on the order of fractions of a nanometer. The AFM consists of a cantilever with a sharp tip (probe) at its end that is used to scan the specimen surface. The cantilever is typically silicon or silicon nitride with a tip radius of curvature on the order of nanometers. When the tip is brought into proximity of a sample surface, forces between the tip and the sample lead to a deflection of the cantilever according to Hooke's law [23].

Atomic force microscopy measurements were performed in a fluid cell of the AFM (Nanoscope III, Digital Instruments, Santa Barbara, CA). The samples were imaged in KCl solutions in contact mode using silicon nitride cantilevers of 100 mm length with integrated sharpened tips (spring constant 0.09 N=m, Olympus, Tokyo, Japan). Height, deflection, and friction were used as image contrast.

### 2.3.6. Electrochemical Methods

#### 2.3.6.1 The 3-electrode cell

In experimental electrochemistry, the 3-electrode cell is one of the most common configurations used to study electrochemical reactions (see Figure 2.3). It consists of a counter electrode (CE) which is used to polarise the electrode of interest, the working electrode. In order to that, the potential (voltage) on the working electrode is precisely known as third electrode, known as the reference electrode (RE) is held close to the surface of the working electrode (WE) and the potential difference measured. This is because the RE has no current passing through it, but merely maintains an invariant constant potential, no matter what is happening around it.

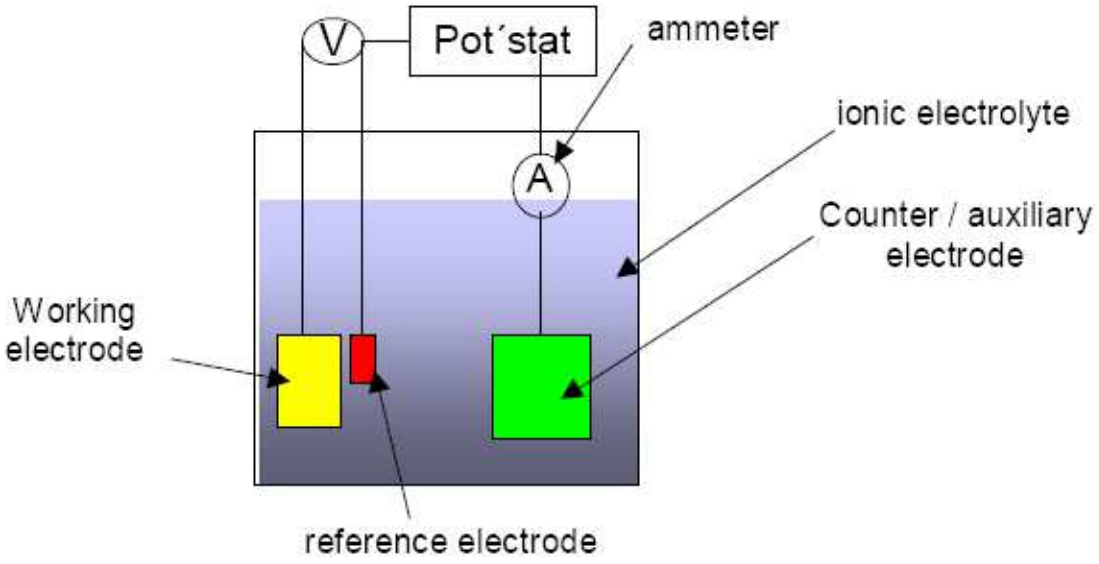


**Figure 2.3.** Typical The 3-electrode cell consists of a counter electrode (CE) reference electrode (RE) and working electrode (WE) immersed in the ionic electrolyte solution and the potential difference measured by Potentiostat.

##### 2.3.6.1.1 Working conditions for the electrochemical experiments

Electrochemical measurements were carried out within a conventional three-electrode cell .The temperature range was from 5°C – 45°C in the case of PMETAC

brushes .For PNIPAMM the temperatures were 20ºC and 40ºC. A platinum sheet with large area and a saturated calomel electrode (SCE) were used as the counter electrode and the reference electrode, respectively. All potentials are referred to the SCE at 25°C. Au substrates coated with brushes served as working electrodes. 0.1 M NaCl , 0.1 M KCl ,50mM NaCl and 0.1 M $NaClO_4$ solutions were used as supporting electrolytes and prepared from analytical grade (Merck) reagents and Milli-Q water for PMETAC and 0.1M KCl solution for PNIPAMM.. Before performing each measurement the working electrode was thoroughly rinsed with Milli-Q water and immersed in the supporting electrolyte solution 10 minutes. Experiments were performed under purified $N_2$ gas saturation in the presence of a 1 mM $K_3[Fe(CN)_6]$ / $K_4[Fe(CN)_6]$ (1:1) and 1 mM $Cl_2[Ru(NH_3)_6]$ / $Cl_3[Ru(NH_3)_6]$ (1:1) both two mixture individually as a redox probe in the supporting electrolytes.

### 2.3.6.2 Cyclic Voltammetry (CV)

#### 2.3.6.2.1 Description of the method

Cyclic voltammetry is the most widely used technique for acquiring qualitative information about electrochemical reactions. It offers a rapid location of *redox potentials* of the electroactive species.

A few concepts have to be introduced before describing briefly this method. For the oxidation reaction involving *n* electrons formally written as:

$$R \leftrightarrow O + ne^{-} \qquad (2.4)$$

the *Nernst Equation* gives the relationship between the equilibrium potential and the concentrations of the oxidized and reduced forms of the redox couple (at 298 K):

$$E = E^{o'} + \frac{0.059}{n} \log \frac{[O]}{[R]} \qquad (2.5)$$

where E is the applied potential and $E^{0'}$ the formal potential; [O] and [R] represent surface concentrations of oxidised and reduced species, respectively, at the electrode/solution interface.

A typical electrode reaction involves the transfer of charge between an electrode and a species in solution in a series of steps:

1. Reactant (O) moves to the interface (this is termed mass transport)
2. Electron transfer can then occur via quantum mechanical tunnelling between the electrode and reactant close to the electrode (typical tunnelling distances are less than 3 nm)
3. The product (R) moves away from the electrode to allow fresh reactant to the surface

A cyclic voltammetric experiment involves potential sweeping according to a ramp function of time between two values at a fixed scan rate (in units of Volt / second), however when the potential reaches the upper limit or final potential, the scan is reversed and the potential is swept back to the lower limit that usually coincides with the initial potential value.

A typical cyclic voltammogram is a recording of current *vs* potential. An example for a solution containing only a single electrochemical reactant is shown in figure 2.4. The characteristics of the voltammogram in each sweep depend on a number of factors including: the rate of the electron transfer reaction(s); mass transport of the electroactive species and potential scan rate. A background current arises from the charge of the interfacial capacitor subjected to a linearly varying applied potential.

As the potential is initially swept during the forward sweep the faradaic current rises as the potential is swept further from its equilibrium position (for null current), thus converting more reactant. A peak occurs, at a potential $E_{pa}$ with an anodic peak current $i_{pa}$ for the oxidation of R to O, since at some point the diffusion layer has grown sufficiently above the electrode so that the flux of reactant to the electrode is not fast enough to satisfy that required by the Nernst or equilibrium equation. In this situation the current begins to drop. When the scan is reversed we simply move back through the equilibrium positions gradually reducing product O back to reactant R. The current flow is now from the solution species back to the electrode and so occurs in the opposite sense to the forward sweep but otherwise the behavior can be explained in an identical manner for a cathodic process.

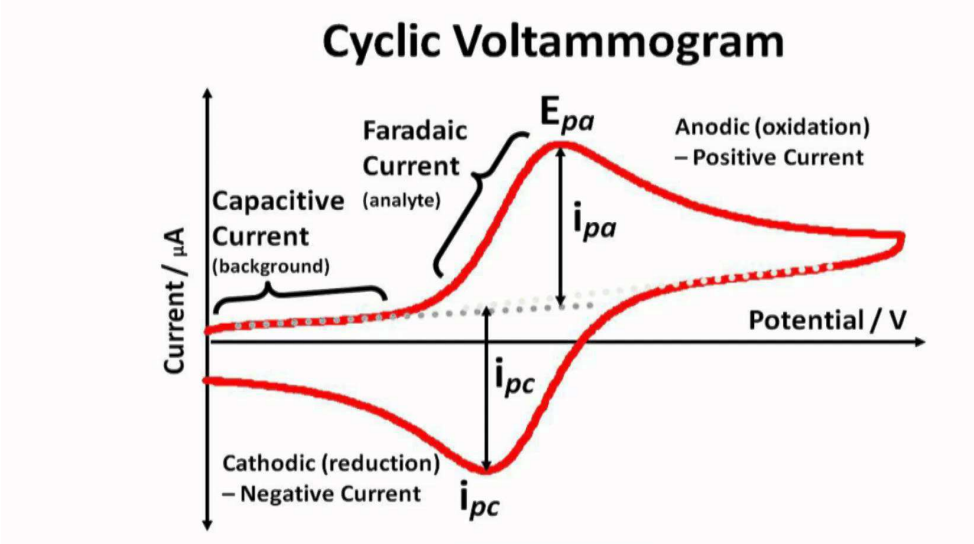


**Figure 2.4.** Typical cyclic voltammogram for a singe redox couple

For a reversible electrochemical reaction the CV recorded has certain well defined characteristics.

1. The potential separation between the current peaks has a fixed value $\Delta E_p = E_{pa} - E_{pc} = 59/n$ mV at all scan rates

2. The peak potentials do not alter as a function of potential scan rate

3. The ratio of the peak currents is equal to one

4. The peak currents are proportional to the square root of the scan rate

#### 2.3.6.2.2 Description of CV experiments

Cyclic voltammetry (CV) measurements were performed by scanning the potential between preset anodic and cathodic switch-potentials, at a scan rate of 0.05 $Vs^{-1}$.

### 2.3.6.3 Electrochemical impedance spectroscopy (EIS)

#### 2.3.6.3.1 Description of the method

EIS, a form of dynamic system analysis, is already established as one of the most efficient experimental techniques to perform an identification of an electrochemical system. The key objective here is to derive a mathematical model of the system containing its dynamic characteristics. To this end it is necessary to deviate the studied system from its steady-state with the help of a deterministic perturbation signal x(t), such as a sinusoidal signal. The system response y(t) can be measured and analysed, either in the time domain or in the frequency domain. Due to experimental and mathematical reasons, it is often much easier to analyze signals and systems when they are represented in the frequency domain. Switching between time-domain and frequency-domain is achieved thanks to the Laplace transformation.

A dynamic model for the studied system can be expressed in many different ways. The essential condition that any of these forms must meet is having enough amount of information to predict the transient response of the system to any input signal.

The behavior of the system becomes defined by the input-output relationship that describes the way in which changes in input signals modify output signals. In this regard, inputs are the origin of the relaxation effects on output signals and consequently, on the behavior of the system. The ratio function of the system in the time domain h(t) and the corresponding transfer function H(s) in the frequency domain relate perturbation and response (Figure 2.5), where ✸ represents the convolution of two temporal functions [24] and s is the Laplace variable.

$$H(s) = \frac{y(s)}{x(s)} \qquad (2.6)$$

The transfer function contains all the dynamic features of the studied system.

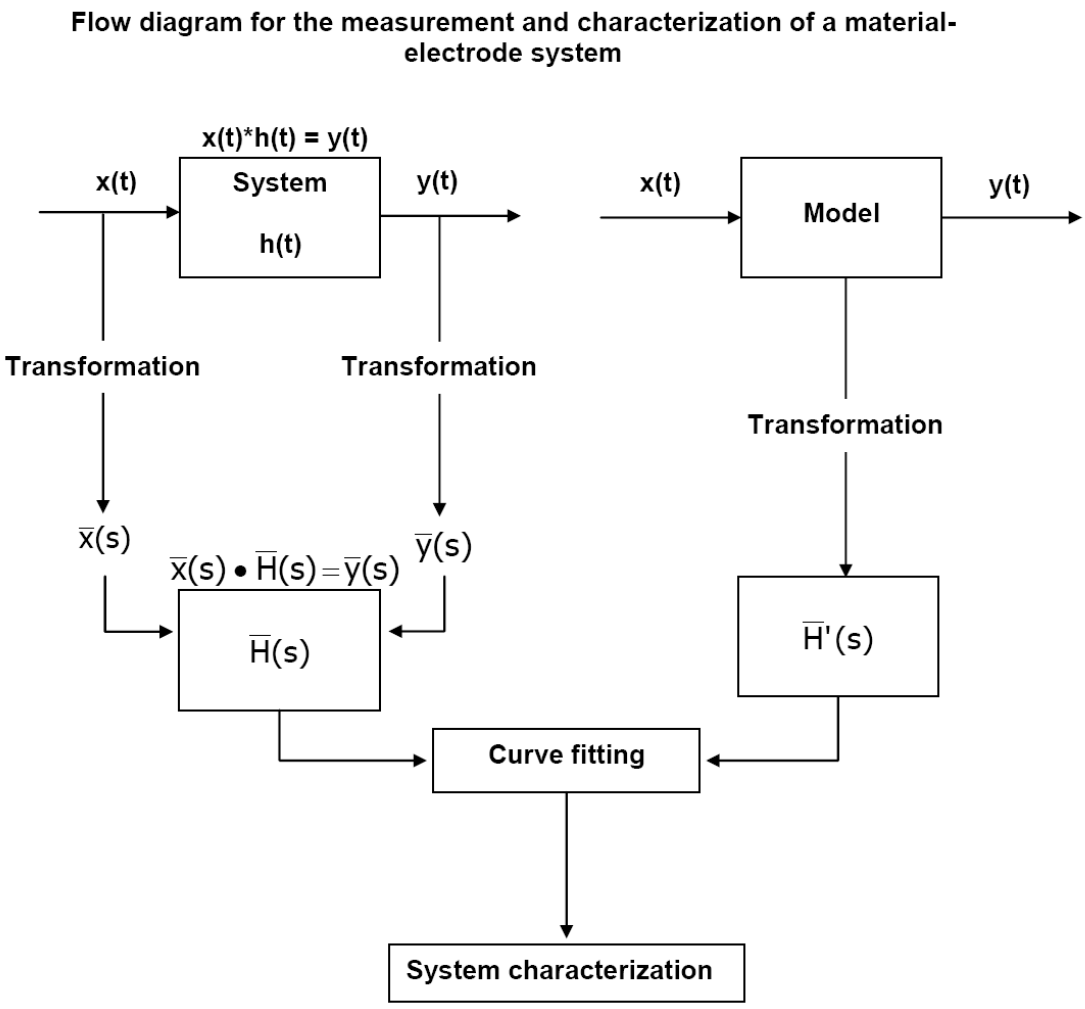


**Figure 2.5.** Scheme of a dynamic system analysis.

A special case of great importance in the field of dynamic system analysis is the one applied to an electrochemical system, where x(t) and y(t) represent the electrical potential E(t) and current i(t), respectively. In this case H(s) corresponds to the admittance of the electrode - solution interface or Y(s)

$$Y(s) = Z(s)^{-1} = \frac{i(s)}{E(s)} \qquad (2.7)$$

and Z(s) represents the impedance.

For a sinusoidal perturbation signal x(t) = a sin ωt, s = j ω and ω = 2 π f, where a is the amplitude measured from the mean value of the function (see Figure 2.6), ω is the angular frequency, f is the oscillation frequency and j = $\sqrt{-1}$ i.e. the imaginary unit, so that Z (s) is a complex number.

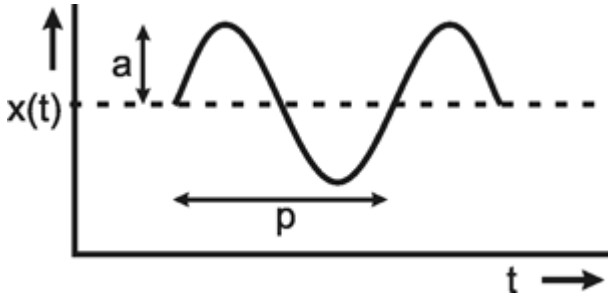


**Figure 2.6** Sine function. Amplitude a, period p = $f^{-1}$. The mean value is shown in dotted line.

In the meantime, this methodology has become a standard technique and has been extensively described in the specific literature [25-29].

The search for a mathematical model of the system involves replacing each block in its functional diagram by the mathematical equation which links outputs to inputs. To this end, one must know the state equations which describe its behaviour. If the block is static, the model will be an equation relating the input variable with the output variable in the following way:

$h(t) = R\ i(t)$ where the block corresponds to a resistance R (2.8)

In the case of a dynamic block the relationship between both variables is a differential equation and consequently in the mathematical model we include not only input and output variables, but also their derivatives

$$h(t) = R\,i(t) + L\,\frac{di(t)}{dt}$$ where the block represents a R,L(inductor) circuit (2.9)

The mathematical model for the global system results from a combination of individual mathematical models for each block and accordingly, a system of differential equations is involved.

If the obtained mathematical models were linear, the study would be much simpler since they adhere to the principle of linearity or superposition, in this case it would be enough to know the model response to a limited set of inputs (usually impulse, step, and / or sinusoidal signals). Indeed, if the superposition principle holds true then, the response to a perturbation signal that is a linear combination of other elementary signals, is the same linear combination of the responses of these elementary signals.

However, most models are nonlinear, especially electrochemical models are highly nonlinear, and for that reason the superposition principle is in general not applicable. Now, for small variations around a **stationary working points** as the ones caused by the application of a low amplitude sinusoidal perturbation signal, the behavior of an electrochemical model can be approximated by its linearized model. This linearized model, does meet the superposition principle, but only in a

small range around the working point and with a slight deviation from the nonlinear model.

The response y(t) to a sine perturbation function is called frequency response. For a linear system, frequency responses are also sinusoidal functions that have the same frequency as the input signal, and usually differ from it in amplitude and phase shift. In this case, the frequency responses take the form $y(t) = A \sin(\omega t + \phi)$. Accordingly, the two components to be measured are $\phi$ (the phase shift between input and output signals) as well as the change in the amplitude.

In order to properly measure the electrochemical impedance, it is necessary to use a perturbation signal with low amplitude. The limits between which the set amplitude defines a **"linear range"** are dependent on the level of electrode polarization. The lower limit is determined by the signal/noise ratio that the measuring equipment can accommodate. The upper limit is determined by the onset of nonlinear distortion (higher order harmonics).

Laplace transformation is a common tool for solving linear differential equations, consequently, by applying Laplace transforms to the differential equation that characterizes the model, we will be able to solve this equation and, therefore, to find the response. Laplace transformation can be used to solve the equation of the model, while it generates a convenient representation of the signals.

It must be highlighted that the primary objective of using the Laplace transformation is not finding a solution for the differential equation, but developing a compact method for representing systems that allows us to disclose in a simple way, the

main features of its behavior. Laplace transformation corresponds to a change of the independent variable, from time to the Laplace complex variable s, in this way switching from the time domain into the frequency domain.

As shown in Figure 2.5, the core of the system identification procedure is the parameter fit of the measured impedance to the transfer function or theoretical impedance. Curve fitting process of the experimental transfer function H(s) to the theoretical transfer function H'(s) generates microscopic parameter values appearing in the impedance equation that characterize the system from a physicochemical point of view.

Diagram in Figure 2.7 schematizes the principle of transfer function measurement using a frequency response analyzer (FRA). The response of the cell y(t) to the perturbation x (t) is correlated with two synchronous reference signals, one in phase with x (t) and the other 90 ° out of phase, i.e. sin ωt and cos ωt, to calculate:

$$Re = \frac{1}{T}\int_0^T y(t)\sin(wt)\ dt \qquad (2.10)$$

$$Im = \frac{1}{T}\int_0^T y(t)\cos(wt)\ dt \qquad (2.11)$$

where T is the integration time, which is an integer number of periods of the perturbating signal.

For a linear system the signal y(t) only contains the first harmonic (fundamental) plus the parasitic noise that can only be completely removed if the integration time

T is infinite. Once both quantities, accounting for the real and imaginary parts of x (t) are known, then the impedance can be calculated.

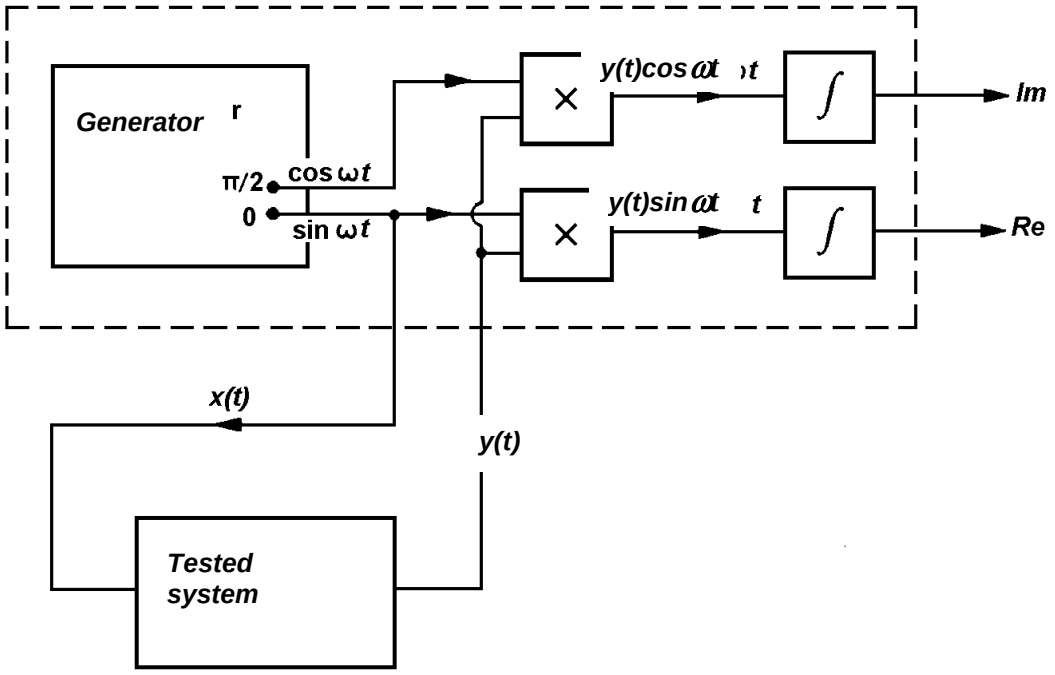


**Figure 2.7.** FRA (frequency response analyser) working principle. Impedance as a complex quantity contains an imaginary part Im and a real part Re.

With the usual cell arrangement of three electrodes the working electrode's potential is controlled by a potentiostat. A space charge or location of charge accumulation, called the electrical double layer is always present on the solution side of the electrode-solution interface. The double layer behavior associated with a charge current can be approximated by a parallel plates capacitor with a capacitance $C_{dl}$ and an impedance component in parallel electrical connection with the Faradaic impedance ($Z_f$) i.e. the impedance related to the electrochemical reaction related to the Faradaic current. Power dissipation by Joule effect in the electrolyte results from the solution resistance, as measured in the electrolytic path between the reference

electrode and the working electrode. The electrolyte resistance ($R_\Omega$ = $R_e$) is connected in series with the parallel connection just mentioned (See Figure 2.8).

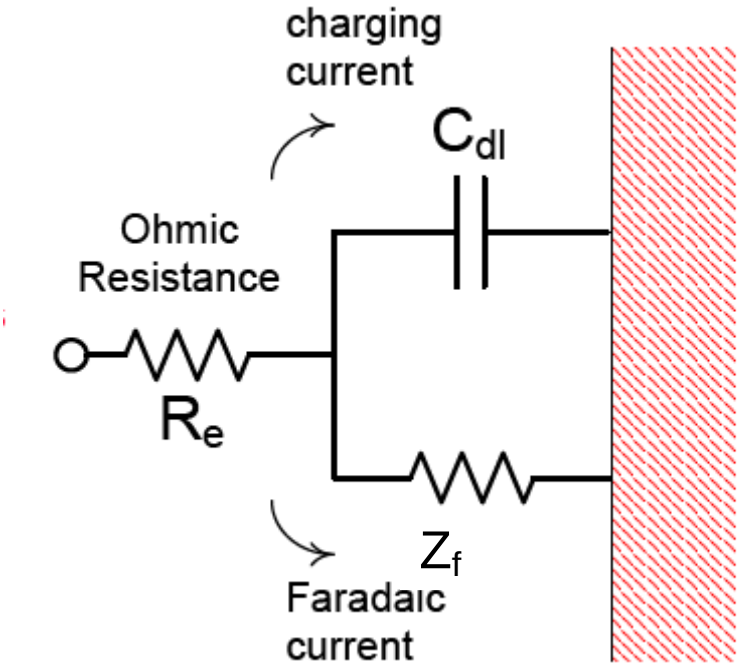


**Figure 2.8.** Schematic diagram of the basic interfacial impedance elements in an electrochemical cell.

Due to the high-frequency capacitive effect attributed to the double layer electrochemical impedance experiments are performed in a wide **range of frequencies** (sometimes up to several hundred kHz) to obtain a high frequency limit of the impedance equal to $R_e$. The lowest frequency at which it is usually required to perform the experiments, according to data published in the last three decades falls in the range of subacustic frequencies $10^{-2}$ – $10^{-3}$ Hz [24]

A practical relevant example of a simple electrochemical system that can be studied by this technique is the corrosion of a metal surface in the so-called active region,

for which the electrochemical reactions occur under activation. Such a system can be represented by an equivalent circuit or electrical analog that results from the combination of passive elements of an electrical circuit with the same response as the considered electrochemical system, as shown in Figure 2.9.

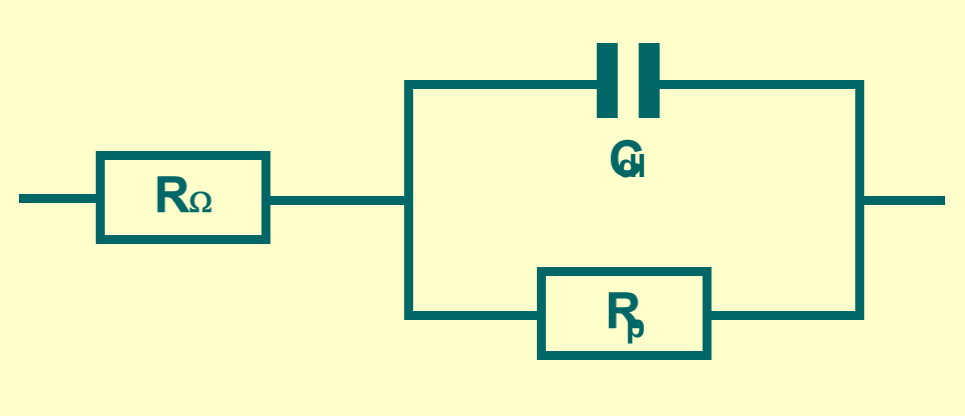


**Figure 2.9.** Equivalent circuit representing a simple corroding metal interface.

Therefore, the Faradaic impedance is simply a resistance Rp called the polarization resistance whose value is

$$R_p = \lim_{s \to 0} Z(s) - \lim_{s \to \infty} Z(s) \qquad (2.12)$$

The impedance representation can be produced in cartesian coordinates with a Nyquist plot [-Im(Z) vs. Re(Z)] or with Bode plots (log IZI vs. Log f and - $\phi$ vs log f) as shown in figure 2.10.

The parallel connection of $C_{dl}$ and $R_p$ results in a characteristic frequency defined as

$$\omega_{car} = \frac{1}{R_p C_{dl}} \qquad (2.13)$$

This frequency $\omega_{car}$ can be calculated as the frequency that exhibit a maximum in the phase angle, as can be seen in the Bode plot (Figure 2.10b). The characteristic angular frequency $\omega_{car}$ is then related to the oscillation frequency $f_{max}$ / Hz at which the imaginary part of the impedance reaches a maximum, according to

$$f_{\max} = \frac{1}{2\pi R_p C_{dl}} = \frac{\omega_{car}}{2\pi} \qquad (2.14)$$

After calculating $\omega_{car}$ and $R_p$ as indicated in equation (2.12) Cdl can be derived from equation (2.14).

The product ($R_p$ $C_{dl}$) has units of time and is a measure of the relaxation time required to reach the new steady state after applying the perturbation, this product is known as the "time constant" of a process stage. Considering a global process comprising successive distinguishable stages a comparison of the different time constants indicates the corresponding frequency ranges (or equivalently, time windows) in which each step can be detected. A step having a small time constant relaxes quickly and will be measured in the high frequency range. On the contrary, a step with a large constant time exhibits a slow relaxation and will be measured in the low frequency range. As already stated, the charging process of the interface capacitor corresponds typically to a step that will be measured at higher frequencies, whereas a diffusion-controlled reaction step, which is typically slow, will be measured at lower frequencies.

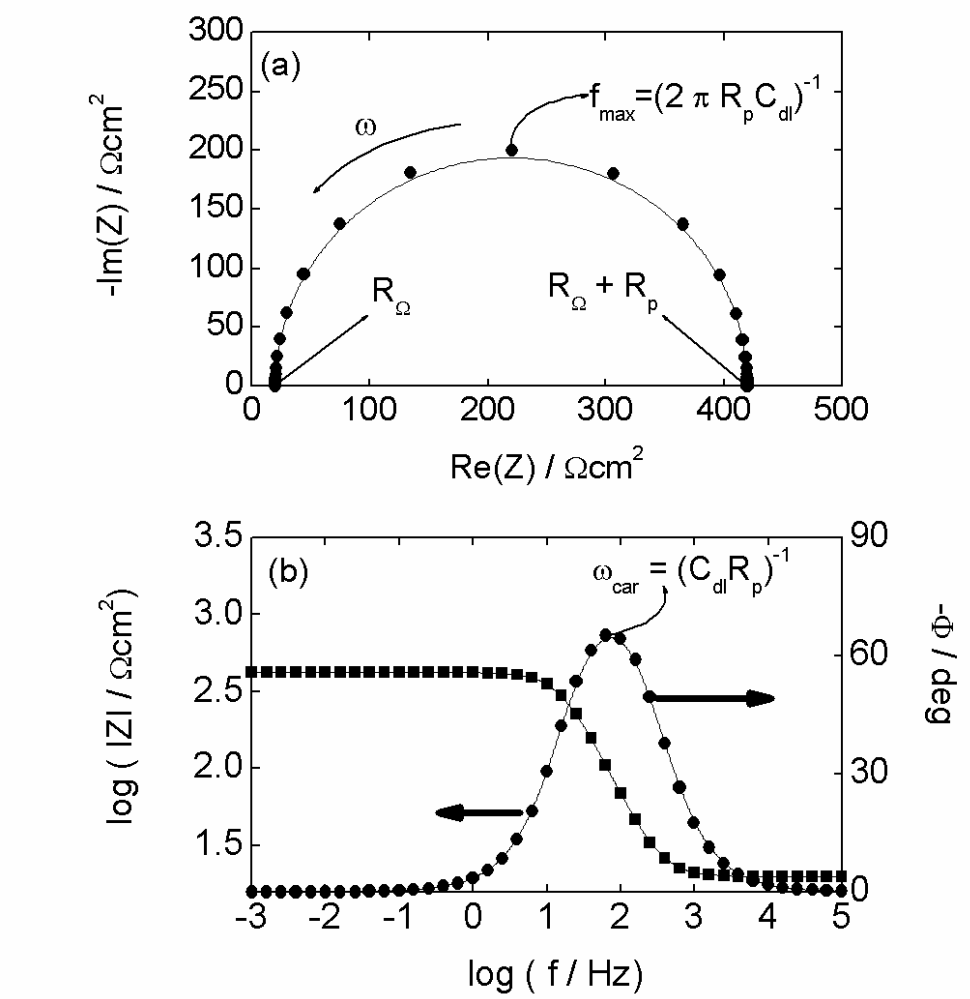


**Figure 2.10.** Simulation of the impedance of an electrode reaction under activation control with the following values for the parameters in the equivalent circuit from figure 2.9: $R_\Omega$ = 20 Ωcm$^2$, $R_p$ = 400 Ωcm$^2$ and $C_{dl}$ = 25 μFcm$^{-2}$. **a)** Nyquist plot, **b)** Bode magnitude plot (■) and Bode phase plot (●).

Perhaps it is worth mentioning here that the use of equivalent circuits to model the electrochemical interface has many limitations. Firstly, the behavior of an electrochemical process rarely corresponds exactly to that of a passive element in the electrical circuit. Secondly, different equivalent circuits having the same elements but with different electrical connections may exhibit the same global

impedance, what demonstrates the ambiguity resulting from the application of electrical equivalent circuits as models. Finally, when the curve fitting procedure yields best-fit macroscopic parameters for the equivalent circuit, a necessary final step remains to be performed. This step, not always considered even in some specialized literature on the subject, involves finding the proper relationships between these parameters and the microscopic physicochemical parameters of the studied system [28].

It is for this reason that in this work EIS is applied according to a strategy based on a proposed theoretical model as derived from the governing differential equations (material and charge balances) that is fitted to the experimental impedance data. The fitting procedure generates directly, in this way, the valuable microscopic parameters that allow to make predictions of the system behavior under different working conditions.

Impedance experiments, like the rest of the electrochemical experiments, were carried out with a Zahner IM6e electrochemical workstation whose operational accuracy limits are shown in Figure 2.11, in the form of an accuracy map. Diagram in Figure 2.11 has the coordinates of a Bode magnitude plot and the violet and green lines enclose areas within which the measured impedance must lie to exhibit any of the two indicated accuracy levels, namely 0.5 % (magnitude) / 0.5 degrees (phase) and 2 % (magnitude) / 3 degrees (phase), respectively. Additionally, the diagram shows areas for galvanostatic operation and operation with a special probe used for high impedance samples (HiZ probe).

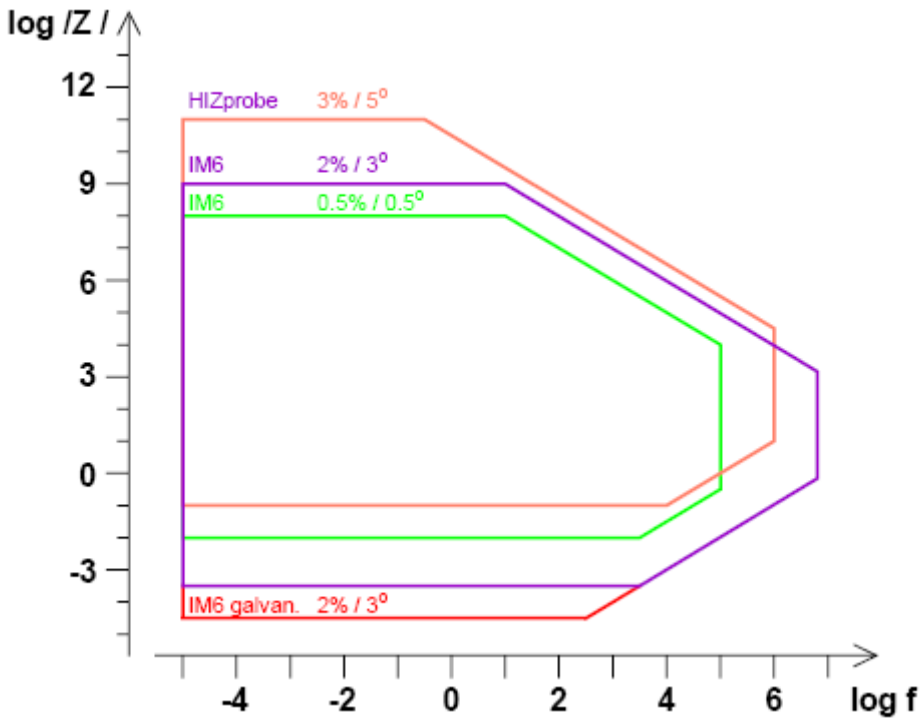


**Figure 2.11.** Accuracy map for the Zahner IM6e electrochemical workstation used for impedance measurements.

Experimental impedance spectra were measured by applying a sinusoidal perturbation of 10 mV amplitude in the frequency range 1 mHz - 100 KHz. Data analysis was performed according to proper procedures for transfer function derivation and identification by using weighted complex non-linear least squares (CNLS) fitting based on the Marquardt-Levenberg algorithm. [28-30]. Fitting the model to the experimental data involves minimization of the cost function J (sum of squared errors), defined as

$$J = \sum_{k=1}^{N} \frac{\left[Z_{r,k} - \bar{Z}_{r,k}(\omega_k, P)\right]^2}{w_{r,k}^2} + \sum_{k=1}^{N} \frac{\left[Z_{j,k} - \bar{Z}_{j,k}(\omega_k, P)\right]^2}{w_{j,k}^2} \qquad (2.15)$$

where $Z_{r,k}$ and $Z_{j,k}$ represent the real and imaginary components of the experimental impedances, respectively, as measured at a frequency with number k that has N values within the experimental frequency range.

$\bar{Z}_{r,k}(\omega_k,P)$ and $\bar{Z}_{j,k}(\omega_k,P)$: are the real and imaginary components of the theoretical impedances, respectively, calculated at the frequency $\omega_k$, and being also a function of the vector of fitting parameters P that appear in the model equation in a nonlinear form and whose fitted values minimize the resultant cost function $w_{r,k}$ and $w_{j,k}$: are the weight factors for the real and the imaginary parts, respectively.

Attention is drawn to the fact that the cost function J contains two terms or sums of squared errors and so, the errors in the real and imaginary parts of the impedance are assumed to be independent of each other. Function J could have also been defined in terms of the errors in phase shift and impedance magnitude. However since it is advisable to calculate J using the impedance components as they were actually measured, equation 2.15 was used in our data analysis, in terms of the measured real and imaginary parts, at each experimental frequency.

As the impedance values can vary over many orders of magnitude between the initial and final frequencies, minimization of J must be weighted. In this case, the weighting strategy is based on using the impedance magnitudes as weight factors at each frequency, both for the real and the imaginary parts. The selected algorithm for the nonlinear regression was the Levemberg-Marquardt's [31].

#### 2.3.6.3.2 Description of EIS experiments

Impedance spectra were obtained with a Zahner IM6d electrochemical workstation. The dc potential of the working electrodes was held at the open circuit potential while a 10 mV amplitude ac potential was applied. The voltage signal frequencies used for EIS measurements ranged from 100 kHz to 1 mHz. Impedance data analysis was performed according to proper procedures for transfer function derivation and identification by using complex non-linear least squares (CNLS) fitting based on the Marquardt-Levenberg algorithm [32] .

## 2.4 REFERENCES


(1). D. M. Jones, A. A. Brown,W. T. S. Huck, Langmuir **2002**, 18,1265.

(2). Matyjaszewski, K.; Gaynor, S.; Grezta, D.; Mardare, D.; Shigemoto, T. *J. Phys. Org. Chem.* **1995**, *8,* 306-315.

(3). Matyjaszewski, K.; Patten, T. E.; Xia, J. *J. Am. Chem. Soc*. **1997**, *119*, 674 - 680.

(4). Janshoff, A.; Galla, H. J.; Steinem, C. Angew. Chem. Int. Ed. **2000**, 39, 4004

(5). Sauerbrey, G. Z. Phys. **1959**, 155, 206.

(6). Domack, A.; Prucker, O.; Rühe, J.; Johannsmann, D. Phys. Rev. **1997**, 56, 680.

(7). Janshoff A, Galla HJ, Steinem C., *Angewandte Chemie International Edition* 2000;39:4004–4032.

(8). Gonçalves, D.; Irene, E. A. Quim. Nova **2002**, 25 (5), 794.

(9). Fowles, G.R. “Introduction to Modern Optics, 2nd ed.” **1975**, Dover, New York .

(10). Pedrotti, F.L.; Pedrotti, L.S.; “Introduction to Optics, 2nd ed.” **1993**, Prentice Hall, NewJersey.

(11). Irene, E. A.; Woolam, J. A. Mater. Res. Soc. Bulletin **1995**, 20, 24.

(12). Landgren, M.; Jönsson, B. *J. Phys. Chem*. **1993**, 97, 1656.

(13). Arnebrant, T.; Bäckström, K.; Jönsson, B.; Nylander, T. *J. Colloid Interface Sci.* **1989**,128, 303.

(14). Wägnerud, P.; Olofsson, G*. J. Colloid Interface* Sci. **1992**, 153, 392.

(15). Wahlgren, M.; Arnebrant. T. *J. Colloid Interface Sci*. **1989**, 136, 259.

(16). Malmsten, M.; Lindman, B. *Langmuir* **1990**, 6, 357.

(17). Tiberg, F.; Malmsten, M.; Linse, P.; Lindman, B. *Langmuir* **1991**, 7, 2723.

(18). Daimon, M.; Masumura, A. Appl. Opt. **2007**, 46, 3811.

(19). *De* Feijter, J. A.; Benjamins, J.; Veer, F. A. Biopolymers **1978**, 17, 1759.

(20). *Halthur, T. J.; Elofsson, U. M. Langmuir* **2004***, 20, 1739*

(21). *Caruso, F.; Niikura, K.; Furlong, D. N.; Okahata, Y. Langmuir* **1997***, 13, 3422.*

(22). Masci, G.; Bontempo, D.; Tiso, N.; Diociaiuti, M.; Mannina, L.; Capitani, D.; Crescenzi, V*. Macromolecules* **2004**, 37, 4464.

(23). Cappella, B; Dietler, G . *Surface Science Reports* ,34 **1999** (1–3):

(24). http://es.wikipedia.org/wiki/Convoluci%C3%B3n

(25). C. Gabrielli, Identification of electrochemical processes by frequency response analysis, Technical Report Nº 004/83, Solartron Instr. Group, Farnsborough, Hamphshire, England, **1984**.

(26). Lasia, Electrochemical Impedance Spectroscopy and Its Applications, Modern Aspects of Electrochemistry, B. E. Conway, J. Bockris, and R.E. White, Edts., Kluwer Academic/Plenum Publishers, New York, 1999, Vol. 32, p. 143-248.

(27). Sluyters-Rehbach, Impedances of Electrochemical Systems, *Pure & Appl. Chem.,* Vol. 66, No. 9, pp. 1831-1891,**1994**.

(28). Impedance Spectroscopy: Theory, Experiment, and Applications, 2nd ed Edited by Evgenij Barsoukov (Texas Instruments Inc.) and J. Ross Macdonald (University of North Carolina, Chapel Hill). John Wiley & Sons, Inc.: Hoboken, NJ. **2005**.

(29). M.E. Orazem and B. Tribollet, Electrochemical Impedance Spectroscopy, John Wiley & Sons, Inc.: Hoboken, NJ. **2008.**

(30). J. Ross Macdonald, Solid State Ionics 176 ,**2005,** 1961 – 1969.

(31). Marquardt, Donald W., Journal of the Society for Industrial and Applied Mathematics, 11, **1963**, 431-441.

(32). Press, W. H.; Teukolsky, S. A.; Vetterling, W. T.; Flannery, B. P. *Numerical Recipes in FORTRAN: The Art of Scientific Computing,* 2nd ed.; Cambridge University Press: Cambridge, U.K., **1992**

# Chapter 3

## MATHEMATICAL MODELING OF THE FARADAIC IMPEDANCE OF A REDOX PROBE INSIDE GRAFTED POLYMER BRUSHES

## 3.1 INTRODUCTION

EIS is a technique with proven capabilities to act as an electronic transducer of molecular level processes occurring inside the brush environment. In most cases, the physicochemical information is obtained after fitting the measured complex impedance to a theoretical impedance expression which includes different elements related to the interfacial physicochemical processes.[1,2]

The choice of a suitable model is a critical step in the characterization procedure. The analysis could be even more complicated when transfer functions, with reasonable physical meaning but different interpretation, can accurately describe the same set of experimental results. In this case the concepts of model distinguishability and parametric identificability are included as part of the analysis. [3]

EIS was applied intensively in this work since it provides a powerful alternative tool for exploring dynamical aspects and elucidating the magnitude of the molecular transport process occurring at macromolecular interfaces and polymer thin films.[4,5] However, as already indicated above, we are fully aware of the fact that a successful application requires some caution in order to describe a realistic scenario. Worth highlighting is also the fact that a good fit of the impedance response is insufficient to validate the proposed model. As discussed by Orazem and Tribollet,[6] impedance spectroscopy is not a standalone technique. In many cases, additional observations and measurements are needed to validate the suggested physical model. This question is particularly critical when circuit analogs are used to provide quantitative information about the physical processes taking

place at the solid-liquid interface in the presence of a polymer film. Consequently, the recommended approach for data analysis and interpretation involves instead developing a theoretical expression for the impedance in terms of microscopic variables and fitting the experimental results to this model. Within this framework, it intends to show how EIS opens up new opportunities to characterize the physical properties of polymer brushes as well as the dynamics of their responsive behavior.

## 3.2 DESCRIPTION OF THE MODEL

With this goal in mind, let’s start considering a schematic representation of an electrochemical working electrode/electrolyte interface and the reference electrode depicted in Figure 3.1. This diagram contains the basic elements necessary to define, from an experimental point of view, an EIS measurement.

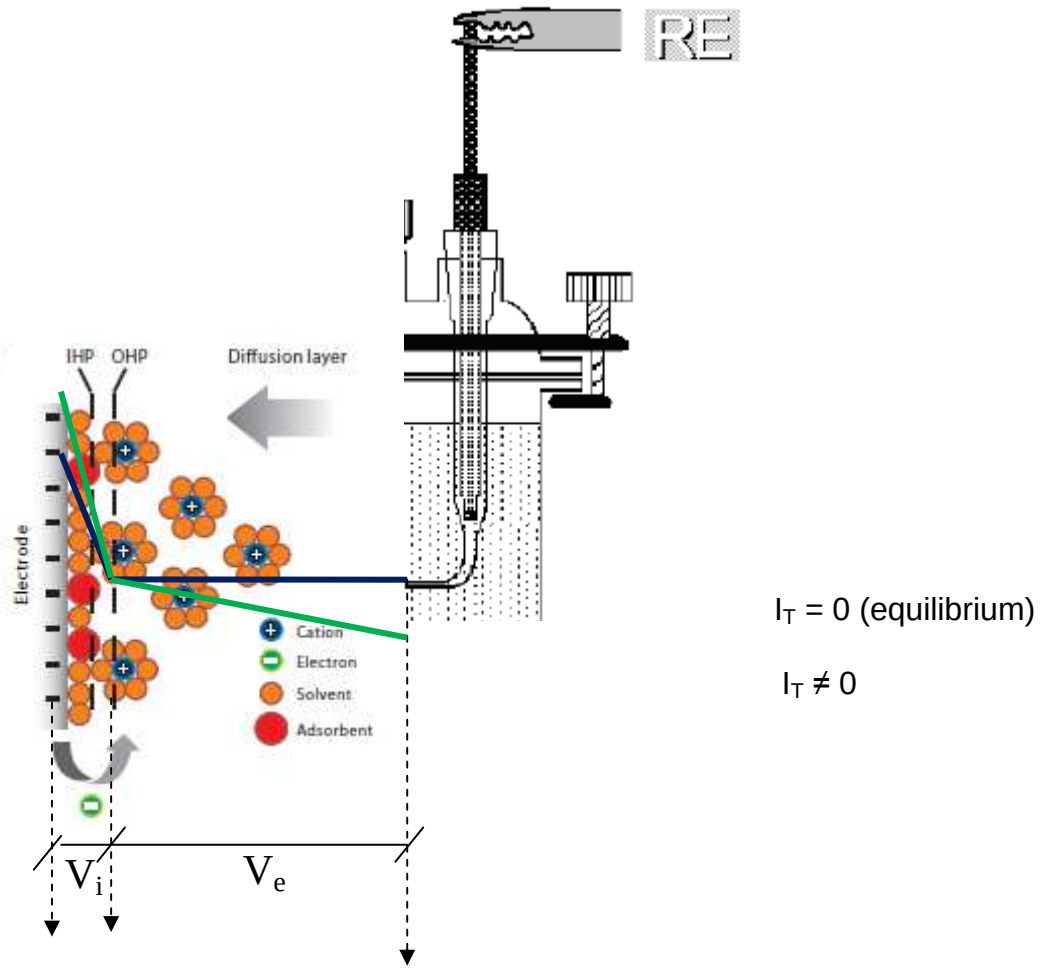


**Figure 3.1.** Electrochemical working electrode/electrolyte interface and the reference electrode

In Figure 3.1, $V_i$ represents the potential drop at the interface between the working electrode WE and the electrolyte, and $V_e$ represents the potential drop in the electrolyte solution that appears when an electric field is applied in a region with mobile charged species.

$V_T$ corresponds with the perturbed total potential drop between the working and reference electrodes.

$V_T = V_i$ ($I_T = 0$)

$V_T = V_i + V_e = V_i + R_\Omega I_T$

$I_T = I_{Cdl} + I_F$

where the total current $I_T$ accounts for two independent processes (currents), the charging current $I_{Cdl}$ of the interfacial capacitances through ionic charge accumulation in a space charge (here at the electrode surface on the electrolyte side, i.e. $C_{dl}$) and the faradaic reaction current (electron transfer through the interface according to Faraday's law characterized by a current $I_F$ ).

$$\frac{V_T}{I_T} = \frac{V_i}{I_T} + \frac{V_e}{I_T}$$

$$Z_T = Z_i + R_\Omega$$

In order to calculate the interfacial impedance $Z_i$, we must first consider the following relationships

$$\frac{I_T}{V_i} = \frac{I_{Cdl}}{V_i} + \frac{I_F}{V_i}$$

$$\frac{1}{Z_i} = j\omega\, C_{dl} + \frac{1}{Z_F}$$

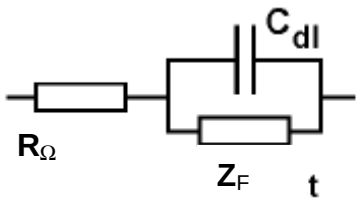


**Figure 3.2.** Basic equivalent circuit of an electrochemical interface

As shown in Figure 3.2, the Faradaic impedance $Z_F$ is in parallel connection with the impedance of the double-layer capacitor $C_{dl}$ and the interfacial impedance in series connection with the ohmic resistance of the electrolyte $R_\Omega$.

Consequently, gaining insight into the actual physicochemical processes governing the impedance response of the studied system, which in our case is a redox probe inside a grafted polymer brush, depends on finding the theoretical expression for $Z_F$. This will also affect the reliability of EIS to provide quantitative data about these processes. In this work, we put a particular emphasis on demonstrating the applicability of EIS to provide quantitative data about the relevant physical and chemical parameters of the system without requiring the use of an equivalent circuit as a first choice. In order to achieve an unambiguous description of the impedance response we attempted the derivation of a theoretical impedance transfer function for the polyelectrolyte brush that describes the experimental data and, more importantly, provides insightful information about the dynamics of the molecular transport inside the brush. The latter represents a key aspect of this work considering that molecular transport of probe molecules through macromolecular assemblies plays a major role in the rational design of time-released drug delivery systems or the time-dependent response of polymer-based sensor materials, just to name a few examples. In this context, this work aims at providing new tools and

methodologies to gain a better understanding of the diffusional phenomena taking place in boundary layers constituted of polymer brushes.

All measured experimental impedance spectra, that will be presented in the next chapters, exhibit a high-frequency capacitive contribution and for sufficiently low frequencies a distinctive contribution that suggests finite-length diffusion inside the polymer brush. Thus, the high-frequency contribution can be associated with the relaxation of the charge transfer process at the surface and the charging of the interfacial capacitor, while the second contribution at low frequencies can be related to ionic transport of the electroactive probe through the polyelectrolyte brush.

Assuming, as a first approximation, that partial coverage area ($\theta$) does not affect significantly linear conditions for the mass-transport step at a planar electrode, the effect of the partial coverage is simply to reduce the active area.

All impedances are inversely proportional to the active area; thus, if the capacity of the covered surface can be neglected with respect to the double-layer capacity of the active surface, all impedance values are inversely proportional to the fractional area of active surface ($1 - \theta$). Regarding the second time constant at low frequencies, it corresponds to a uniformly accessible electrode to mass transfer through a polyelectrolyte brush of finite thickness. The diffusion impedance response of the brush-containing electrode, when the resistance of the brush to diffusion is much larger than that of the bulk electrolyte, can be approximated by the diffusion impedance of the brush. Moreover, the thickness of the diffusion layer depends significantly on the time scale of a transient experiment, or equivalently on

the frequency scale of impedance experiments. If there is a finite length associated with the diffusion layer beyond which the electrode process can have no effect on concentrations, then there is a frequency range for sufficiently low frequencies where impedance response departs from a pure Warburg behavior. Noteworthy, for our experiments we set the lowest measurement frequency at a lower value than that used in comparable experiments from the literature.[7] Thus, it can be anticipated that the brush layer represents a diffusion-limiting barrier of finite thickness for electroactive molecular probes (Figure 3.3).

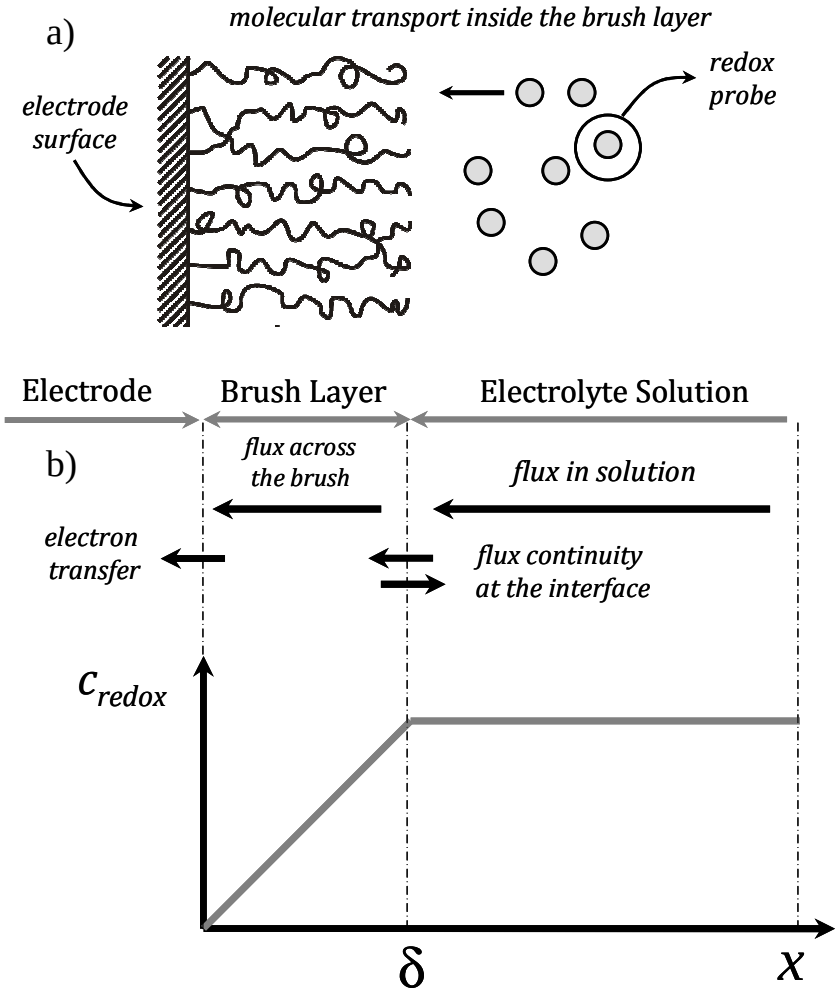

**Figure 3.3 (a)** Schematic illustration of a gold electrode modified with polymer brushes in the presence of redox probe molecules in solution. **(b)** Qualitative description of the steady-state concentration profile of redox species under finite-length diffusion conditions (only a concentration profile for the reactive species is considered).

## 3.3 MATHEMATICAL DEVELOPMENT OF THE MODEL

The electrochemical reaction can formally be written as

$$O + e^- \underset{k_a}{\overset{kc}{\rightleftharpoons}} R \qquad (3.1)$$

where O is an oxidised species like $[Fe(CN_6)]^{3-}$ and R represents the corresponding reduced form i.e. $[Fe(CN)_6]^{4-}$.

The potential (V) dependence of the rate constants can be expressed by an exponential law:

$$k_a = k_a^0 \exp[b_a(V - V_r)] \qquad (3.2)$$

$$k_c = k_c^0 \exp[b_c(V - V_r)] \qquad (3.3)$$

where $b_c = -\alpha_c F/RT$ and $b_a = \alpha_a F/RT$, $k^o$ is a constant independent of V, $\alpha$ is the transfer coefficient and $V_r$ the Nernst equilibrium potential.

Charge balance is given by:

$$I_f = -A_e F[k_c C_O(0) - k_a C_R(0)] \quad (3.4)$$

where $C_O(0)$ and $C_R(0)$ represent concentrations of the oxidized and reduced species at the surface and $A_e$ is the apparent electrode area. The negative sign arises from the assumed convention in which the cathodic current is negative.

When a small ac perturbation signal $\Delta V = \tilde{V}\exp(j\omega t)$ is applied, the current and concentrations oscillate around steady-state values: $I_f = I^{dc} + \Delta I$, $C = C^{dc} + \Delta C$ (for both O and R), where the superscript dc indicates a parameter that changes only slowly with time (i.e. either a steady-state term or one that does not change with the frequency of the perturbation $\omega$), and the symbol $\Delta$ indicates a parameter oscillating periodically with time t. The resulting oscillations with time may be written as: $\Delta I = \tilde{I}\exp(j\omega t)$ and $\Delta C = \tilde{C}\exp(j\omega t)$. $\tilde{V}$ and $\tilde{I}$ represent the phasors of potential and current. Taking $\tilde{V}$ as the reference signal and considering the phase shift $\phi$ between them results $\tilde{E} = E_o$ and $\tilde{I} = I_o \exp(j\phi)$, where $E_o$ and $I_o$ are the amplitudes of the applied potential and the resulting current waves, respectively.

For simplicity, we write a single generic expression for O and R mass balances according the second Fick's law, as:

$$\frac{dC}{dt} = -\nabla J = D\frac{\partial^2 C}{\partial x^2} \quad (3.5)$$

for the flux J along the x coordinate perpendicular to the electrode surface. D refers to the diffusion coefficient of the redox probe.

Or, equivalently,

$$\frac{d\Delta C}{dt} = D\frac{\partial^2 \Delta C}{\partial x^2} \tag{3.6}$$

which in the Fourier domain can be expressed as

$$j\omega\,\Delta C(x,\omega) = D\,\frac{d^2\Delta C(x,\omega)}{dx^2} \tag{3.7}$$

with $j = \sqrt{-1}$.

The general solution of the second-order differential equation (3.7) is

$$\Delta C(x,\omega) = P\exp(x\sqrt{\frac{j\omega}{D}}) + Q\exp(-x\sqrt{\frac{j\omega}{D}}) \tag{3.8}$$

subject, in this case, to the following boundary conditions corresponding to a finite-length diffusion in a system having a transmissive boundary,

$$x = 0 \qquad A_e F\Delta J = \Delta I_f \tag{3.9}$$

which expresses the flux continuity condition at the interface, and

$$x = \delta \qquad \Delta C = 0 \tag{3.10}$$

which indicates that transfer of electroactive species O and R is possible at $x = \delta$ (thickness of the diffusion layer), while for $x \geq \delta$, C remains unaltered and equal to $C^{dc}$.

Using equations 3.8 and 3.10 we can write,

$$\Delta C(0,\omega) = -2\,Q\,\exp(-\delta\sqrt{\frac{j\omega}{D}})\,\sinh(-\delta\sqrt{\frac{j\omega}{D}}) \qquad (3.11)$$

and calculate $\Delta J$ at the surface in the Fourier domain

$$\Delta J(0,\omega) = -D\frac{d\Delta C(x,\omega)}{dx}\bigg|_{x=0} = 2\,Q\,D\sqrt{\frac{j\omega}{D}}\,\exp\left(-\delta\sqrt{\frac{j\omega}{D}}\right)\cosh\left(-\delta\sqrt{\frac{j\omega}{D}}\right) \qquad (3.12)$$

Lets call $M(0,\omega)$ the mass transfer function, defined as [8,9]

$$M(0,\omega) = \frac{\Delta C(0,\omega)}{\Delta J(0,\omega)}$$

Considering the boundary condition at the surface (equation 3.9), results

$$M(0,\omega) = \frac{\Delta C(0,\omega)}{\Delta J(0,\omega)} = \frac{A_e F\,\Delta C(0,\omega)}{\Delta I_f} = \frac{1}{D\sqrt{\frac{j\omega}{D}}}\tanh\left(\delta\sqrt{\frac{j\omega}{D}}\right) \qquad (3.13)$$

In order to calculate the reaction impedance $Z_f$, equation 3.4 describing the rate of charge transfer should be linearized, according to Taylor series expansion retaining only terms with first-order derivatives, giving:

$$\frac{1}{Z_f} = \frac{\Delta I_f}{\Delta V} = \left(\frac{\partial I_f}{\partial V}\right)_{dc} + \left(\frac{\partial I_f}{\partial C_O(0)}\right)_{dc} \frac{\Delta C_O(0)}{\Delta I_f}\frac{\Delta I_f}{\Delta V} + \left(\frac{\partial I_f}{\partial C_R(0)}\right)_{dc} \frac{\Delta C_R(0)}{\Delta I_f}\frac{\Delta I_f}{\Delta V} \qquad (3.14)$$

Derivatives in equation (3.14) correspond to stationary conditions and may be obtained from equation (3.4).

$$\left(\frac{\partial I_f}{\partial V}\right)_{dc} = \frac{1}{R_{ct}} = A_e F\left[C_O^{dc}(0)\left(\frac{k_c \alpha_c F}{RT}\right) + C_R^{dc}(0)\left(\frac{k_a \alpha_a F}{RT}\right)\right] \qquad (3.15)$$

$$\left(\frac{\partial I_f}{\partial C_O(0)}\right)_{dc} = -A_e F k_c \qquad (3.16)$$

$$\left(\frac{\partial I_f}{\partial C_R(0)}\right)_{dc} = A_e F k_a \qquad (3.17)$$

and equation 3.14 becomes

$$\frac{1}{Z_f} = \frac{1}{R_{ct}} + \left(\frac{\partial I_f}{\partial C_O(0)}\right)_{dc} \frac{M_O(0)}{A_e F}\frac{1}{Z_f} + \left(\frac{\partial I_f}{\partial C_R(0)}\right)_{dc} \frac{M_R(0)}{A_e F}\frac{1}{Z_f} \qquad (3.18)$$

For simplicity we assume $D_O = D_R = D$, and so $M_O(0) = M_R(0) = M(0)$ that can be calculated according to equation 3.13.

Consequently, the reaction impedance can be identified as

$$Z_f = R_{ct} + R_{ct}\frac{(k_c - k_a)}{D\sqrt{\frac{j\omega}{D}}}\tanh\left(\delta\sqrt{\frac{j\omega}{D}}\right) \qquad (3.19)$$

which, after rearranging reduces to

$$Z_f = R_{ct} + \frac{\sigma}{\sqrt{\omega}}\tanh\left(B\sqrt{j\omega}\right)(1-j) \qquad (3.20)$$

where the so-called mass transfer coefficient $\sigma$ contains the contributions of the forms O and R and $B = \delta/\sqrt{D}$.

Finally, the electrode impedance consists of the electrolyte resistance $R_s$ connected in series with a parallel connection of the double layer capacitance $C_{dl}$ and the reaction impedance $Z_f$.

Some of the parameters that can be estimated through fitting of the experimental impedance spectra to the theoretical mathematical model are listed in Table 3.1. (the brush thickness ($\delta$) was independently measured using the protocols described related to other experimental techniques).

**Table 3.1.** List of some of the fit parameters: $R_\Omega$, $C_{dl}$ and those from the reaction impedance $Z_f$ according to Equation (3.20)

| $R_\Omega$ ($\Omega$) | $C_{dl}$ ($\mu$F) | $R_{ct}$ ($\Omega$) | B ($s^{1/2}$) | D ($cm^2s^{-1}$) |
|---|---|---|---|---|
| | | | | |

Data analysis was performed according to the transfer function derivation above described and identification procedures, while avoiding the use of ambiguous equivalent circuit models. Moreover, this analysis provides a plausible explanation for the distinct features of the experimental impedance data recorded under different working conditions.

A most relevant parameter obtained from the fitting procedure is the diffusion coefficient, D, that provides insightful information about the molecular transport of probe species within the macromolecular environment provided by the polymer brush.

However, full capabilities of the electrochemical approach were obtained, as usual, with complementary results from other measuring techniques.

As a consequence, this work clearly shows that EIS can be used as a valuable tool to study the effect of different experimental variables, e.g: solvent, ionic strength or temperature, on the diffusion of probe species inside a brush layer.

## 3.4 REFERENCES

(1). Choi, E.-Y.; Azzaroni, O.; Cheng, N.; Zhou, F.; Kelby, T.; Huck, W.T.S. *Langmuir* **2007**, *23* ,10389-10394.

(2). Moya, S.E.; Azzaroni, O.; Kelby, T.: Donath, E.; Huck. W.T.S. *J. Phys. Chem. B,* **2007**, *111*, 7043-7040.

(3). P. E. Alvarez, C. A. Gervasi, A. E. Vallejo, *J. Biol. Phys.*, **2007**, *33* (5-6) 421-431.

(4). *"Diffusion in Polymers"* edited by Crank, J.; Park, G.S. (Academic Press, London, **1968**).

(5). Bridges, T.E.; Uibel, R.H.; Harris, J.M. *Anal. Chem.* **2006**, *78*, 2121-2129.

(6). M.E. Orazem, B. Tribollet, in *"Electrochemical Impedance Spectroscopy",* Ch. 23., John Wiley & Sons, New Jersey, **2008**

(7). Zhou, F.; Hu, H.; Osborne, V.L.; Huck, W.T.S.; Liu, W. *Anal. Chem.* **2007**, *79*, 176-182

(8). Jacobson, T.; West, K. *Electrochim. Acta* **1995**, *40*, 255-262.

(9). Castro, E.B.; Milocco, R.H. *J. Electroanal. Chem.* **2005**, *579/1*, 113-123

# Chapter 4

## MOLECULAR TRANSPORT IN THIN THERMO-RESPONSIVE POLY (N-ISOPROPYLACRYLAMIDE) BRUSHES WITH VARYING GRAFTING DENSITY

## ABSTRACT

The effect of the grafting density on the molecular transport through thermo-responsive brushes of poly(N-isopropylacrylamide) (PNIPAM) grafted onto flat gold substrates was investigated using voltammetry and impedance spectroscopy. PNIPAM brush layers were synthesized at four different grafting densities using surface-initiated atom transfer radical polymerization (SI-ATRP) from mixed self-assembled monolayers of ω-mercaptoundecyl bromoisobutyrate and undecanethiol chemisorbed on gold surfaces. Tethered PNIPAM layers with grafting densities resulting from initiator concentrations lower than 25 % in the thiol monolayer show the same transport properties as the initial self assembled monolayer before brush synthesis. For higher grafting densities, the diffusion coefficients, D, of the $K_3[Fe(CN)_6]/K_4[Fe(CN)_6]$ redox probe is seven orders of magnitude smaller than those typically measured in aqueous solutions and independent of whether the brush is collapsed or swollen. Collapse of the PNIPAM brush drives a hydrophilic/hydrophobic transition in addition to structural/conformational transformations of the grafted layers resulting in still smaller values of D. However, these changes do not lead to a blocking effect on the active area of the gold surface which is only determined by pinholes or discontinuities in the thiol initiator monolayer. These results are only observed for thin PNIPAM brush layers.


## 4.1. INTRODUCTION

Poly(N-isopropylacrylamide) (PNIPAM) is the most studied among the thermo-responsive polymers used to obtain brushes that exhibit measurable changes in

their thickness with temperature.[1] PNIPAM exhibits phase-transition in aqueous environments in a narrow temperature range around 32 °C. Above this temperature, called lower critical solution temperature (LCST), the hydrogen bonding between amide groups of PNIPAM and water molecules is broken, and replaced by intramolecular hydrogen bonds between amide groups. As a consequence, the polymer becomes more hydrophobic, excluding water. PNIPAM precipitates in solution above the LCST. In a brush PNIPAM collapses reducing thickness besides losing water. These phenomena are reversible. Reducing the temperature below the LCST, the polymer dissolves in water again and the brush recovers its original thickness.

The actual value of the LCST varies slightly depending on solution conditions, i.e ionic strength, pH or the configuration of the polymeric system (free, self assembled or grafted).[2] In addition, for PNIPAM brushes the value of the LCST depends on the grafting density and molecular weight of the polymer.[3,4]

The temperature responsive character of PNIPAM has attracted a lot of attention for the fabrication of “smart” surface modifiers acting like molecular actuators.[5-8]

A clear potential application of PNIPAM brushes is as thermoresponsive barriers. The collapse of PNIPAM above the LCST could generate a hydrophobic layer that restricts transport of water soluble molecules. Also, the change in thickness of the PNIPAM brush after collapse could increase the volume flow through a pore coated with this polymer as shown by Yameen et al.[9] In this article swollen PNIPAM brushes below the LCST dramatically decrease ionic transport through nanopores with reduced effective cross section.

Even though a great deal of effort has been devoted to characterize the thermo-responsive structural change of PNIPAM brushes considerably less effort has been put in the characterization of molecular transport through the brush. Among the scarce work dealing with this subject, it is worth mentioning that by Reuber et al.[10] where the ionic permeability is studied using cyclic voltammetry on electrodes covered with thick PNIPAM brushes synthesized via electrochemically induced free-radical polymerization. A diffusion coefficient of $10^{-11}$ $cm^2$ $s^{-1}$ was calculated for the diffusion of ferricyanide ions across a film of about 100 nm thick.

There is indeed a lack of knowledge of how the architecture of the brush, i.e. chain density, chain length, can affect the transport through PNIPAM brushes below and above the LCST. Understanding the transport properties of brushes in relation to their nanoscale organization is extremely important for the design of surfaces and devices with tailored properties as barriers or protecting coatings. Moreover, in the case of PNIPAM it is not clear how the thermally induced collapse transition affects both molecular transport through the brush and its blocking character of the modified surface, respectively.

To address these issues we have synthesized thin PNIPAM brushes with varying grafting densities and studied ionic transport through their electrochemical response in presence of a $K_3[Fe(CN)_6]/K_4[Fe(CN)_6]$ redox probe by means of voltammetry and impedance spectroscopy. We aim at measuring the diffusion coefficient of the probe at temperatures below and above the LCST. From the changes in the diffusion coefficient with grafting density and temperature we intend to evaluate the

role on transport of the initiator monolayer and the nanoscale arrangement of the polymer chains in the brush after the collapse.

## 4.2. EXPERIMENTAL

### 4.2.1 Chemicals

N-isopropylacrylamide (NIPAM), 2,2´bipyridine (bpy), cooper chloride(I), N,N´-dimethyl formamide (98%) and blank thiol (1-undecanethiol) were purchased from Sigma-Aldrich (Spain) and used without further purification. Ethanol was purchased form Scharlau S.A. Water purification was performed with a Nanopure purification system. ω-Mercaptoundecyl bromoisobutyrate, the thiol initiator, was synthesized as described elsewhere.[11]

### 4.2.2 Sample preparation

Au substrates were prepared by sputtering deposition, cleaned by sonication, followed by water rinsing while the final cleaning step comprised exposure to UV radiation in a Bioforce Nanosciences chamber for 30 minutes just before modification step. Modification of Au surfaces was carried out by immersion in 10 mM thiol solutions in ethanol for 16 hours in order allow the spontaneous formation of the initial assembled monolayer (SAM). In other to obtain brushes with four different grafting densities, four different thiol solutions were prepared mixing initiator and inhibitor thiols with the following content of the initiator: 100%; 50%; 25% and 5%.

Polymer brushes were grown from the different mixed self-assembled monolayers constituted of ω-mercaptoundecyl bromoisobutyrate (thiol initiator) and 1-

undecanethiol (blank thiol) chemisorbed on gold, which ultimately defines the grafting density of the polymer chains. Polymer synthesis was accomplished by surface-initiated aqueous atom transfer radical polymerization (SI-ATRP).[12,13]

Polymer brushes were prepared as follows: thiol functionalized surfaces were immersed in a mix of CuCl/ Bipyridine/ monomer in a ratio of 1:2:10 in DMF/water (3:2) as solvent, at 40 ºC in an inert atmosphere of $N_2$.The polymerization was left to proceed for 5 hours. At the end the subtrates were rinsed with water, acetone, ethanol and water.

### 4.2.3 Experimental techniques

Ellipsometric thickness determinations were performed with a spectroscopic rotating compensator ellipsometer (M2000V, Woollam, NE, USA). Ellipsometric data, Δ and ψ, were acquired simultaneously, over a wavelength range from λ = 380 to 1000 nm, at an angle of incidence of 65° and with a time resolution of 5 s. The working temperature was 20 °C for dry film conditions, while thicknesses were also determined at 20° and 40°C in KCl 0.1M in a custom-built fluid cell (Q-Sense AB, Västra Frölunda, Sweden) with a total volume of ≈ 300 μL. Reported thickness values result from an average over five measurements at different spots on the PNIPAM brush surfaces.

Atomic force microscopy measurements were performed in a fluid cell of the AFM (Nanoscope III, Digital Instruments, Santa Barbara, CA). The samples were imaged in KCl solutions in contact mode using silicon nitride cantilevers of 100 mm length with integrated sharpened tips (spring constant 0.09 N=m, Olympus, Tokyo, Japan). In order to minimize drift, the whole set-up was allowed to equilibrate for 3–5 h, and

images were taken with relatively high scan frequencies (one image, of 512 lines, was taken in 8 or 16 s, at 20–30 Hz). Height, deflection, and friction were used as image contrast.

Electrochemical measurements were carried out at room temperature in a conventional three-electrode cell. A large area platinum sheet was used as the counter electrode, and a saturated calomel electrode (SCE) served as the reference electrode. All potentials in the text and figures are referred to the SCE. As working electrodes we used the modified Au substrates coated with the initial thiol monolayer, or PNIPAM brushes grown on top of the mixed reactive thiol monolayer. Solutions of 0.1 M KCl were used as supporting electrolytes and prepared from analytical grade (Merck) reagents and Milli-Q water. Before performing each measurement, the working electrode was thoroughly rinsed with Milli-Q water and immersed in the supporting electrolyte solution for 10 min. Experiments were performed under purified $N_2$ gas saturation at 20 ºC and 40º C in the presence of a 1 mM $K_3[Fe(CN)_6]/K_4[Fe(CN)_6]$ (1:1) mixture as a redox probe in the supporting electrolyte.

Cyclic voltammetry measurements were performed by scanning the potential in the window where oxidation and reduction of the redox couple takes place at a scan rate of 50 mV $s^{-1}$.

Impedance spectra were obtained with a Zahner IM6d electrochemical workstation on modified working electrodes with 0.50 $cm^2$ apparent area. The dc potential was held at the open circuit potential while a 10 mV amplitude AC voltage was applied.

The measuring frequency f used for EIS measurements ranged from 100 kHz to 1 mHz. Impedance data analysis was performed according to proper transfer function derivation and identification procedures, that involved complex nonlinear least-squares (CNLS) fitting based on the Marquardt-Levenberg algorithm.[14]

## 4.3. RESULTS AND DISCUSSION

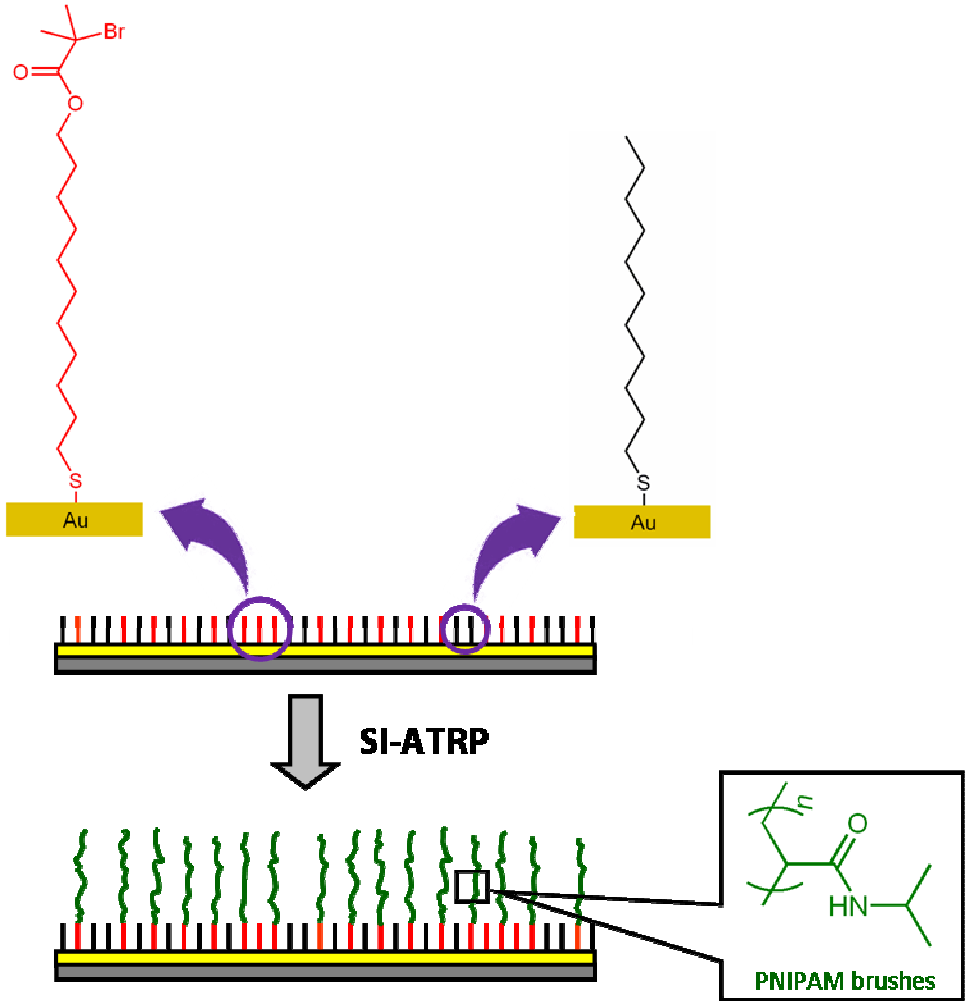


**Figure 4.1.** Schematic representation of a Au substrate modified with an initial SAM containing a mixture of initiator/inhibitor thiols (upper sketch) and the resulting surface after growth of a PNIPAM brush via ATRP (lower sketch).

The mixed initial SAM, graphically outlined in Figure 4.1, provides initiating sites for brush growth as well as a barrier of hydrophobic molecules between the electrode surface and hydrophilic electroactive species in the electrolyte.[15] Moreover, as is well known, most SAMs contain a certain density of defects or pinholes, at which electron transfer reactions between electroactive molecules and the electrode surface may take place with considerable less hindrance. If the pinhole density is large enough, currents due to electron tunneling through the blocking layer become negligible.[16] Furthermore, for impedance experiments recorded at the open circuit potential where a very low overpotential (essentially the amplitude of the AC voltage) is applied, tunneling currents are anticipated to have a minimal effect on the pinhole currents.[17] Under these conditions the electrochemically active area of the substrate corresponds to the fractional area determined solely by pinhole sites and other defects in the initial SAM. In the case studied here, the fractional area of pinholes may be affected by the collapse of the brush with the temperature, which could block the surface. The concept of fractional coverage is essential for the interpretation of voltammetric and impedance data obtained with SAM-coated electrodes.[18] Clearly, the best way to estimate the fractional coverage is to measure the charge-transfer resistance in the presence of the SAM/brush system and compare these values with those for an electrode that is unmodified.

We will first consider the voltammetric response of the SAM/Brush coated electrodes.

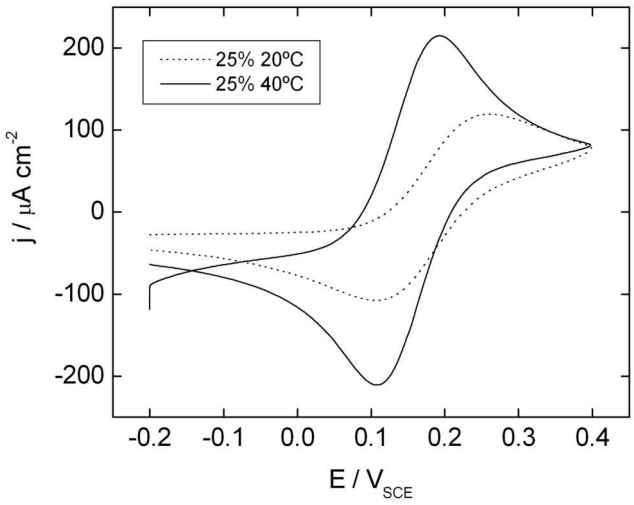


**Figure 4.2.** Cyclic voltammograms for a single electrode modified with a PNIPAM brush grown from an initial SAM containing 25 % thiol initiator. Voltammograms were recorded at a sweeping rate of 50 mV $s^{-1}$ and at two electrolyte temperatures (•••••) 20 ºC and (——) 40 ºC.

In Fig.4.2 we observe the effect of switching the electrolyte temperature T from a value below the LCST to a value above the LCST on the voltammetric response of an electrode modified with a PNIPAM brush grown from an initial SAM containing 25 % thiol initiator. The separation of peak potentials was 75 mV at 40 ºC. These data for a Au electrode are consistent with a quasi-reversible electron transfer model. When a bare gold electrode is modified with a SAM a noticeable decrease in the peak current is observed in the cyclic voltammogram as well as an increase in the splitting of the peak potentials and a tendency of the voltammogram to adopt a sigmoidal line shape. These observations are in agreement with those obtained for ultramicroelectrodes and indicate that the electron transfer reaction might be occurring at pinhole sites.[19] Higher peak current densities and a smaller peak separation were obtained as the measuring temperature is increased. This

response can be interpreted in terms of faster electrochemical kinetics exhibited by the couple for higher temperature values.

At this point it is probably worth mentioning briefly that for quasi-reversible electrode reactions[20]: i) a decrease in the diffusion coefficient D reduces the shift in the peak potentials $E_p$ away from the formal potential of the electrode; ii) the same effect is also obtained with an increase in T. However, in this system an increase in T leading to a collapsed brush is expected to reduce D and hence it is not possible from the voltammetric results to uncouple both effects. Consequently, the observed changes of the voltammetric responses shown in Figure 4.2 can not be solely ascribed to a marked reduction of D related to a collapsed brush but also to considerably more facile kinetics of the heterogeneous electron transfer reactions after increasing T.

In Figure 4.3 we observe the voltammetric responses of the electrodes coated with PNIPAM synthetized from a SAM with 50% thiol initiator and recorded at 20 ºC and 40 ºC. Current densities j in both Figures 4.2 and 4.3 were calculated relative to the apparent electrode area, what precludes a direct comparison of absolute j values between these two Figures, unless the real active areas are known. Figure 4.3 shows a similar behavior as Figure 4.2.

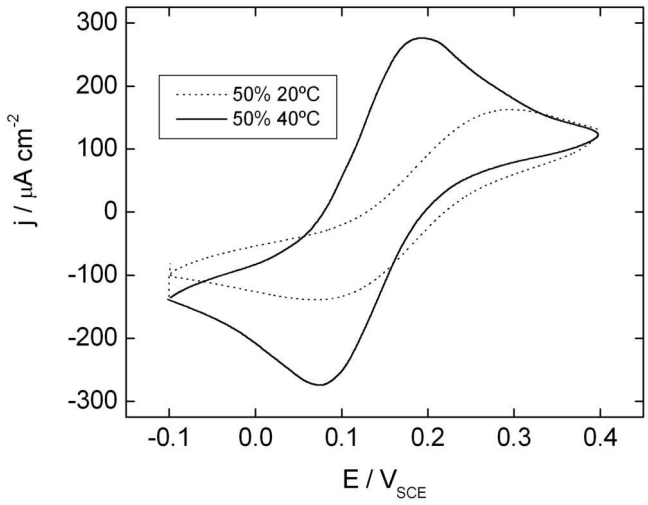


**Figure 4.3.** Cyclic voltammograms for a single electrode modified with a PNIPAM brush grown from an initial SAM containing 50% thiol initiator. Voltammograms were recorded at a sweeping rate of 50 mV $s^{-1}$ and at two electrolyte temperatures (•••••) 20 ºC and (——) 40 ºC.

These results differ strongly from those obtained for thick PNIPAM brushes where the redox probe exhibits a quasi-reversible wave at 25 °C i.e. for the swollen, extended conformation of the polymer brush, while the redox voltammetric response becomes almost undetectable after raising the temperature to 45 °C. In this case results are explained in terms of a brush in a collapsed state hindering charge transfer between the redox probe and electrode surface.[21] On the other hand, Reuber et al.[10] claim that the voltammetric response of ferricyanide ions on electrodes covered with a thick PNIPAM hydrogel arises from the hindered diffusion of the electroactive ions between the bulk electrolyte and the collapsed film.

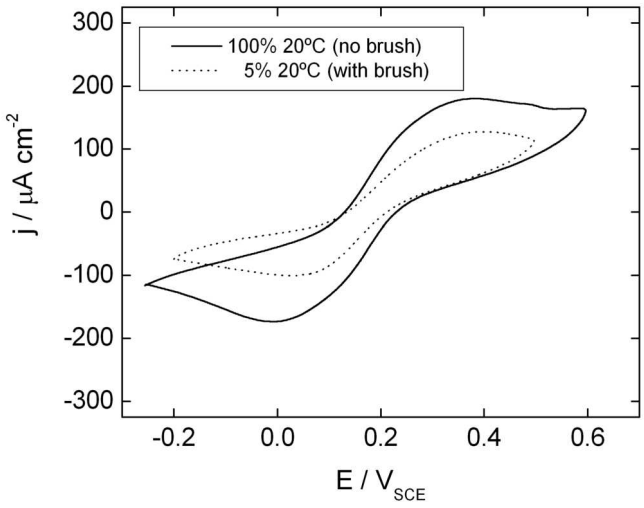


**Figure 4.4** Cyclic voltammograms for an electrode modified with an initial SAM containing 100% thiol initiator (——) and for a second electrode modified with an initial SAM containing 5% thiol initiator from which the PNIPAM brush was grown (•••••). Voltammograms were recorded at a sweeping rate of 50 mV $s^{-1}$ and at 20 ºC.

Figure 4.4 shows voltammetric responses for an electrode modified with an initial SAM containing 100 % thiol initiator and for a second electrode modified with an initial SAM containing 5 % thiol initiator from which the PNIPAM brush was grown. Since the resulting real active area after covering the electrode with the initial SAM varies from sample to sample no comparison can be made between the absolute values for the peak current densities in Figure 4.4 that were calculated relative to the electrode's geometric area. In both cyclic voltammograms an increase in the splitting of the peak potentials relative to the expected value for a bare Au electrode can be clearly observed, as well as a tendency of the voltammograms to adopt a sigmoidal shape that is in agreement with the results also measured at 20 ºC and discussed above. Moreover, the separation of peak potentials is practically the same for both electrodes. This behavior can be interpreted as resulting from the

presence of the initial SAM alone independent of the presence of the brush. Such a brush grown with low grafting density proves unable to affect the diffusion coefficient in the system. It is worth emphasizing here that D at the electrode without a grown brush corresponds to the ionic species in solution and consequently, it is much larger than that expected for diffusion through the polymer film. Based on theoretical postulates and numerical simulations it has been claimed that brushes of low grafting density may display a lateral “phase separation”, with grafted chains forming isolated clusters with free space among them.[2] In order to either confirm or rule out a possible phase separation effect in the initial SAMs formulated with two different thiols AFM images were obtained of the initiating layers by a phase-sensitive technique such as AFM in lateral force mode. Results for a SAM obtained with 5% thiol initiatior and a SAM with a 100% inert thiol are shown in Figure 4.S1 from the Supporting Information. Comparison of AFM topography reveals the same overall morphology for both samples and the absence of phase-separated nanometer scale domains in the mixed SAM.

For an initial mixed SAM without phase-segregated domains inhomogeneous coverage by the brush chains along the SAM surface would result in semi-infinite diffusion conditions for the redox probe at the electrode. Thus, at low grafting density, i.e., if the distance between two neighboring polymer chains is greater than the radius of gyration of free polymer chains, two tethered chains feel no interaction and two conformations of polymers end-attached to a surface are possible, described as "mushroom-like" and "pancake-like". If polymer chains are well soluble in the solvent, they form a “mushroom” structure that might explain similar results presented in Figure 4.4 for both samples. Indeed, AFM topographic images of the

brush grown from an initial SAM containing 5% thiol initiator display randomly distributed patches of uncovered surface where the underlying substrate features can be clearly recognized (Figure 4.5). These brush-free spaces are absent in AFM images obtained from the brush grown from an initial SAM containing 100% thiol initiator (Figure 4.6).[22]

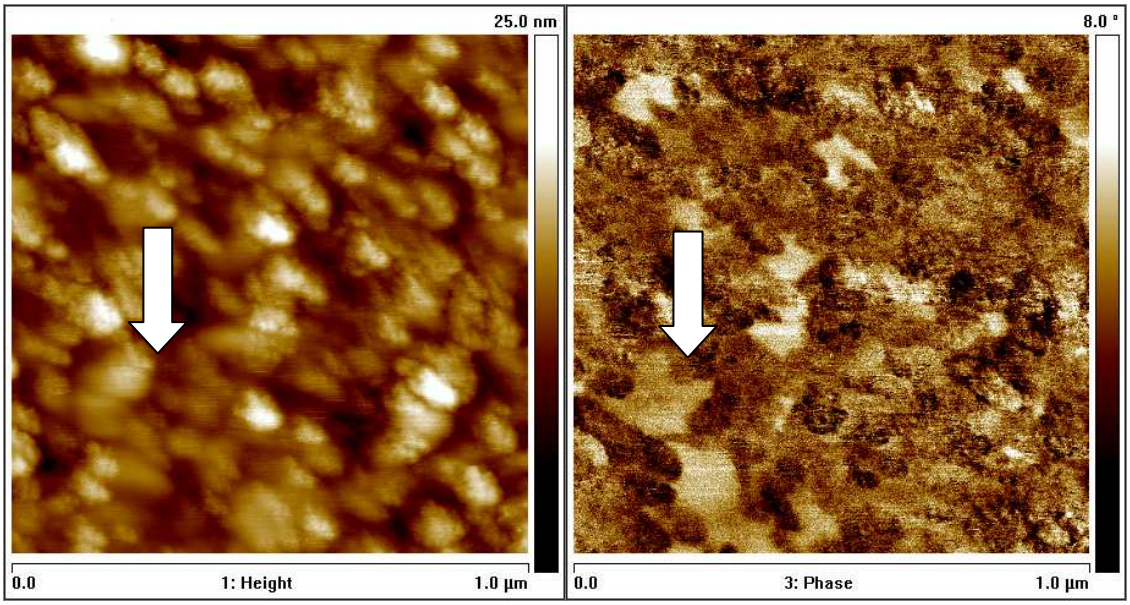


**Figure 4.5.** AFM topographic images of the brush grown from an initial SAM containing 5% thiol initiator, image contrast in terms of height and phase. Arrows indicate patches of substrate uncovered by the brush.

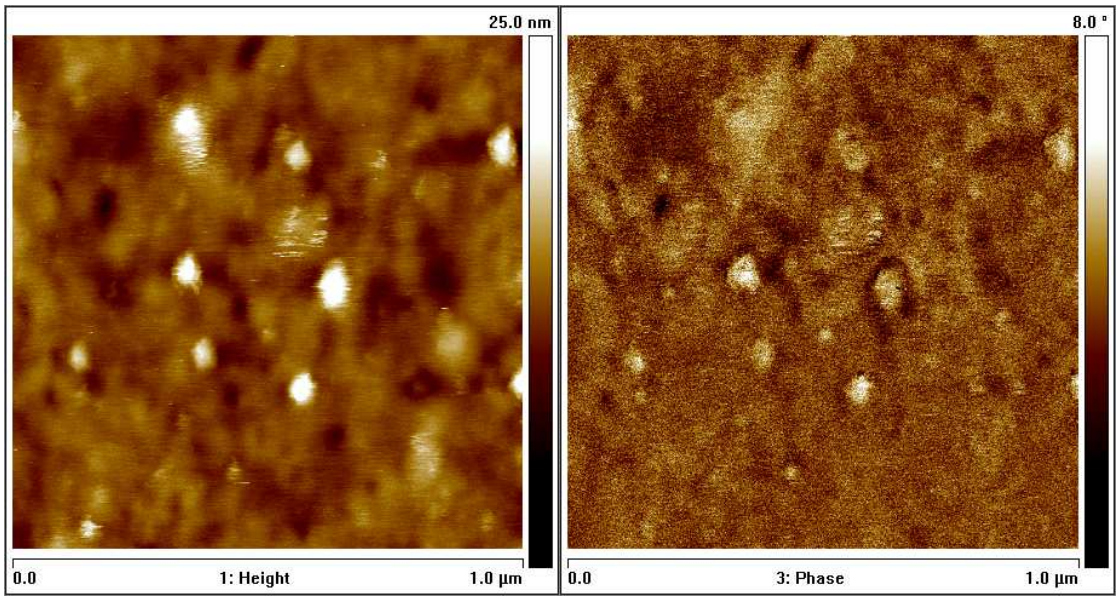


**Figure 4.6.** AFM topographic images of the brush grown from an initial SAM containing 100% thiol initiator, image contrast in terms of height and phase.

To gain a deeper insight into the transport through PNIPAM and the possible blocking effect of collapsed PNIPAM layers we performed impedance experiments. Figure 4.7 shows impedance spectra for an electrode modified with an initial SAM containing 100% thiol initiator without subsequent brush growth. Nyquist diagrams in Figure 4.7a exhibit a semicircle in the high frequencies f region followed by a straight line with slope approaching -45º at low frequencies. The semicircle is related to electron transfer-limited processes at the uncovered gold surface, whereas the straight line is compatible with semi-infinite linear diffusion or Warburg diffusion of the redox probe in the electrolyte. Hence, the electron transfer kinetics and the diffusional characteristics can be extracted from the EIS data. The semicircle diameter represents the charge transfer resistance $R_{ct}$ whereas the intercept of the semicircle with the real part of the impedance Re(Z)-axis for $f \rightarrow \infty$ corresponds to the solution resistance, $R_s$. Measured impedance data were corrected by the apparent electrode area. Data representation in terms of Bode

plots is also included in Figure 4.7b since they show the frequency response characteristic of the system over the entire measured frequency range, with points equally spaced in the frequency axis.

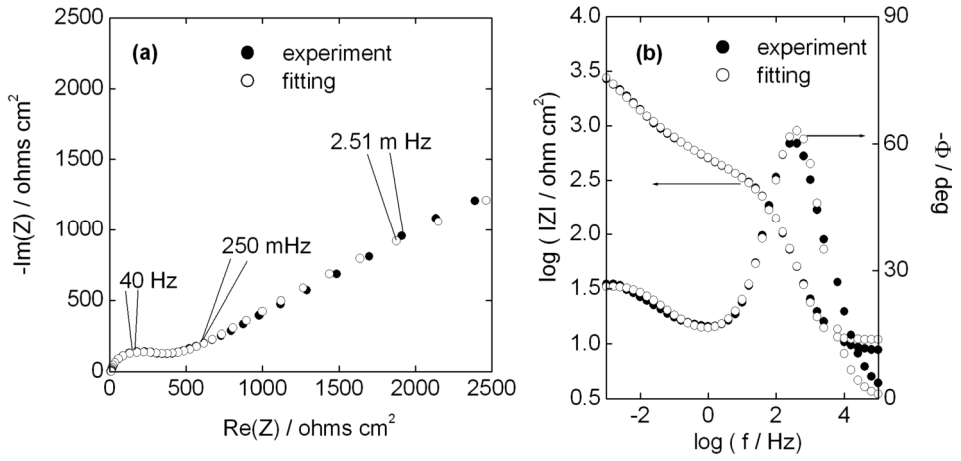


**Figure 4.7.** Impedance spectra for an electrode modified with an initial SAM containing 100% thiol initiator without subsequent brush growth. Measured and fitted data represented as Nyquist diagrams **(a)** and Bode plots **(b)**. Experimental data (●) and fit results (○) according to the equivalent circuit (Fig. 4.11a) and the reaction impedance $Z_f$ from Equation (4.7).

The same qualitative behavior was measured for an electrode modified with an initial SAM containing 5 % thiol initiator from which the PNIPAM brush was grown (Figure 4.8). A comparison between the dynamic behavior in the low frequency regions shown in Figures 4.7 and 4.8 indicate that for low grafting densities, resulting for example from an initiator concentration of 5 % in the initial self assembled monolayer, the polymer brush is incapable of affecting the transport properties in the system. This observation is in agreement with the corresponding information derived from voltammetric data.

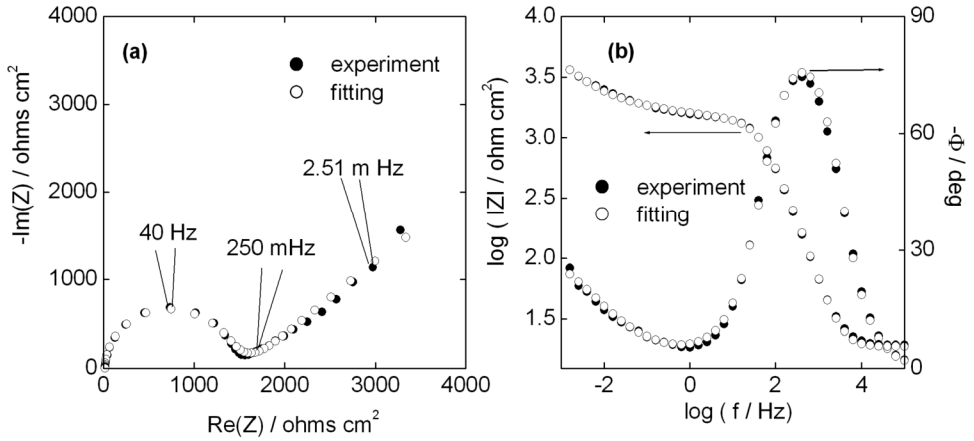


**Figure 4.8.** Impedance spectra for an electrode modified with an initial SAM containing 5% thiol initiator from which the PNIPAM brush was grown. Measured and fitted data represented as Nyquist diagrams **(a)** and Bode plots **(b)**. Experimental data (●) and fit results (○) according to the equivalent circuit (Fig. 4.11a) and the reaction impedance $Z_f$ from Equation (4.7).

Impedance spectra were measured at 20 ºC and 40 ºC for an electrode modified with an initial SAM containing 50 % thiol initiator from which the PNIPAM brush was grown. Experimental data and fitting results are presented in Figures 4.9 and 4.10, respectively.

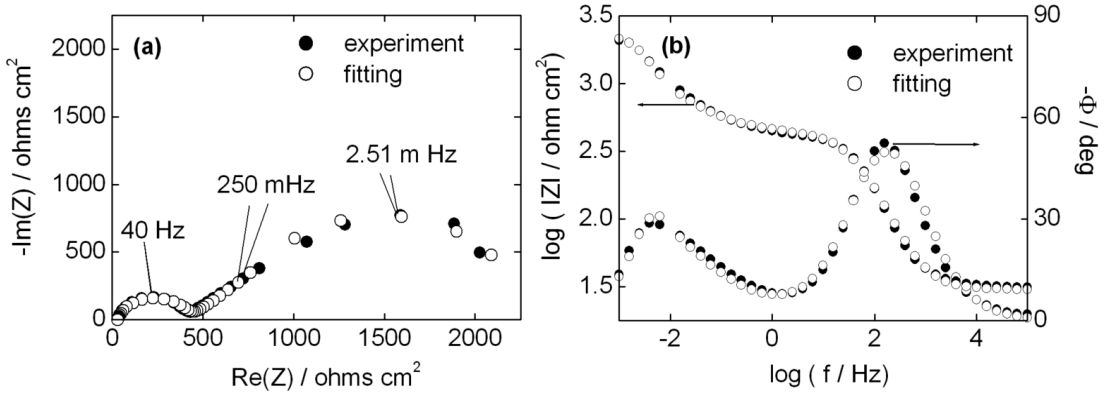

**Figure 4.9.** Impedance spectra recorded at 20 ºC for an electrode modified with an initial SAM containing 50 % thiol initiator from which the PNIPAM brush was grown. Experimental data (●) and fit results (○) according to the equivalent circuit (Fig. 4.9b) and the reaction impedance $Z_f$ from Equation (4.6).

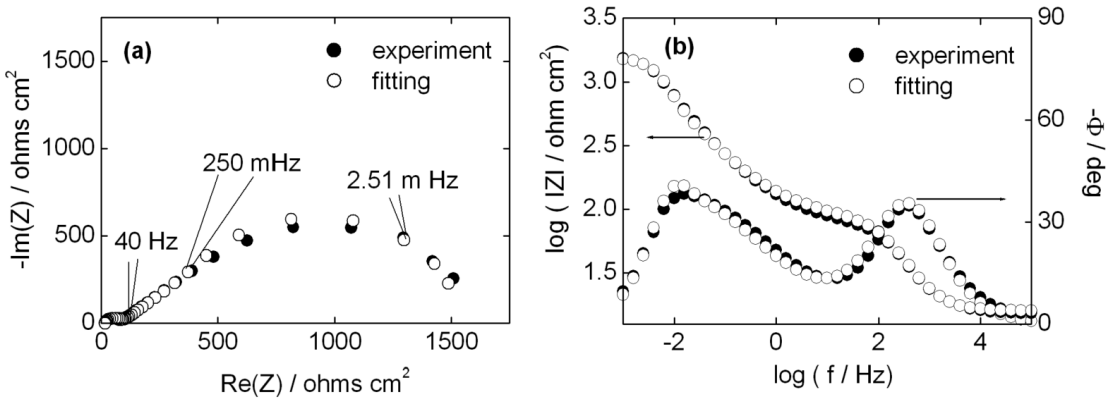


**Figure 4.10.** Impedance spectra recorded at 40ºC for an electrode modified with an initial SAM containing 50% thiol initiator from which the PNIPAM brush was grown. Experimental data (●) and fit results (○) according to the equivalent circuit (Fig. 4.9b) and the reaction impedance $Z_f$ from Equation (4.6).

Similarly to the impedance data discussed before the high frequency region of Nyquist spectra in Figures 4.9 and 4.10 is characterized by a semicircle related to the electron transfer reactions at the uncovered gold surface. However, the main difference with data in Figures 4.7 and 4.8 is associated with the low frequency region containing diffusion effects that are now compatible with finite-length diffusion-type impedances. It is only quite recently that it has become clear that this type of behavior can be observed for electrodes modified with PMETAC polymer brushes.[23] For this purpose, it has been shown that impedance spectra should be

recorded over as wide a range of frequency as possible before any attempt is made to interpret the data.[24]

The same qualitative behavior was observed for each electrode modified with an initial SAM containing a percentage of thiol initiator larger than 5 % and from which the PNIPAM brush was grown.

Since both sets of data (Figures 4.9 and 4.10) were obtained from the same electrode it is possible here to compare the absolute values of the measured impedance between the two experiments. Clearly, charge transfer resistance $R_{tc}$ becomes smaller as the temperature is raised from 20 ºC to 40 ºC but the resistive term of the diffusional impedance at low frequencies $R_d$ remains practically unaltered. Bearing in mind that each impedance value is inversely proportional to the electroactive area, we can conclude that by switching the temperature from 20 ºC to 40 ºC the active area of electrode is not affected but the charge transfer at the surface becomes faster. An additional indication that the charge transfer process becomes faster is given by a change in the frequency range for which the corresponding semicircle in the Nyquist plots is detected. For example, at 20 ºC the experimental point measured at 40 Hz barely exceeds the semicircle's maximum, while at 40 ºC the same point is measured when the high frequency semicircle has been completely measured (see Figures 4.9a and 4.10a).

Dynamic behavior related to diffusion effects can be preliminarily analyzed, on a qualitative basis, also by comparison of the spectra shown in Figures 4.9 and 4.10. Thus, the characteristic frequency value $f_{char}$ of the inflection point at which the

diffusional part of the impedance departures from the linear Warburg behavior and starts to describe a concave downward arch reaching the Re(Z)-axis, increases with an increase in the diffusion coefficient D and decreases as the diffusion path length δ augments. Assuming that δ is the thickness of the polymer brush, as explained below, it is expected that the thermally collapsed brush (40 ºC) be associated with a higher $f_{char}$ due to a thinner diffusion path or with a lower $f_{char}$ if the major effect is to reduce D. In this case $f_{char} \approx 15$ mHz for both experiments in Figures 4.9 and 4.10. Consequently, the expected decrease in δ values due to the polymer brush collapse must be compensated for by a decrease in D, thus leaving $f_{char}$ nearly invariant.

It has been shown in the previous qualitative discussion of impedance data that, the technique allows separating the individual effects of the thermally induced collapse transition on both the molecular transport through the brush and the blocking character of the modified surface, respectively. However, the points made require confirmation through a quantitative analysis of impedance data.

As previously pointed out, the impedance response of the system can be described in terms of a partially blocked electrode surface determined by the initial SAM. Then, the main influence of the polymer brush would be to slow down the mass transfer rate of the redox probe. A physical model of the interface of the modified electrode is suggested on the basis of the equivalent circuit for the impedance in Figure 4.11a, with $R_e$ the electrolyte resistance, $C_{dl}$ the double layer capacitance, $R_l$ the resistance of the ionic path within the brush, $C_l$ the capacitance of the intact SAM, and $Z_f$ the Faradaic impedance associated with the electrochemical reactions

of the redox probe at the fraction of area of the electrode that is not blocked, i.e. at the defect sites of the initial SAM.

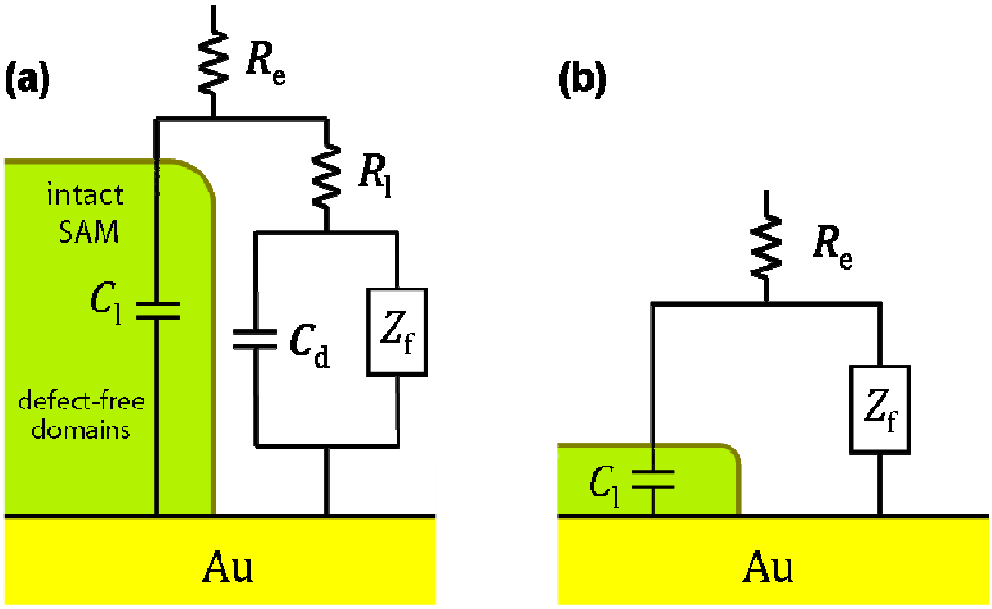


**Figure 4.11.** Schematic representation of an electrode modified with a SAM from which the PNIPAM brushes were grown. The SAM contains defects exposing the bare Au surface. The corresponding equivalent circuit is presented in its general form **(a)** and in a simplified form **(b)**.

The equivalent circuit in Figure 4.11b is a simplification of that in Figure 4.11a and corresponds to a condition prevailing in many of our experiments, where $R_l$ is negligible and $C_l$ is considerably larger than $C_{dl}$.

Theoretical derivation of the interfacial impedance $Z_f$ requires the following assumptions that are partially supported by the voltammetric analysis and the qualitative aspects of the experimental impedance, as presented above.

As a first approximation, partial coverage $\theta$ does not affect significantly linear conditions for the mass-transport step at a planar electrode; the effect of the partial coverage is simply to reduce the active area. All impedances, with the exception of the electrolyte resistance $R_e$ and the capacitive reactance related to $C_l$, are inversely proportional to the active area; thus, $Z_f$ is inversely proportional to the fractional area of active surface (1 - $\theta$). The brush layer represents a diffusion-limiting barrier of finite thickness $\delta$ for electroactive molecular probes. In this way the electrode is uniformly accessible to mass transfer through a hydrated brush of finite thickness. The diffusion impedance response of the brush-covered electrode, when the resistance of the brush to diffusion is much larger than that of the bulk electrolyte, can be approximated by the diffusion impedance of the brush alone.

The electrochemical reaction can formally be written as

$$O + e^- \underset{k_a}{\overset{kc}{\rightleftharpoons}} R \qquad (4.1)$$

where O is the oxidized species $[Fe(CN_6)]^{3-}$ and R represents the reduced species $[Fe(CN)_6]^{4-}$.

The potential (V) dependence of the rate constants can be expressed by an exponential law:

$$k_a = k_a^o \exp[b_a(V - V_r)] \qquad (4.2)$$

$$k_c = k_c^o \exp[b_c(V - V_r)] \qquad (4.3)$$

where $b_c = -\alpha_c F/RT$ and $b_a = \alpha_a F/RT$, $k^o$ is a constant independent of V, $\alpha$ is the transfer coefficient and $V_r$ the Nernst equilibrium potential.

Charge balance is given by:

$$I_f = -A_e F[k_c C_O(0) - k_a C_R(0)] \qquad (4.4)$$

where $C_O(0)$ and $C_R(0)$ represent concentrations of the oxidized and reduced species at the surface and $A_e$ is the active electrode area. The negative sign arises from the assumed convention in which the cathodic current is negative. For simplicity we assume $D_O = D_R = D$.

Consequently, the reaction impedance can be identified as

$$Z_f = R_{ct} + R_{ct}\frac{(k_c - k_a)}{D\sqrt{\frac{j\omega}{D}}}\tanh\left(\delta\sqrt{\frac{j\omega}{D}}\right) \qquad (4.5)$$

which, after rearranging reduces to

$$Z_f = R_{ct} + \frac{\sigma}{\sqrt{\omega}}\left[\tanh\left(B\sqrt{j\omega}\right)\right](1-j) \qquad (4.6)$$

where $j = \sqrt{-1}$, $\omega = 2\,\pi\,f$, is the angular frequency of the potential perturbation and the so-called mass transfer coefficient $\sigma$ contains the contributions of the forms O and R and $B = \delta/\sqrt{D}$.

However, when the polymer brush is absent or it has been grown with a very low grafting density e.g. 5% content of thiol initiator in the initial SAM, $\delta$ corresponds to the diffusion length in the electrolyte solution. More specifically, $\delta$ becomes infinitely large and the conditions correspond to those of semi-inifinite linear diffusion that is described by a Warburg impedance. Since tanh (x) tends asymptotically to the value 1 as x tends to infinity [25], equation (4.6) reduces to

$$Z_f = R_{ct} + \frac{\sigma}{\sqrt{\omega}}(1-j) \qquad (4.7)$$

Experimental impedance spectra in Figures 4.7 and 4.8 together with spectra recorded with the same electrodes but at 40º C, were fitted to a model comprising the equivalent circuit in Figure 4.11a and the expression for $Z_f$ from equation (4.7).

Fit results are also included in Figures 4.7 and 4.8 together with the corresponding experimental data. A very good agreement between theory and experiment can be observed. Best-fitting parameters are assembled in Table 4.1.

**Table 4.1.** Best-fitting parameters obtained for the experimental spectra shown in Figs. 4.7 and 4.8 and spectra recorded with the same electrodes but at 40º C. Data fitted to the theoretical impedance resulting from the equivalent circuit (Fig. 4.11a) and the reaction impedance $Z_f$ according to Equation (4.7).

| %init / T (ºC) | $R_e$ ($\Omega cm^2$) | $C_l$ ($Fcm^{-2}$) | $R_l$ ($\Omega cm^2$) | $C_{dl}$ ($Fcm^{-2}$) | $R_{ct}$ ($\Omega cm^2$) | $\sigma$ ($\Omega cm^2 s^{-1/2}$) |
|---|---|---|---|---|---|---|
| 5 / 20 | 18.88 | $1.18 \times 10^{-4}$ | <0.1 | $2.4 \times 10^{-6}$ | 1620 | 0.0033 |
| 5 / 40 | 13.53 | $5.68 \times 10^{-5}$ | <0.1 | $2.2 \times 10^{-6}$ | 595 | 0.0052 |
| 100 % no brush / 20 | 11 | $8.2 \times 10^{-4}$ | <0.1 | $7.6 \times 10^{-6}$ | 1118 | 0.00154 |
| 100 % no brush / 40 | 12.14 | $6.7 \times 10^{-4}$ | <0.1 | $8.7 \times 10^{-6}$ | 491 | 0.00524 |

During the fitting process all parameters were allowed to vary freely until they reached their optimized values. As indicated in the qualitative analysis $R_{ct}$ values are smaller at 40 ºC, i.e. in conditions of thermally induced collapse of PNIPAM brushes. Moreover, the ratio of $R_{ct}$ values measured at 20° C and 40° C is nearly the same for the electrode covered only with the initial SAM (100% initiator) and the electrode covered by the initial SAM (5 % initiator) from which a brush was grown with very low grafting density. The same is true for the ratio of the Warburg

coefficients. These facts confirm that the effect of changing T is restricted to the electrochemical kinetics and that the polymer brush grafted from a SAM with very low initiator concentration (5% in the initial SAM) does not set up a diffusion barrier for the redox probe.

A charge transfer resistance $R_{ct}^{\text{bare Au}} = 24.43\ \Omega cm^{-2}$ for a Au(111) surface in 0.01 M $HClO_4$ at 25 ºC was measured by Janek and Fawcett [18] which we use to make a rough estimation of the apparent fractional electrode coverage θ in our experiments. Thus, we can write

$$\theta = \left(1 - \frac{R_{ct}^{\text{bare Au}}}{R_{ct}^{\text{initial SAM}}}\right) \qquad (4.8)$$

Where $R_{ct}^{\text{initial SAM}}$ corresponds to the charge transfer resistance measured at 20 ºC for the electrodes modified with: i) an initial SAM containing 5 % thiol initiator from which the PNIPAM brushes were grown and ii) an initial SAM containing 100 % thiol initiator without subsequent brush growth. These values are shown in Table 4.1. In spite of some differences with the experiments in the work from the literature taken as reference, like e.g. electrolyte T and composition, θ results 0.988 and 0.978, respectively, which are in good agreement with those calculated for the following comparable electrodes: Au(111) modified with decanethiol (DT) and Au(111) modified with ω-hydroxydecanethiol (HDT).[18] This fact, in turn, can be taken as a validation of the theoretical model used in this work.

Experimental impedance spectra in Figures 4.9 and 4.10 together with spectra recorded with the electrodes where the brushes were grown from an initial SAM containing 25 % and 100 % thiol initiator at 20 ºC and 40º C (impedance data not

shown), were fitted to a model comprising the equivalent circuit depicted in Figure 4.11b and the expression for $Z_f$ from equation (4.6). Fit results are also included in Figures 4.9 and 4.10 together with the corresponding experimental data. A very good agreement between theory and experiment can be observed. Best-fitting parameters are assembled in Table 4.2.

**Table 4.2.** Best-fitting parameters obtained from the fitting of the experimental spectra shown in Figs. 4.9 and 4.10 and spectra recorded with the electrodes where brushes were grown from initial SAMs containing 25 % and 100 % thiol initiator at 20 ºC and 40º C. Impedance data were fitted to the theoretical impedance derived from the equivalent circuit (Fig. 4.11b) and the reaction impedance $Z_f$ according to Equation (4.6). Measured values for the brush wet thickness $\delta$ and calculated values for the diffusion coefficient D of the redox probe.

| %init / T (ºC) | $R_e$ ($\Omega cm^2$) | $C_l$ ($Fcm^{-2}$) | $R_{ct}$ ($\Omega cm^2$) | B ($s^{1/2}$) | Wet $\delta$ (nm) | D x $10^{13}$ ($cm^2s^{-1}$) |
|---|---|---|---|---|---|---|
| 100 / 20 | 42 | 6.26 x $10^{-6}$ | 7650 | 5.62 | 38 ± 5.1 | 4.6 ± 0.6 |
| 100 / 40 | 27.57 | 1.51 x $10^{-5}$ | 286 | 6.72 | 21 ± 2.5 | 0.98 ± 0.1 |
| 50 / 20 | 30.14 | 2.19 x $10^{-5}$ | 392 | 11.83 | 40 ± 2.1 | 1.1 ± 0.06 |
| 50 / 40 | 16 | 4.4 x $10^{-5}$ | 71.05 | 8.8 | 17 ± 1.0 | 0.4 ± 0.02 |
| 25 / 20 | 26.6 | 2.05 x $10^{-5}$ | 498 | 6.64 | 39 ± 0.9 | 3.5 ± 0.08 |
| 25 / 40 | 26.58 | 2.77 x $10^{-5}$ | 66 | 6.52 | 19 ± 0.4 | 0.9 ± 0.02 |

As before $R_{ct}$ values are smaller at 40 ºC, i.e. under conditions of thermally induced collapse of PNIPAM brushes and in agreement with an activated process.

Consequently, for all studied grafting densities of thin grafted PNIPAM brushes, increasing T above LCST results in faster electrochemical kinetics without detectable changes in the electrodes' surface coverage.

Using fit parameter B in table 4.2 we can derive the diffusion coefficient D of the electroactive molecule, independent of the actual value for the active area of the electrode or the need to derive $A_e$ from a different source, when it is different from the electrode's geometric area, like in the present system. Independent calculations of D cannot be made from voltammetric results or results obtained with another electroanalytical technique, because $A_e$ and D are always part of the same fitting parameter in the corresponding theoretical equations. Generally speaking, electrochemical techniques are best suited for studying mass transport processes through thin polymer films. However, for the present study, the possibility of obtaining a parameter like B that is independent of $A_e$, represents a considerable advantage of impedance spectroscopy over other electrochemical techniques.

In order to estimate D we need to consider the brush thickness $\delta$ under the different working conditions.

Thicknesses of polymer brushes as measured in the dry state with ellipsometry are shown in Figure 4.12.

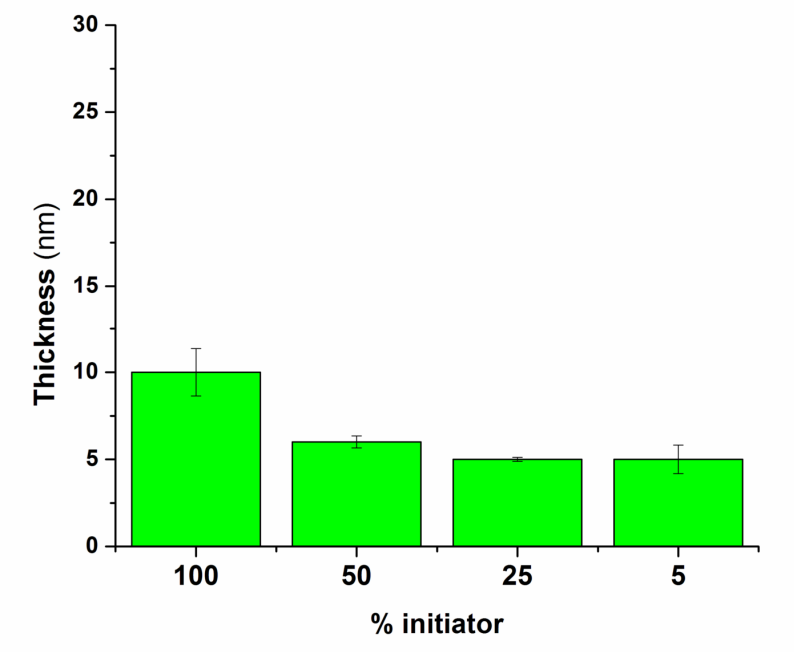


**Figure 4.12.** Ellipsometric thicknesses of PNIPAM brushes grown from thiol monolayers with different percentages of initiator as measured in the dry state.

The following swelling factors according to the grafting density, whether high (HD), medium (MD) or low (LD), were obtained after measuring wet thickness values at 20 ºC: 3.8 (HD for 100% initiator), 6.7 (MD for 50% initiator) and 7.8 (LD for 25% initiator). These factors are in good agreement with comparable literature data. [26] Finally, the following relationship [27] was confirmed to be valid for the change in thickness of PNIPAM brushes due to the thermally-induced collapse

$$\delta_{wet}^{20^oC} = 2\,\delta_{wet}^{40^oC} \qquad (4.9)$$

The measured values of $\delta_{wet}$ and the calculated values for D are assembled in Table 4.2. It can be clearly observed that D values for the redox molecule in the brush are much smaller than the corresponding value in an aqueous electrolyte and similar to those obtained in thick surface-attached PNIPAM gel layers[10] or in comparable grafted PMETAC brushes.[23,24] Finally, comparing D values measured

below LCST and above that temperature, at each grafting density, an additional hindrance to diffusion associated with the brush collapse can be observed. For all studied grafting densities D results *ca* 4 times smaller above LCST which is compatible with a decrease in wet δ of 2 times to leave $f_{char}$ practically invariant, as indicated above. Accordingly, derived values of D match exactly the proportionality existing between $f_{char}$ and $B^{-2}$. This, in turn, supports the validity of equation (4.9) to relate $\delta_{wet}^{20°C}$ and $\delta_{wet}^{40°C}$. It must be emphasized that the effect on D is still more decisive since it results opposite to the expected behavior of the thermally-activated diffusional process.

The fact that a grafted PNIPAM brush builds a barrier to molecular diffusion, irrespective of its conformational state, is particularly relevant in the design of certain thermally nanoactuated ion gating.[9]

## 4.4 CONCLUSIONS

A number of open questions related to thin grafted PNIPAM brushes with varying grafting density were thoroughly discussed on the basis of an electrochemical characterization strategy. In particular, answers were given for individual effects of the thermally-induced collapse transition on both molecular transport through the brush and blocking character of the modified surface, respectively. In addition, further insight into the transport behavior of brushes synthesized from SAM monolayers was gained and consequently, some clarity was brought to otherwise unanswer aspects of earlier findings. A quantitative description of mass transport processes through the PNIPAM brushes could be achieved thanks to the use of

impedance spectroscopy. We were able to describe how conformational changes due to the thermal collapse of the PNIPAM brush influence transport properties.

More specifically, we have shown that:

1) when the brush is absent or it has been grown from an initial SAM with low concentration of the initiatior thiol (5 %) semi-infinite diffusion limiting step takes place in the electrolyte while the charge transfer step remains also unaffected by the brush.

2) in thin brushes reaction sites on the surface are given by hydrophilic regions or defects on the initial SAM that determine the active area of the electrode. The fractional surface coverage does not vary with the polymer brush conformational changes. This behavior is related only to thin brushes.

3) characteristic features of the voltammetric responses, e.g. peaks separation and sharpness, may be used to confirm results obtained by impedance spectroscopy. However, obtaining a fit parameter like B that is independent of $A_e$, represents a considerable advantage of impedance spectroscopy over other electrochemical techniques in calculating the diffusion coefficient.

4) the calculated fractional coverage and other calculated microscopic variables are in agreement with comparable literature data. This validates the proposed impedance theoretical model. According to this model it is possible to separate individual effects of the thermally induced collapse transition on both molecular transport through the brush and blocking character of the modified surface, respectively.

5) grafted PNIPAM brushes grown from an initial SAM containing a concentration of thiol initiator ≥ 25% sets up a barrier to molecular diffusion irrespective of its

conformational state. An additional hindrance to diffusion is associated with the brush collapse.

## 4.5 REFERENCES


(1) .Jhon, Y. K.; Bhat, R. R.; Jeong, C.; Rojas, O. J.; Szleifer, I; Genzer, J. *Macromol. Rapid Commun.* **2006,** *27,* 697-701.

(2) .Malham, I. B.; Bureau, L. *Langmuir* **2010,** *26,* 4762–4768.

(3) .Plunkett, K. N.; Zhu, X.; Moore, J. S.; Leckband, D. E.; *Langmuir* **2006,** *22,* 4259-4266.

(4) .Goldstein, R. E. J. *Chem. Phys.* **1984,** *80,* 5340-5341.

(5) .Luzinov I.; Minko, S.; Tsukruk, V. V. *Prog. Polym. Sci.* **2004,** *29,* 635-698.

(6) .Gil, E. S.; Hudson, S. M. *Prog. Polym. Sci.* **2004,** *29,* 1173-1222.

(7) .Cole, M. A.; Voelcker, N .H.; Thissen, H.; Griesser, H. J. *Biomaterials* **2009,** *30,* 1827-1850.

(8) .Guo, W.; Xia, H. ; Xia, F.; Hou, X.; Cao, L.; Wang, L.; Xue, J.; Zhang, G.; Song, Y.; Zhu, D.; Wang, Y.; Jiang, L. *ChemPhysChem* **2010,** *11,* 859–864.

(9) .Yameen, B.; Ali, M.; Neumann, R.; Ensinger, W.; Knoll, W.; Azzaroni, O. *Small* **2009,** *5,* 1287–1291.

(10) .Reuber, J.; Reinhardt, H.; Johannsmann, D. *Langmuir* **2006,** *22,* 3362-3367.

(11) .Jones, D. M., Brown, A. A., Huck, W. T. S. *Langmuir* **2002,** *18,* 1265-1269.

(12) .Matyjaszewski, K.; Gaynor, S.; Grezta, D.; Mardare, D.; Shigemoto, T. *J. Phys. Org. Chem.* **1995,** *8,* 306-315.

(13) .Matyjaszewski, K.; Patten, T. E.; Xia, J. *J. Am. Chem. Soc*. **1997,** *119*, 674-680.

(14) .Press, W. H.; Teukolsky, S. A.; Vetterling, W. T.; Flannery, B. P. *Numerical Recipes in FORTRAN: The Art of Scientific Computing,* 2nd ed.; Cambridge University Press: Cambridge, U.K., 1992

(15) .Liu, X.; Ye, Q.; Yu, B.; Liang, Y.; Liu, W.; Zhou, F. *Langmuir* **2010,** *26,* 12377–12382.

(16) .Kaifer, A.; Gómez-Kaifer, M. *Supramolecular Electrochemistry*, Wiley-VCH: Weinheim, Germany, 1999; pp 193-194.

(17) .Finklea, H.O. In Electrochemistry of Organized Monolayers of Thiols and Related Molecules on Electrodes, *Electroanalytical Chemistry* Vol. 19, Bard, A. J.; Rubinstein I. Eds., Marcel Dekker Inc.: New York, 1996; pp 160-239.

(18) .Janek, R.P.; Fawcett, W.R. *Langmuir* **1998,** *14,* 3011-3018.

(19) .Finklea, H. O.; Snider, D. A.; Fedyk, J., *Langmuir* **1993**, *9,* 3660-3667.

(20) .Bard, A. J.; Faulkner, R. L. *Electrochemical Methods. Fundamentals and Applications*. 2nd Edition; John Wiley & Sons, Inc.: New York, 2001; pp 236-238.

(21) .Zhou, J.; Liu, J.; Wang, G.; Lu, X.; Wen, Z.; Li, J. *Adv. Funct. Mater.* **2007**, *17,* 3377–3382.

(22) .Alonso García T., Gervasi C.A., Rodríguez Presa M.J., Irigoyen Otamendi J., Moya S.E., Azzaroni O., in preparation.

(23) .Rodríguez Presa, M. J.; Gassa, L. M.; Azzaroni, O.; Gervasi, C. A.; *Anal. Chem.* **2009,** *81,* 7936–7943.

(24) .Azzaroni, O.; Gervasi, C. A. In *Functional Polymer Films,* Vol. 2 *Characterization and Applications*, First Edition; Knoll, W.; Advincula, R C.

Eds; Wiley-VCH Verlag GmbH & Co. KgaA: Weinheim, Germany, 2011; Chapter 26, pp. 809-830.

(25) .Berry, J.; Norcliffe, A.; Humble, S. *Introductory mathematics through science applications*, Cambridge University Press: New York, 1996; p 57

(26) .Sui, X. ; Chen, Q.; Hempenius, M. A.; Vancso, G. J.; *Small* **2011,** *7,* 1440–1447.

(27) .Kidoaki, S.; Ohya, S.; Nakayama, Y, Matsuda, T. *Langmuir* **2001,** *17,* 2402-2407.

## 4.6 SUPPORTING INFORMATION CHAPTER 4

### 4.6S1. CONTENT:

-AFM images in lateral force mode of the initiating layers corresponding to a SAM obtained with 5% thiol initiator and a SAM with a 100% inert thiol.

-A discussion of these images in terms of the absence of phase separation domains in the mixed thiol SAM and equivalent literature data.

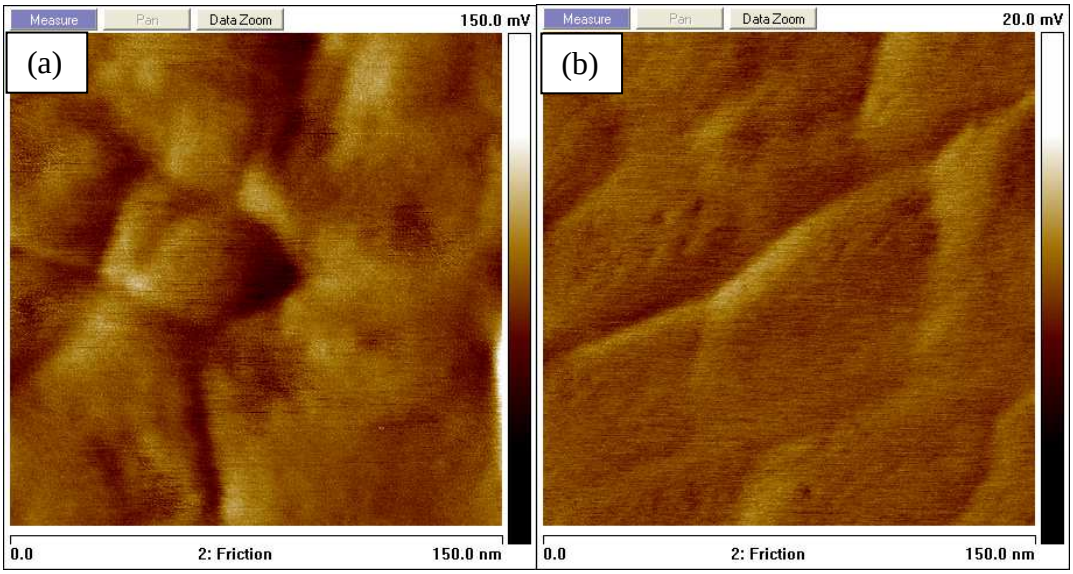


**Figure 4.S1.** Lateral-force AFM images of a) a sample of Au covered by a SAM of the inert thiol (1-undecanethiol) and b) a sample of Au covered by a SAM prepared with a mix of initiator (5% ω-mercaptoundecyl bromoisobutyrate) and inert thiols.

Comparison of AFM friction images reveals the same overall morphology for both samples and the absence of phase-separated nanometer scale domains in the mixed SAM. The absence of phase separation in the SAMs used in this work agrees with previous studies by Wang et. al.[28] . These authors have shown that

using an inert analogue with the highest chemical similarity to its reactive initiator typically minimizes the segregation in mixed initiator monolayers and polymer brushes of varied grafting density. Thus, studies performed on a comparable binary SAM of 1-undecanethiol (UDT) and 11-mercaptoundecanoic acid (MUA) on Au(111) showed that these two thiols having the same number of methylene units are well-mixed in the SAMs, and no distinct domain formation takes place. [29] Moreover, transition regions between adjacent domains in phase-separated SAMs of mixed thiols are characterized by a less close-packed structure corresponding to highly disordered borders. [30] Consequently, the presence of these morphological features are expected to lead to numerous site defects in the SAM and to a lower coverage $\theta$. However, it has been shown in connection with impedance results that in the present work measured $\theta$ is practically the same for the SAMs in Figure 4.S1. Thus, these observations also lend support to the absence of a phase separation process.

## 4.6S2.REFERENCES


(28) Wang S.; Zhu Y., *Langmuir* **2009**, 25, 13448–13455.

(29) Kakiuchi T, Iida M., Gon N., Hobara D., Imabayashi S., Niki K., *Langmuir* **2001**, 17, 1599–1603.

(30) J.P. Folkers, Laibinis P.E., Whitesides G.M., *Langmuir* **1992**, 8, 1330-1341.

# Chapter 5

## ELECTROCHEMICAL DETERMINATION OF THE GLASS TRANSITION TEMPERATURE OF THIN POLYELECTROLYTE BRUSHES AT SOLID-LIQUID INTERFACES BY IMPEDANCE SPECTROSCOPY

## ABSTRACT

Devising strategies to assess the glass transition temperature ($T_g$) of polyelectrolyte assemblies at solid-electrolyte interfaces is very important to understand and rationalize the temperature-dependent behavior of polyelectrolyte films in a wide range of settings. Despite the evolving perception of the importance of measuring $T_g$ under aqueous conditions in thin film configurations, its straightforward measurement poses a challenging situation that still remains elusive in polymer and materials science. Here we describe a new method based on electrochemical impedance spectroscopy (EIS) to estimate the glass transition temperature of planar polyelectrolyte brushes at solid-liquid interfaces. To measure $T_g$, the charge transfer resistance ($R_{ct}$) of a redox probe diffusing through the polyelectrolyte brush was measured, and the temperature corresponding to the discontinuous change in $R_{ct}$ was identified as $T_g$. Furthermore, we demonstrate that impedance measurements not only facilitate the estimation of $T_g$ but also enable a reliable evaluation of the transport properties of the polymeric interface, *i.e.:* determination of diffusion coefficients, close to the thermal transition. We consider that this approach bridges the gap between electrochemistry and the traditional tools used in polymer science and offers new opportunities to characterize the thermal behavior of complex polymeric interfaces and macromolecular assemblies.


## 5.1.INTRODUCTION

Knowledge of the influence of temperature on the physical properties of thin polymer films as well as appearance of thermal transitions in surface-grafted

macromolecular systems are key aspects that play major roles in many technological applications [1]. For many years, now, and particularly within the last decade, special interest has been paid to the estimation of the glass transition temperature ($T_g$) of thin polymer films, *i.e.*: the temperature at which the polymer film experiences a transition from a glassy to a rubbery state.[2,3] In most of cases, determination of $T_g$ in thin film configurations is much more difficult to accomplish than in typical bulk samples. The main reason for that is the reduction in signal strength because less material is being probed and concomitantly, this effect could also have an impact in the slopes of the curves relating a property being measured versus temperature that characterize the glass and melt regions.[4] Nevertheless, different groups developed different successful strategies based on ellipsometry [5], surface plasmon resonance spectroscopy,[6] x-ray reflectivity [7] or fluorescence spectroscopy [8] to achieve such a goal. More recently, there has been great emphasis on studying the thermal behaviour and estimating $T_g$ of polyelectrolyte-based thin films in aqueous environments [9]. Interfacial architectures based on polyelectrolytes, like layer-by-layer assemblies or polyelectrolyte brushes, have become versatile materials for the design and fabrication of a broad variety of smart functional devices including self-assembled capsules, membranes, sensors or drug delivery systems.[10] In all of these applications, the same experimental scenario takes place: polymeric assemblies are in contact with a liquid phase. As mentioned above, a number of techniques and protocols are available to determine $T_g$ in thin films at the gas-solid interface; however, the choice is much more limited for estimating $T_g$ in thin films fully immersed in electrolyte solutions. Therefore, it is crucial to develop straightforward but reliable techniques that enable an *in-situ* estimation of $T_g$ of polyelectrolyte assemblies without drawing upon complex

experimental setups, specific sample preparation or even arguable assumptions for data analysis. In this context, electrochemical (Faradaic) impedance spectroscopy (EIS) is rapidly evolving as a very versatile electrochemical technique fully compatible with the *in-situ* characterization of polyelectrolyte brushes grafted on solid surfaces.[11] This technique has facilitated the accurate electronic transduction [12] of a series of stimuli-triggered responses in different polymer brushes.[13] For example, Minko, Katz and co-workers explored the switchable properties of mixed polymer brushes arising from morphological transitions in the polymer brush layer using EIS under different conditions in liquid environments.[14] So far, temperature-dependent EIS studies on polymer brushes have been exclusively circumscribed to the characterization of the switchable gating properties of polymer brushes bearing thermoresponsive monomers, e.g.: isopropylacrylamide (NIPAM).[15]In this work, we describe for the first time the use EIS as an electrochemical method to estimate the glass transition temperature of polyelectrolyte brushes in aqueous electrolyte environments. We show the capabilities of EIS to demonstrate that ion-paired polycationic thin polymer brushes display a well-defined $T_g$ near room temperature. Although solvent-driven glass transition was reported previously for polyelectrolyte brushes,[16] a temperature-driven glass transition like the one reported here was not and this could have immediate implications in their molecular transport properties.

### 5.1.1 Synthesis of Polyelectrolyte Brushes.

Polyelectrolyte brushes growth starts with self-assembly of an initiator thiol (□–mercaptoundecylbromobutyrate) onto clean gold substrates. The polymerization solution was prepared as follows: commercially–available (Aldrich) METAC (10 mL (75 wt. % solution in water), 40 mmol) was dissolved in water (2 $cm^3$) and

dimethylformide (DMF) 99.85% (3 $cm^3$) at 20 ºC and degassed by passing a continuous stream of dry $N_2$ through the solution whilst being stirred (15 minutes). To this solution was added 2,2'-bipyridyl (416 mg, 2.7 mmol), $Cu^{I}Cl$ (105 mg, 1.1 mmol) and $Cu^{II}Cl_2$ (14 mg, 0.11 mmol). The mixture was then further stirred and degassed with a stream of dry $N_2$ (15 minutes). Initiator coated samples (1.0 $cm^2$ each) were sealed in Schlenk tubes, degassed (4 x high-vacuum pump / $N_2$ refill cycles) and left at 20 ºC under $N_2$. The polymerization solution was then syringed into each Schlenk tube, adding enough solution to submerge each sample completely. Once polymerization step is accomplished, the samples were removed, washed with water, then methanol, and dried under a stream of $N_2$. Replacement of chloride counterions by perchlorate ions was accomplished by placing PMETAC brushes in 0.1 M $NaClO_4$ (aqueous solution) during 4-6 hours.

### 5.1.2 Preparation of Gold Substrates.

Au substrates were prepared by sputtering deposition, cleaned by sonication, followed by water rinsing while the final cleaning step comprised exposure to UV radiation in a Bioforce Nanosciences chamber for 30 minutes just before modification step. Modification of Au surfaces was carried out by immersion in 10 mM thiol solutions in ethanol for 16 hours in order allow the spontaneous formation of the initial assembled monolayer (SAM).

### 5.1.3 In situ spectroscopic ellipsometry.

The growth of the polymer brushes and the resulting brush thickness were monitored by ellipsometry under the corresponding liquid environment. Measurements were performed using a purpose-built flow cell with a total volume of

~300 µL. The flow cell was mounted on a spectroscopic rotating compensator ellipsometer (M2000V, Woollam, NE, USA), providing access to ellipsometric data. Ellipsometric data, Δ and Ψ, were acquired over a wavelength range from λ = 380 to 1000 nm, simultaneously, at 65º angle of incidence, and with a time resolution of ~5 s. The thickness of PMETAP brushes in aqueous 0.1 M $NaClO_4$ was ~ 21 nm.

### 5.1.4 Electrochemical techniques.

Electrochemical measurements were carried out within the 5°C – 45°C temperature range in a conventional three-electrode cell. A large area platinum sheet was used as the counter electrode and a saturated calomel electrode (SCE) was the reference electrode. All potentials are referred to the SCE at 25°C. Brush-modified Au substrates served as working electrodes. Solutions of 0.1 M $NaClO_4$ were used as supporting electrolytes and prepared from analytical grade (Merck) reagents and Milli-Q water. Before performing each measurement the working electrode was thoroughly rinsed with Milli-Q water and immersed in the supporting electrolyte solution for 10 minutes. Experiments were performed under purified $N_2$ gas saturation in the presence of a 1 mM $K_3[Fe(CN)_6]$ / $K_4[Fe(CN)_6]$ (1:1) mixture as a redox probe in the supporting electrolytic solutions

Impedance spectra were obtained with a Zahner IM6d electrochemical workstation on modified gold electrodes. The dc potential was held at the open circuit potential while a 10 mV amplitude ac potential was applied. The voltage signal frequencies used for EIS measurements ranged from 100 kHz to 1 mHz. Impedance data analysis was performed according to proper transfer function derivation and

identification procedures by using complex non-linear least squares (CNLS) fitting based on the Marquardt-Levenberg algorithm.

## 5.2 RESULTS AND DISCUSSION

Cationic poly(2-(methacryloyloxy)ethyltrimethylammonium perchlorate) (PMETAP) brushes were synthesized by surface-initiated atom transfer radical polymerizacion (SI-ATRP) of the monomer 2 (methacryloyloxy)ethyltrimethylammonium followed by counterion exchange in the presence of 0.1 M $NaClO_4$ (Fig. 5.1). [17] Polymer brushes were then characterized by *in-situ* ellipsometry to estimate the thickness of the PMETAP brushes.

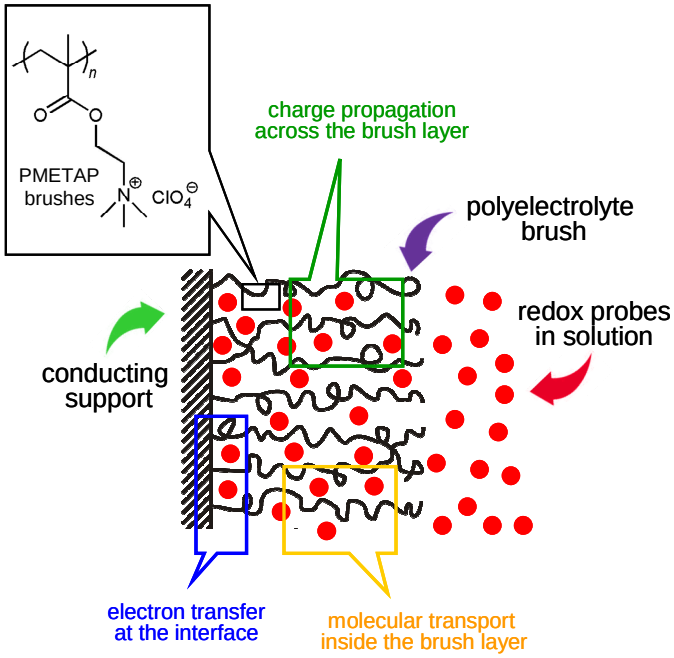


**Figure 5.1.** Schematic representation of the different charge- and mass-transport processes taking place in the system constituted of a gold substrate modified with

PMETAP brushes in a solution containing redox probes. See the text for the full description of the transport processes prevailing under our experimental conditions.

Thereafter, we carried out the EIS characterization of PMETAP brushes in an electrolyte solution 0.1 M $NaClO_4$ containing 1 mM $K_3[Fe(CN)_6]/K_4[Fe(CN)_6]$ (1:1) mixture (redox probes) at different temperatures. EIS is a versatile method for probing the features of surface-modified conducting supports.[18] A small-amplitude perturbing sinusoidal voltage signal is applied to the electrode surface and the resulting current response is measured.

This particular feature renders EIS a very sensitive technique to monitor subtle changes in electrical properties of solid-liquid interfaces. [19] Moreover, EIS probes not exclusively the solid-liquid interface but also bulk processes, like mass transfer, that govern the value of the surface concentration of the electroactive molecules. In the studied system the diffusion layer spans the whole brush thickness. Figure 5.2 shows the impedance spectra of PMETAP brushes measured at different temperatures. These plots are presented in the form of complex plane graphs (the so-called Nyquist plots), in which the semicircle diameter corresponds to the electron transfer resistance ($R_{ct}$) of the redox reporters, *i.e.*: $Fe(CN)_6^{3-/4-}$, at the electrode surface. In order to derive accurate values of $R_{ct}$ from the experimental spectra, the data were fitted to a theoretical equivalent circuit (inset in Fig. 5.2). For the high frequency data in Figure 5.2 the faradaic impedance $Z_f = R_{ct}$. A plot displaying the electron transfer resistance versus temperature is presented in Figure 5.3.

As expected, electron transfer is an activated process and consequently $R_{ct}$ decreases upon increasing temperature. However, EIS is able to detect within the experimental temperature domain two well-defined regions that are associated, in principle, to two different activation energies. Straight lines drawn in Figure 5.3 are not intended as an indication of strict linear behaviour but as a clarification of the bounds of each region. The $R_{ct}$ vs. T curve displays a kink, which is attributed to the thermally induced glass transition. As is discussed below, the changes in activation energies for the diffusion and electron transfer processes measured after lowering the temperature below a certain critical value are not arbitrarily linked here with a glassy-rubbery state transition but rather this event appears as the only plausible interpretation of the experimental results. It is also important to mention here that similar experiments performed in the absence of polymer brushes, *i.e.:* gold electrodes modified with ATRP initiator-terminated self-assembled monolayers, revealed plots with a single value for the activation energy. Hence, the presence of a break-point in Fig. 5.3 leading to temperature domains with different activation energies is a clear indication that the thermal transition occurring in the brush layer is responsible for altering charge transfer resistance values. Charge transfer dynamics at electrode surfaces chemically modified with polymeric building blocks is strongly influenced by structural changes in the macromolecular array and provides an assessment of physical changes in the polymer layer.[20] The different slopes of the straight lines in the $R_{ct}$ vs T plot reveal the transition between glassy and rubbery states. Traditionally, the physical changes occurring in the polymer film at $T_g$ have been explained on the basis of free volume and cooperative motion of the macromolecular assembly.[21] In our case electron transfer of redox probes

embedded in a “glassy” polymer brush represents a process with high activation energy.

This fact might be ascribed to the reduced segmental motion of polymer chains and free volume at the electrode surface that render the electron transfer a costly process.[22]

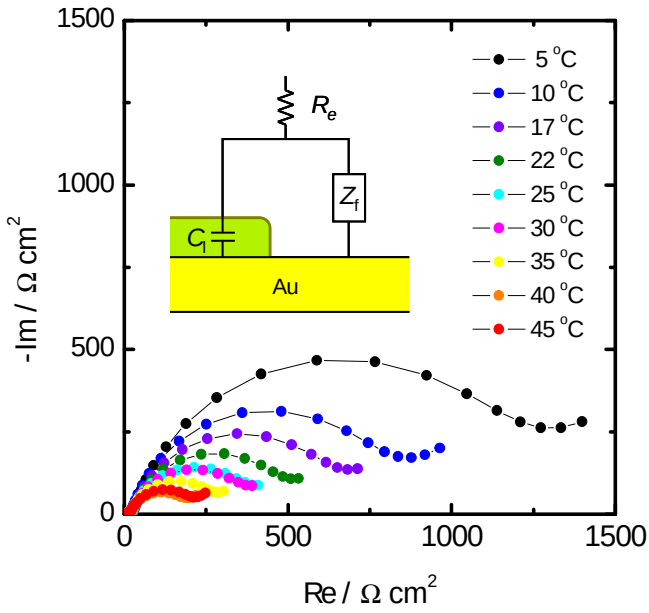


**Figure 5.2.** Nyquist plot ($Z_{Im}$ vs $Z_{Re}$) for the Faradaic impedance measurements performed at different temperatures in the presence of $5\times10^{-3}$ M $Fe(CN)_6^{3-/4-}$ + 0.1 M $NaClO_4$ at a Au electrode modified with poly(2 (methacryloloxy)ethyltrimethyl ammonium perchlorate)

(PMETAP) brushes. Measuring frequency range $10^5$ Hz - $10^{-1}$ Hz. The inset displays the theoretical equivalent circuit used to fit the experimental data. $R_e$: electrolyte resistance; $C_l$: interfacial capacitance; $Z_f$: faradaic impedance.

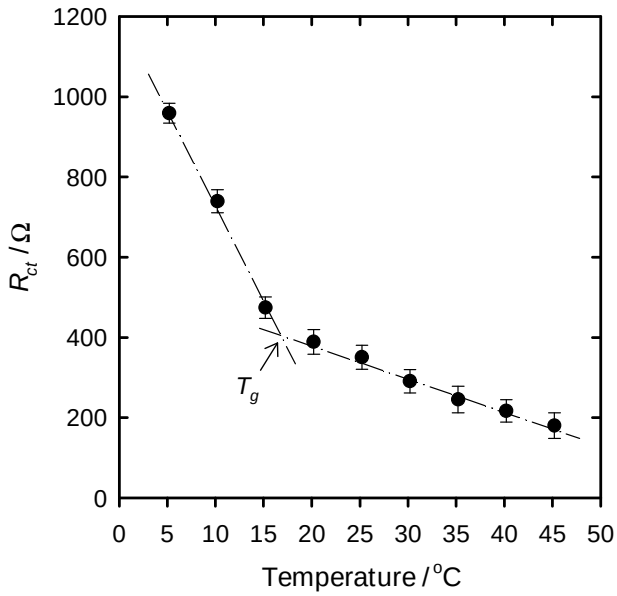


**Figure 5.3**. Representation of the charge transfer resistance ($R_{ct}$) derived from EIS measurements plotted in figure 5.2 as a function of temperature (T).

In the most general case the electroactivity in polyelectrolyte films hosting redox counterions not only relies on the charge transfer of the redox species at the electrode surface but also on the movement of electrons in a diffusive manner among the neighboring redox centers (Fig. 5.1). For instance, the redox process is coupled to the incorporation of ions and solvent molecules into the film in which swelling or shrinkage of the polymer brush can take place.[20] Thus, the electrochemical process with the polyelectrolyte brush in the presence of the redox probes can be, under certain experimental conditions, rather complicated, particularly due to the possible interaction between the $Fe(CN)_6^{-3/-4}$ anions and the brush chains. $Fe(CN)_6^{-3}$ once mixed with the cationic polyelectrolyte brushes, would preferentially replace and release the monovalent counter anion perchlorate from the brush film and introduce ionic crosslinking of the brush chains.[23] However, in our experiments the concentration of perchlorate anion is 100 times that of each

redox species, what in principle reduces substantially the occurrence of this event. In principle, the charge transport mechanism might involve either movement of the electroactive ions by diffusion or hopping/tunneling of electrons from one redox site to the next at fixed positions in the polymer chain.[24] Interestingly, Huck and co-workers [25] demonstrated that in $[Fe(CN)_6]^{3-}$-coordinated PMETAC brushes ion diffusion rather than electron hopping is the charge transport mechanism taking place even for comparable concentrations of the redox species and the counter ion. Hence, in the case of PMETAP brushes upon increasing temperature above $T_g$ the reorganization and higher mobility of grafted chains facilitates not only the movement of redox probes to close proximity of the electrode surface but also the charge propagation across the film. Hence, this electron transfer process is energetically more favorable than a similar one occurring below $T_g$.

Differences between both thermal regimes, glassy and rubbery, are clearly manifested by a well-defined variation in activation energy for the electron transfer process of the redox probe. Figure 5.4 shows a plot of ln ($T/R_{ct}$) versus 1000/T. As already shown for this kind of experiments ($T/R_{ct}$) is proportional to the reaction rate constant $k$ (see Supporting Information and references therein). From this figure it is evident that the electron transfer requires different activation energies whether the process occurs below or above $T_g$.

Activation energy values calculated from the experimental data are 53.3 kJ/mol and 26.6 kJ/mol for temperature domains below and above $T_g$, respectively.[26,27] These results indicate that the activation energy for the electron transfer taking place

within the brush in the “glassy” state is twice the activation energy in the “rubbery” state.

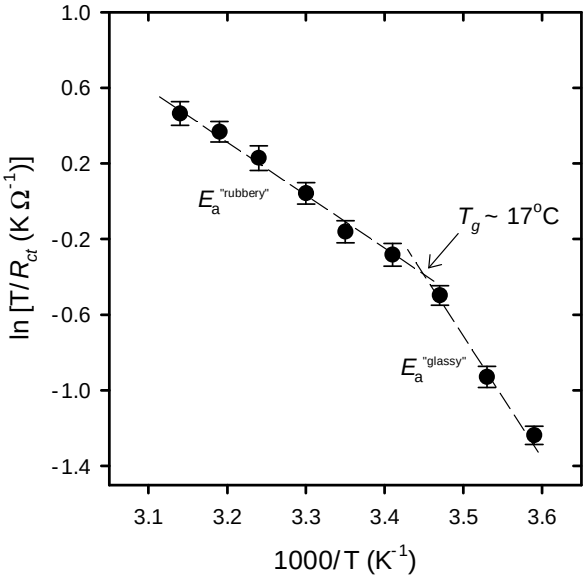


**Figure 5.4.** Arrhenius-type plot showing the dependence of ln ($T/R_{ct}$) on the inverse temperature ($T^{-1}$). At T = $T_g$ there is a marked difference in the slope of the correlation line, indicative of a higher activation energy, Ea.

This quantitative comparison of activation energies further confirms the critical role of the thermally activated macromolecular organization and the mobility the grafted polymer chains in defining the electron transfer characteristics of a chemically modified electrode.[28] It is a well-known fact that $T_g$ has a significant impact on the diffusion of molecular species through the macromolecular matrix.[29] In most cases involving ionic transport through polymeric materials, increasing temperature above $T_g$ is reflected as a sudden increase in diffusion coefficient values.[30]This feature is commonly ascribed to changes in segmental mobility and the formation of free volume between polymer chains that greatly facilitate the diffusion of small

molecules through the “rubbery” film. From the EIS data we were able to estimate the diffusion coefficients of $Fe(CN)_6^{4-/3-}$ (see Supporting information for details) at different temperatures and the resulting values are consistent with prior reports. [31] As seen in Figure 5.5, there is a significant jump in *D* upon increasing temperature above $T_g$. Diffusion of the redox probe is approximately nine times faster above $T_g$. If we consider that many applications of polymer brushes demand new strategies to manipulate and/or activate transport and permeability of small molecules passing through these films, the manipulation of *D* using $T_g$ as a thermal trigger can be an interesting practical step to achieve such goal.

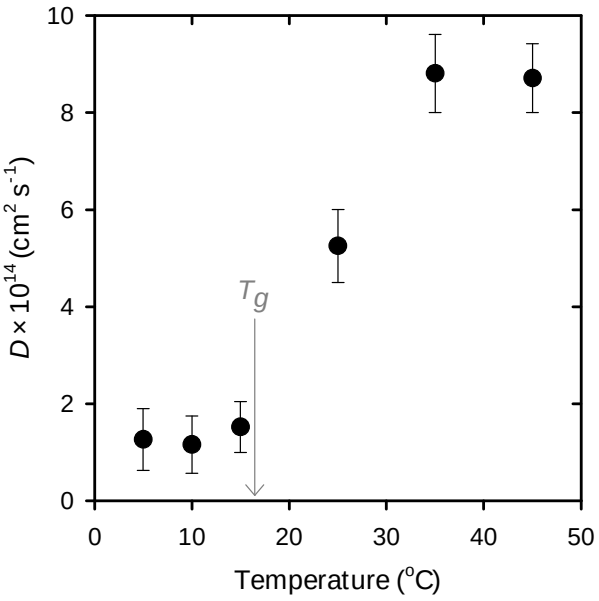


**Figure 5.5**. Representation of the diffusion coefficient (*D*) of the redox probe as a function of temperature. For the sake of clarity, the glass transition temperature ($T_g$ ~ 17 $^o$C) is indicated by a gray arrow.

## 5.3 CONCLUSIONS

In conclusion, we showed for the first time the capabilities of Faradaic impedance spectroscopy as a tool to estimate the glass transition temperature of ultrathin polymer brushes at solid-liquid interfaces.[32] This is a fundamental parameter in thin films that accounts for the presence of thermally induced structural transitions. To measure the glass transition temperature, the charge transfer resistance was measured as a function of temperature, and the temperature corresponding to the near discontinuous change in $R_{ct}$ was identified as $T_g$. Further results from the modeling of the impedance response as a function of temperature enabled the estimation of the diffusion coefficient of the redox probes close to the thermal transition temperature. Impedance measurements corroborated the typical scenario in which diffusion coefficients sharply increase at temperatures higher than $T_g$. From the functional viewpoint our results gain particular relevance not only because this is the first estimation of $T_g$ in *polyelectrolyte* brushes at *solid-liquid* interfaces but also because we demonstrate that this transition occurs close to room temperature.

## 5.4 REFERENCES


(1). (a) Jones, R.A.L., *Curr. Op. Colloid. Interf. Sci.* **1999**, *4*, 153. (b) Forrest, J.A. Dalnoki-Veress, K., Dutcher, J.R. *Phys. Rev. E* **1997**, *56*, 5705.

(2). Keddie, J.; Jones R.A.L.;Cory, R. Faraday Diss.1994, 98, 219.

(3). (a) Forrest, J.A.; Mattsson, J. *Phys. Rev. E.,* **2000**, *61*, R54. (b) Forrest, J.A.; Dalnoki-Veress, K., *Adv. Colloid Interf. Sci.* **2001**, 94, 16. (c) Ellison, C.J..; Torkelson, J.M., *Nat. Mater.* **2003**, *2*, 695.

(4). Roth, C.B.; Dutcher, J.R., *J. Electroanal. Chem.* **2005**, *584*, 13.

(5). (a) Lee, H.; Ahn, H.; Naidu, S.; Seong, B.S.; Ryu, D.Y.; Trombly, D.M.; Ganesan, V., *Macromolecules* **2010**, *43*, 9892. (b) Clough, A.; Peng, D.; Yang, Z.; Tsui, O.K.C., *Macromolecules* **2011**, *44*, 1649. (c) Yamamoto, S.; Tsujii, Y.; Fukuda, T., *Macromolecules* **2002,** *35,* 6077.

(6). Prucker, O.; Christian, S.; Bock, H. Rühe, J.; Frank, C.W.; Knoll, W. in *"Organic Thin Films"* Frank, C (ed.) (ACS Symposium Series; American Chemical Society, Washington, DC, 1998), Ch. 17, pp.233-249.

(7). (a) Fryer, D.S.; Peters, R.D.; Kim, E.J.; Tomaszewski, J.E.; de Pablo, J.J.; Nealey, P.F.; White, C.C.; Wu, W.-l., *Macromolecules*, **2001**, *34,* 5627. (b) Cecchetto, E.; de Souza, N.R.; Jerome, B., *J. Phys. IV France* **2000**, *10*, 247.

(8). (a) Ellison, C.J.; Ruszkowski, R.L.; Fredin, N.J.; Torkelson, J.M., *Phys Rev.Lett.* **2004**, *92*, 095702 (b) Mok, M.M.; Kim, J.; Marrou, S.R.; Torkelson, J.M. *Eur. Phys. J. E* **2010**, *31*, 239–252.

(9). (a) Köhler, K.; Shchukin, D.G.; Möhwald, H.; Sukhorukov, G.B., *J. Phys. Chem. B* **2005**, *109,* 18250. (b) Köhler, K.; Möhwald, H.; Sukhorukov, G.B., *J. Phys. Chem. B* **2006,** *110,* 24002. (c) Fortier-McGill, B.; Reven, L. *Macromolecules* **2009**, *42*,

247. (d) Vidyasagar, A.; Sung, C.; Gamble, R.; Lutkenhaus, J.L., *ACS Nano*, **2012**, *6*, 6174. (e) Sung, C.; Vidyasagar, A.; Hearn, K.; Lutkenhaus, J.L., *Langmuir* **2012**, *28*, 8100. (f) Ghostine, R.A.; Schlenoff, J.B., *Langmuir*, **2011**, *27*, 8241.

(10). (a) Azzaroni, O. *J.Polym.Sci., Part A: Polym. Chem.*, **2012**, *50*, 3225 (b) Advincula, R.C.; Brittain, W.J.; Caster, K.C.; Rühe, J. (eds.) "*Polymer Brushes: Synthesis, Characterization, Applications"*, (VCH-Wiley Verlag GmbH, Weinheim, 2004) (b) Mallapragada, S.K.; Chin, S.-F., in *"Tailored Polymeric Materials for Controlled Delivery Systems"* McCulloch, I.; Shalaby, S.W. (eds.)(American Chemical Society, Washington, 1998), Ch. 14, p. 176. (c) Siepmann, J.; Lecomte, F.; Bodmeier, R., *J. Controlled Release* **1999**, *60*, 379.

(11). (a) Bai, D.; Habersberger, B.M.; Jennings, G.K. *J. Am. Chem. Soc.*, **2005**, *127*, 16486. (b) Bai, D.; Ibrahim, Z.; Jennings, G.K. *J. Phys. Chem. C*, **2007**, *111*, 461. (c) Bai, D.; Hardwick, C.L.; Berron, B.J.; Jennings, G.K. *J. Phys. Chem. B*, **2007**, *111*, 11400.

(12). Pardo-Yissar, V.; Katz, E.; Lioubashevski, O.; Willner, I., *Langmuir* **2001,** *17,* 1110.

(13). Zhou, F.; Hu, H.; Yu, B.; Osborne, V.L.; Huck, W.T.S.; Liu, W., *Anal. Chem.*, **2007**, *79*, 176.

(14). M. Motornov, R. Sheparovych, E, Katz, S. Minko, *ACS Nano*, **2008**, *2*, 41.

(15). (a) Sheeney-Haj-Ichia, L.; Sharabi, G.; Willner, I., *Adv. Funct. Mater.* **2002**, *12*, 27. (b) Zhou, J., Wang, G., Hu, J., Lu, X., Li, J. *Chem. Commun.*, **2006**, 4820. (c) Alonso García, T.; Gervasi, C.A.; Rodríguez Presa, M.J.; Irigoyen Otamendi, J.; Moya, S.E.; Azzaroni, O., *J. Phys. Chem. C* **2012**, *116*, 13944.

(16). Laschitsch, A.; Bouchard, C.; Habicht, J.; Schimmel, M.; Rühe, J.; Johannsmann, D.; *Macromolecules* **1999**, *32,* 1244-1251.

(17). (a) Farhan, T.; Azzaroni, O.; Huck, W.T.S., *Soft Matter,* **2005**, *1*, 66. (b) Azzaroni, O.; Moya, S.; Farhan, T.; Brown, A.A.; Huck, W.T.S., *Macromolecules*, **2005**, 38, 10192.

(18). Katz, E; Willner, I, *Electroanalysis*, **2003**, *15*, 913.

(19). Lvovich, V.F. in *"Impedance Spectroscopy: Applications to Electrochemical and Dielectric Phenomena"* (JohnWiley & Sons, New York, 2012).

(20). *Techniques of Chemistry: Molecular Design of Electrode Surfaces,* Murray, R.W. (ed.) (Wiley-Interscience, Hoboken, 1992).

(21). George S.C.; Thomas, S., *Prog. Polym.Sci.* **2001**, *26*, 985.

(22). Inzelt, G., *Electrochimica Acta* **1989**, *34*, 83.

(23). Combellas, C.; Kanoufi, F.; Sanjuan, S.; Slim, C.; Tran, Y. *Langmuir*, **2009**, *25*, 5360–5370.

(24). Bard, A. J.; Faulkner, L. R. *Electrochemical Methods, Fundamentals and Applications*, 2nd ed.; Wiley: New York, 2001.

(25) . Spruijt, E.; Choi, E.-Y.; Huck, W.T.S. *Langmuir*, **2008**, *24*, 11253–11260. (26). It is worth mentioning that polyelectrolyte brushes are in collapsed conformation at all experimental temperatures due to the high concentration of perchlorate ions (0.1 M $NaClO_4$). Thus, it is very unlikely that a decrease in temperature might lead to a further collapse of the structure within our experimental temperature domain. *In-situ* ellipsometric mesurements corroborated that the brush thickness remained independent of the electrolyte temperature within the working temperature range. Further details can be found in: (a) T. Farhan et.al. Soft Matter, **2005,** 1, 66–68, (b) O. Azzaroni et.al. *Macromolecules* **2005,** *38,* 10192-10199, (c) M.J. Rodríguez-Presa et al Anal. Chem. **2009,** 81, 7936–7943. (d) Jagoba Jon Iturri Ramos. *"Assembly and Physico-Chemical Characterization of Supramolecular*

*Polyelectrolyte Nanostructures"*. PhD Thesis, Doctor Europeus, San Sebastián, Spain, 2011.

(27). We should mention that, apart from the glass transition, there is no other studied process in supported polymer films that could account for the existence of a critical temperature below which *k* values exhibit much larger activation energies. Since the glass transition temperature is the temperature at which the spacing and free internal volume available for molecular motions achieve minimum values it is reasonable to expect that a glass transition may lead to increased reorganization energy for the redox species during the electron jump (Eckermann *et al.*, *Coord Chem Rev*. **2010**; 254, 1769] and also to decreased molecular mobility within the diffusion layer [Spruijt *et al. Langmuir* **2008,** *24,* 11253]. Both events, in turn, are related to higher activation energies as estimated from *k* values in the lower temperature range.

(28). Inzelt, G. in *Encyclopedia of Electrochemistry – Vol. 10*: *Modified Electrodes*, Bard A.J.; Stratmann, M.; Fujihira, M.; Rubinstein, I.; Rusling, J.F. (eds.) (Wiley-VCH, Weinheim, 2007) Ch. 9, p. 651.

(29). Flier, B.M.I.; Baier, M.C.; Huber, J.; Müllen, K.; Mecking, S.; Zumbusch, A.; Wöll, D., *J. Am. Chem. Soc.* **2012**, *134*, 480.

(30). Chandra, A.; Agrawal, R.C.; Mahipal, Y.K., *J. Phys. D: Appl. Phys.,* **2009**, *42*, 135107.

(31). Rodríguez Presa, M.J.; Gassa, L.M.; Azzaroni, O.; Gervasi, C.A., *Anal. Chem.*, **2009**, *81*, 7936.

(32). It is generally accepted that for a polymer film attached to a solid substrate at one end, $T_g$ displays lower values at the other end where the polymer chains are able to move freely. Thus, as with other measuring techniques, EIS measurements

only generate average values for the transition temperature. See, for example: Fryer, D.S.; Peters, R.D.; Kim, E.J.; Tomaszewski, J.E.; de Pablo, J.J.; Nealey, P.F.; White, C.C.; Wu, W.-l. *Macromolecules* **2001**, *34,* 5627-5634.

## 5. 5 SUPPORTING INFORMATION CHAPTER 5

### 5. 5S1.ESTIMATION OF DIFFUSION COEFFICIENTS.

EIS experiments were used to estimate diffusion coefficients of the redox probe being transported within the brush. Experimental impedance spectra of the electrode modified with the polyelectrolyte brush exhibit in the region of low ac-signal frequency a typical impedance contribution compatible with finite-length diffusion-type impedances. Interfacial Faradaic impedance $Z_f$ can be properly described according to the following expression:

$$Z_f = R_{ct} + \frac{\sigma}{\sqrt{\omega}}\left[\tanh\left(B\sqrt{j\omega}\right)\right](1-j) \qquad (5.S1)$$

where $R_{ct}$ is the charge transfer resistance, $j = \sqrt{-1}$, $\omega = 2\ \pi\ f$, is the angular frequency of the potential perturbation and the so-called mass transfer coefficient $\sigma$ contains the contributions of the oxidised and reduced forms of the redox couple and $B = \delta / \sqrt{D}$. $\delta$ is the thickness of the polymer brush (the brush layer represents a diffusion-limiting barrier of finite thickness) and *D* is the diffusion coefficient. The complete mathematical treatment used to derive equation (5.S1) can be found in Chapter 3. From the B values derived through fitting of the experimental impedance to the theoretical transfer function and $\delta$ values derived from in-situ ellipsometry, diffusion coefficients *D* were estimated (Figure 5.5 in Chapter 5).

### 5.5S2.ESTIMATION OF THE ACTIVATION ENERGY FOR THE CHARGE TRANSFER PROCESS.

The activation energy for the electrode reaction was obtained from an Arrhenius plot of the rate constant which, in turn, was derived from $R_{ct}$ values resulting from

the fitting of impedance data. $R_{ct}$ contains kinetic information according to the following expression : [33,34]

$$\frac{1}{R_{ct}} = A_e\, F \left[ C_O^{dc} \left( \frac{k_c \alpha_c F}{RT} \right) + C_R^{dc} \left( \frac{k_a \alpha_a F}{RT} \right) \right] \qquad (5.S2)$$

where $k_a$ and $k_c$ correspond to the rate constants for the anodic and cathodic reactions, respectively, $C_O$ and $C_R$ represent concentrations of the oxidized and reduced species at the surface for dc conditions and $A_e$ is the electrode area. Assuming that the transfer coefficients $\alpha$ are equal for both anodic and cathodic reactions and remembering that the applied dc potential corresponds to the formal potential of the redox couple ($C_O^{dc} = C_R^{dc} = C$**)** results $k_a = k_c = k$ and equation (5.S2) reduces to:

$$\frac{T}{R_{ct}} = A_e\, F\, C \left( \frac{\alpha F}{R} \right) 2\, k \qquad (5.S3)$$

Since $k$ obeys the Arrhenius equation from the slope of the linear plot $\ln(T/R_{ct})$ vs. $T^{-1}$ the activation energy was calculated.

**5.5S3.IMPEDANCE MEASUREMENTS FOR AN EXTENDED FREQUENCY RANGE.**

Figure 5.S1 shows impedance data recorded at 10 °C for which the lowest measurement frequency is 1 mHz. The main difference with data in Figure 5.2 in

Chapter 5 is associated with the low frequency region containing diffusion effects that are now compatible with finite-length diffusion-type impedance $Z_d$ with a permeable boundary at the brush/solution limit. Theoretical data shown were obtained through fitting to the equivalent circuit depicted in the inset of figure 5.2 in Chapter 5 but this time with $Z_f = R_{ct} + Z_d$.

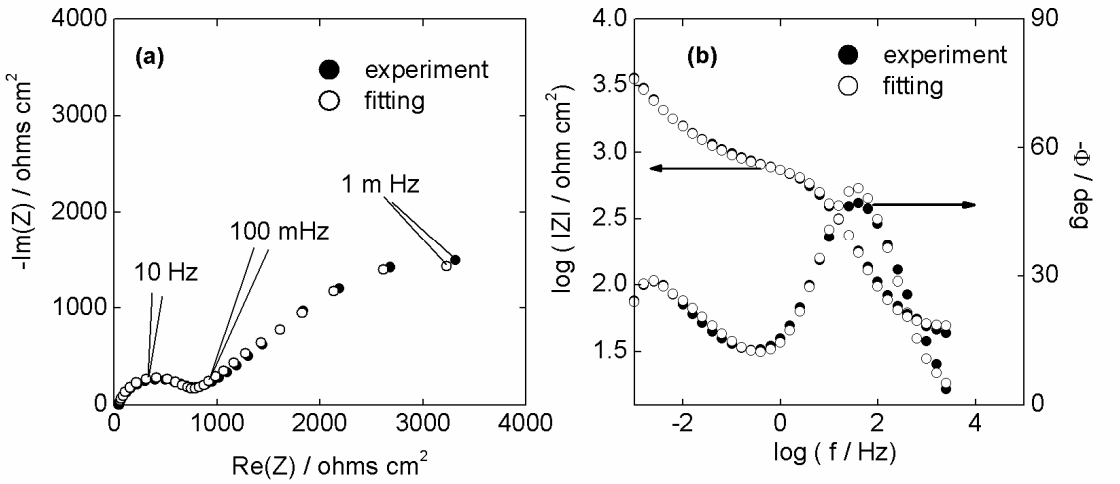


**Figure 5.S1.** Nyquist (a) and Bode (b) plots of impedance data for PMETAP-modified electrodes in 0.1 M $NaClO_4$ containing 1 mM $K_3[Fe(CN)_6]/K_4[Fe(CN)_6]$ (1:1) mixture at T = 10°C. Experimental data (●) and fit results (○).

Figure 5.S2 shows impedance spectra for an electrode modified with an initial SAM containing 100% thiol initiator without subsequent brush growth recorded at 40° C. Nyquist diagrams exhibit a semicircle in the high frequencies f region followed by a straight line with a slope approaching -45º at low frequencies. The semicircle is related to electron transfer-limited processes at the uncovered gold surface, whereas the straight line is compatible with semi-infinite linear diffusion or Warburg diffusion of the redox probe in the electrolyte.

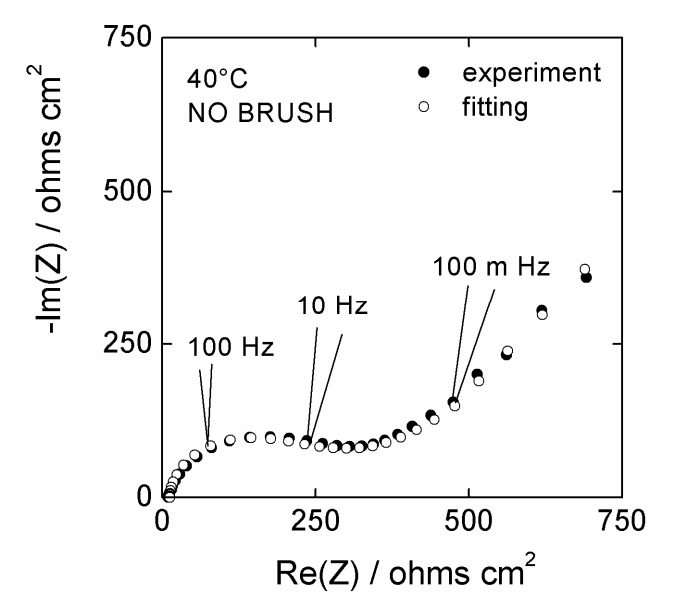


**Figure 5.S2.** Impedance spectra recorded at 40°C for an electrode modified with an initial SAM containing 100% thiol initiator without subsequent brush growth. Measured and fitted data represented as Nyquist diagrams. Experimental data (●) and fit results (○) according to the equivalent circuit (Fig. 5.2 Chapter 5) and the faradaic impedance $Z_f$ according to Equation (5.S4).

The main difference with spectra obtained for brush-modified electrodes is the type diffusion observed in the low frequency region. Consequently, data in Figure 5.S2 can be fitted using the same equivalent circuit but with an expression for $Z_f$ in terms of the Warburg impedance

$$Z_f = R_{ct} + \frac{\sigma}{\sqrt{\omega}}(1 - j) \qquad (5.S4)$$

where $\sigma$ represents the Warburg coefficient. Finally, Figure 5.S3 shows impedance spectra for an electrode modified with an initial SAM containing 100% thiol initiator without subsequent brush growth recorded at 15° C. The same dynamic behavior is

obtained as in the spectra shown in Figure 5.S2 in the whole frequency range, but with smaller charge transfer resistance due to the temperature effect.

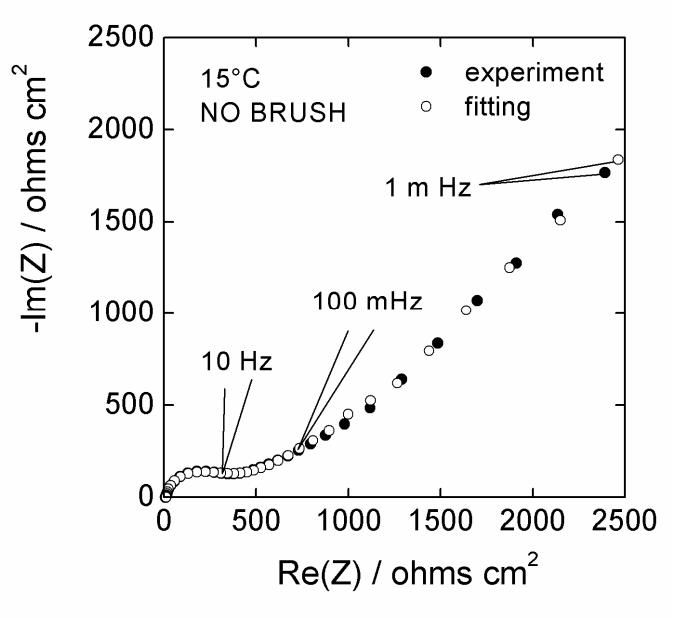


**Figure 5.S3.** Impedance spectra recorded at 15°C for an electrode modified with an initial SAM containing 100% thiol initiator without subsequent brush growth. Measured and fitted data represented as Nyquist diagrams. Experimental data (●) and fit results (○) according to the equivalent circuit (Fig. 5.2 Chapter 5) and the faradaic impedance $Z_f$ according to Equation (5.S4).

## 5. 5S4.TEMPERATURE EFFECTS ON THE CHARGE TRANSFER RESISTANCE OF INITIATOR-TERMINATED SELF-ASSEMBLED MONOLAYERS.

The charge transfer resistance is directly related to the electron transfer reaction of the probe molecules at the gold surface. Both in presence and in absence of a polymer brush the electron-transfer reaction takes place at bare spots or pinhole sites on the electrode surface. Consequently, the fractional coverage of the (initiator) thiol monolayer determines the absolute value of the measured charge-

transfer resistance. Charge transfer resistance was obtained after fitting experimental data measured in the high frequency range ($10^5$ Hz - $10^{-1}$ Hz).

Hence, it is important to note that the charge transfer resistance values informed here cannot be compared directly with data reported in the literature, without considering: (a) apparent electrode area and (b) surface coverage. Calculation of the apparent fractional coverage for the charge transfer resistance at 25°C informed in the present work yields the value 0.93 and consequently within the range of typical coverages reported in the literature. Coverage was calculated according to equation 9 in Ref. 5.S3, for an electrode with 1 $cm^2$ apparent area and considering that the charge-transfer resistance for $Fe(CN)_6]^{4-/3-}$ on bare gold is 24.4 ohms $cm^{-2}$. It should be recognized that under environmental conditions leading to strongly collapsed brushes, e.g.:1 M LiClO4,, charge transfer resistance values can be strongly affected by the conformational state of the polymer layer. However, this is not the case in our experimental systems where $R_{ct}$ is only affected by the glass transition.

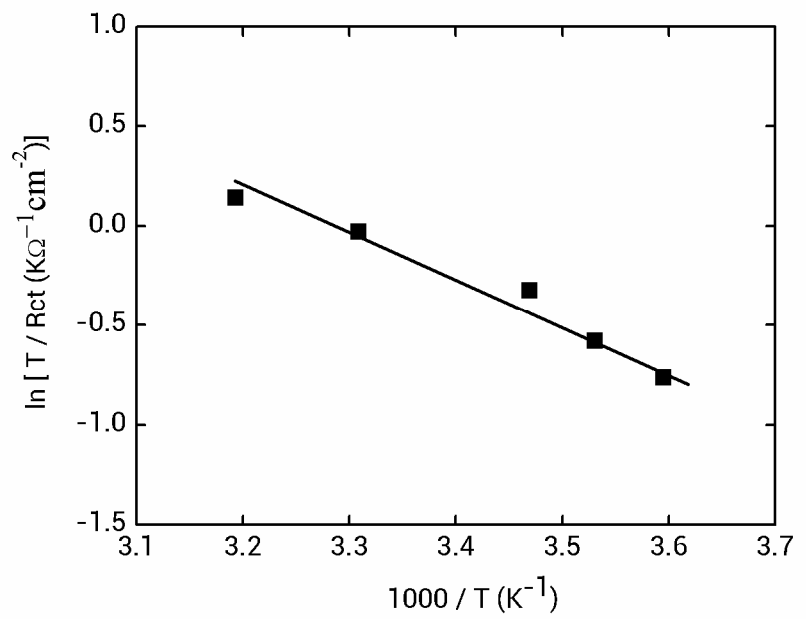


**Figure 5.S4.** Arrhenius-type plot showing the dependence of ln ($T/R_{ct}$) on the inverse temperature ($T^{-1}$) for a gold electrode modified with an ATRP initiator-terminated self-assembled monolayer. The slope of the correlation line hints that a single value of activation energy, Ea, is governing the process within the experimental temperature range.

Regarding the temperature dependence of the SAM resistance, it is worth clarifying here that no thermal transitions associated with this process are expected within our experimental temperature range. Figure 5.S4 shows that in the absence of the polyelectrolyte brush and with the electrode covered by the initiator-terminated SAM there is no breaking point in the Arrhenius plot for the rate constant since no thermal transition takes place. On the other hand, in the presence of the brush for temperatures lower than 17 °C the Arrhenius plot exhibit a much larger value for the activation energy and consequently, much larger charge transfer resistance values were measured (Fig. 5.4 Chapter 5). Finally, as already described above, with the

electrode covered by the initial SAM the low frequency region of the impedance spectra correspond to semi-infinite diffusion in the electrolyte, while in the presence of the brush this spectral region is related to a finite-length diffusion of the electroactive probe inside the brush. This shows that impedance measurements can sense in a distinctive way the effect of thermally induced transitions on both electron transfer and diffusion processes occurring in the polymer brush.

## 5.5S5.REFERENCES

(33). Azzaroni, O.; Gervasi, C. A. In *Functional Polymer Films,* Vol. 2 *Characterization and Applications*, First Edition; Knoll, W.; Advincula, R C. Eds; Wiley-VCH Verlag GmbH & Co. KgaA: Weinheim, Germany, **2011**; Chapter 26, pp. 809-830.

(34). R. P. Janek, W.R. Fawcett, *Langmuir* **1998,** *14,* 3011-3018.

# Chapter 6

## TEMPERATURE-DEPENDENT TRANSPORT PROPERTIES OF POLY [2(METHACRYLOYLOXY)ETHYL] TRIMETHYLAMMONIUM CHLORIDE BRUSHES RESULTING FROM ION SPECIFIC EFFECTS.

## ABSTRACT

Combined use of electrochemical techniques (EIS and CV) and QCM-D allowed to resolve separately the thermal effects on diffusion and electron-transfer steps of the electrochemical reaction of the $[Fe(CN)_6]^{3-/4-}$ redox couple at a Au electrode modified with poly[2-(methacryloyloxy)ethyl]trimethylammonium chloride (PMETAC) brushes. Arrhenius-type dependences of the kinetic constant and the diffusion coefficient with temperature were observed in different electrolytes. Ion-paired collapsed polyelectrolyte brushes in $NaClO_4$ result in compact stiff structures with less amount of entrapped water and markedly different from the same brushes with a collapse driven by pure Coulombic screening in NaCl. A remarkable difference related to the type of counterion is the occurrence of a thermal transition for the polyelectrolyte brush in the presence of $ClO_4^-$ ions at near-ambient temperature (~17°C). Activation energies for electron transfer and diffusion processes become twice as large as those for temperatures above the thermal transition. These electrochemical studies demonstrate not only the critical role of ion-pairing interactions in determining the physicochemical properties of the macromolecular system but also provide experimental evidence of counterion-induced thermocontrolled transport functionality in the polyelectrolyte brush layer.


## 6.1. INTRODUCTION

Polyelectrolyte (PE) brushes are assemblies of charged macromolecules tethered at one end of their chains to a substrate while the other end is free. PE brushes normally exhibit a responsive behavior (transition between extended and collapsed

conformational states) with changes in the ionic strength of the solution inside the polymer matrix. Thus, brush thickness, mechanical properties, friction and wettability can be varied changing the ionic strength and in some cases by means of specific ion interactions, i.e., the so-called hydrophobic or ion-pairing collapse. This responsive character of PE brushes has been explored in the design of surfaces with a "smart" function. [1]

Poly [2-(methacryloyloxy)ethyl]trimethylammonium chloride (PMETAC) brushes are cationic PE brushes that have been shown to suffer a hydrophobic collapse as mentioned above.[2] This hydrophobic collapse is explained as a result of a strong interaction between the quaternary ammonium groups of the brushes with large polarizable ions such as $ClO_4^-$ or $I^-$. These ions have affinity for unstructured water and find a suitable environment in the bulky hydrophobic region of the quaternary ammonium groups, contributing at the same time to an increase in their hydrophobic character. As a consequence, brush collapse in presence of these ions takes place at lower counterion concentrations than when collapse is driven purely by changes in the solution ionic strength, e.g., in the presence of NaCl. Moreover, the hydrophobic collapse results in a much larger water loss for the brush and induces a significant change in surface wettability. The percentage of water removed reaches ca. 54% in 0.1 M $ClO_4^-$ in contrast to slightly more than 17% in 0.1 M $Cl^-$ solution.[3,4]

Among the different properties of the brush that are affected by the brush collapse the transport properties are of particular importance since they are essential for the application of brushes as coating or barriers. It has been indeed shown how the

swelling/collapse behavior of thin polyelectrolyte brushes governs the interfacial impedance. [5,6] Transport phenomena have been recently studied by impedance methods in PMETAC brushes under collapse due to both pure charge screening and ion-pairing, in presence of NaCl and $NaClO_4$, respectively. Results obtained at 25°C show that the diffusion of an electroactive probe is significantly restricted inside the brush in both electrolytes with diffusion coefficient values ranging from 2 x $10^{-13}$ $cm^2s^{-1}$ to 5 x $10^{-14}$ $cm^2$ $s^{-1}$. Clearly, differences in probe mobility between both electrolytes are relatively small at 25°C. Slightly lower diffusion coefficients measured in $NaClO_4$ solution as compared with NaCl solution can be understood on the basis of the lower water content that restricts the diffusive pathways of the probe within the brush and limits polymer chain mobility of the brushes.

Recently we have also shown that measuring the electrochemical behavior of PMETAC brushes in presence of $ClO_4^-$ ions a steep thermal transition at 17 °C can be observed for the brushes. In this article we aim at addressing the activity of the brush-modified electrode according to the temperature and in relation to the nature of the counter ion and the type of collapse associated, either by Coulombic screening or ion-paring interactions. By doing so, we intend to obtain a deeper insight into the brush structure during the collapse. Transport studies according to the temperature are also fundamental for the application of brushes as barriers or for permeability control. Moreover, the study of transport phenomena in relation to the temperature can provide fundamental information to interrogate the mechanisms of diffusion of electroactive probes through brushes. Indeed, an electrochemical reaction on the surface of an electrode has two limiting mechanisms: the reaction is under kinetic control or the reaction is controlled by the

diffusion of the electroactive species. Recently, in order to describe the electrochemical response of the modified electrode a model was presented considering a planar diffusion step for an electroactive molecular probe, where the brush layer acts as a diffusion-limiting barrier of finite thickness, followed by the electron transfer step at the electrode surface. [7] In these studies, it was shown that the conformational transition of the polymer brush affects the mass transport of the redox probe through the new structure of the macromolecular array and, for a strongly collapsed brush, this also affects the fraction of active surface available for the electron transfer. Since both diffusion and electron transfer are activated processes, but only the electron transfer rate is dependent on the active surface (unlike the diffusion coefficient), a study of the temperature dependence of the rate constant and the diffusion coefficient allows to deepen our understanding on this subject. Therefore, in a scenario of a possible temperature-affected characteristic for this interface it is essential to assess whether the polymer brush suffering a transition process preferentially restricts mass transport or blocks electron transfer at the active electrode surface. Additionally, quantifying temperature effects on both the diffusion coefficient and the rate constant, represents a useful way to validate the proposed theoretical model and derive useful thermodynamic data to get an insight as to how the relative contributions of each reaction step determine the reaction control according to the brush conformational state.

In the present article the interfacial electrochemical behavior of Au electrodes modified with PMETAC brushes was characterized varying bulk temperature in 0.1 M NaCl and $NaClO_4$-solutions by electrochemical impedance spectroscopy (EIS) and cyclic voltammetry (CV) using $[Fe(CN)_6]^{3-/4-}$ as the redox probe. Additionally,

quartz crystal microbalance with dissipation (QCM-D) studies were performed to asses changes in brush thickness and water content with the different salts studied.

## 6.2. Experimental

### 6.2.1 Synthesis of Polyelectrolyte Brushes

PE brushes were grown from self-assembled monolayers of ω–mercaptoundecylbromobutyrate as the initiator thiol. The thiol monolayers were deposited on clean gold substrates whose preparation is described in detail elsewhere.[8] The assembly of the thiol was perfomed from a $10^{-2}$ M methanolic solution of the initiator. Brushes were synthesized by atom transfer radical polymerization (ATRP). The polymerization solution was prepared as follows: 1 mL of commercially available (Aldrich) METAC monomer (75 wt. % solution in water), 40 mmol, were dissolved in a mixture of 2 $cm^3$ of water and 3 $cm^3$ of dimethylformamide (DMF), 99.85%, at 20 ºC and degassed by passing a continuous stream of dry $N_2$ through the solution whilst being stirred, approximately for 15 minutes. 2,2'-Bipyridyl (416 mg, 2.7 mmol), $Cu^{I}Cl$ (105 mg, 1.1 mmol) and $Cu^{II}Cl_2$ (14 mg, 0.11 mmol) were added to this solution. The mixture was then further stirred and degassed with a stream of dry $N_2$ for another 15 minutes. Gold substrates coated with the initiator were sealed in Schlenk tubes, degassed and left at 20 ºC under $N_2$. The polymerization solution was then syringed into each Schlenk tube, adding enough solution to submerge each sample completely. Once the polymerization step is accomplished, the samples were carefully removed from the Schlenck tubes, washed with water, then with methanol, and finally dried under a stream of $N_2$.

### 6.2.2 Characterization Techniques

#### *6.2.2.1 In situ* QCM-D measurements

Growth of the polymer brush and brush thickness were measured by QCM-D on the same surface and in the same liquid environment. Measurements were performed using a purpose-built flow cell (Q-Sense AB, Västra Frölunda, Sweden) with a total volume of ~300 µL. The flow cell was attached to a Q-Sense E1 setup, providing access to QCM-D data. QCM-D data, $\Delta f$ and $\Delta D$, were acquired at 6 overtones ($i$ = 3, 5 … 13, corresponding to resonance frequencies of $f_i \approx$ 15, 25 … 65 MHz) simultaneously, with sub-second time resolution.

#### 6.2.2.2 Electrochemical techniques

Electrochemical measurements were carried out within the 5°C – 45°C temperature range in a conventional three-electrode cell. A platinum sheet with large area and a saturated calomel electrode (SCE) were used as the counter electrode and the reference electrode, respectively. All potentials are referred to the SCE at 25°C. Au substrates coated with brushes served as working electrodes. 0.1 M NaCl and 0.1 M $NaClO_4$ solutions were used as supporting electrolytes and prepared from analytical grade (Merck) reagents and Milli-Q water. Experiments were performed under purified $N_2$ gas saturation in a solution of the redox couple consisting of 1 mM $K_3[Fe(CN)_6]$ / $K_4[Fe(CN)_6]$ (1:1) mixture in the supporting electrolytes. As already discussed by Huck and co-workers, due to their much larger concentration, counterions will preferentially displace redox probe molecules coordinated with PMETAC brush chains, and consequently, conformational collapse of PMETAC brushes proceeds only affected by the presence of chloride and perchlorate ions. [9]

Cyclic voltammetry (CV) measurements were performed by scanning the potential at a scan rate of 0.05 $Vs^{-1}$.

Impedance spectra were obtained with a Zahner IM6d electrochemical workstation. The dc potential of the working electrodes was held at the open circuit potential while a 10 mV amplitude ac potential was applied. The voltage signal frequencies used for EIS measurements ranged from 100 kHz to 1 mHz. Impedance data analysis was performed according to proper procedures for transfer function derivation and identification by using complex nonlinear least-squares (CNLS) fitting based on the Marquardt-Levenberg algorithm.

## 6.3. RESULTS AND DISCUSSION

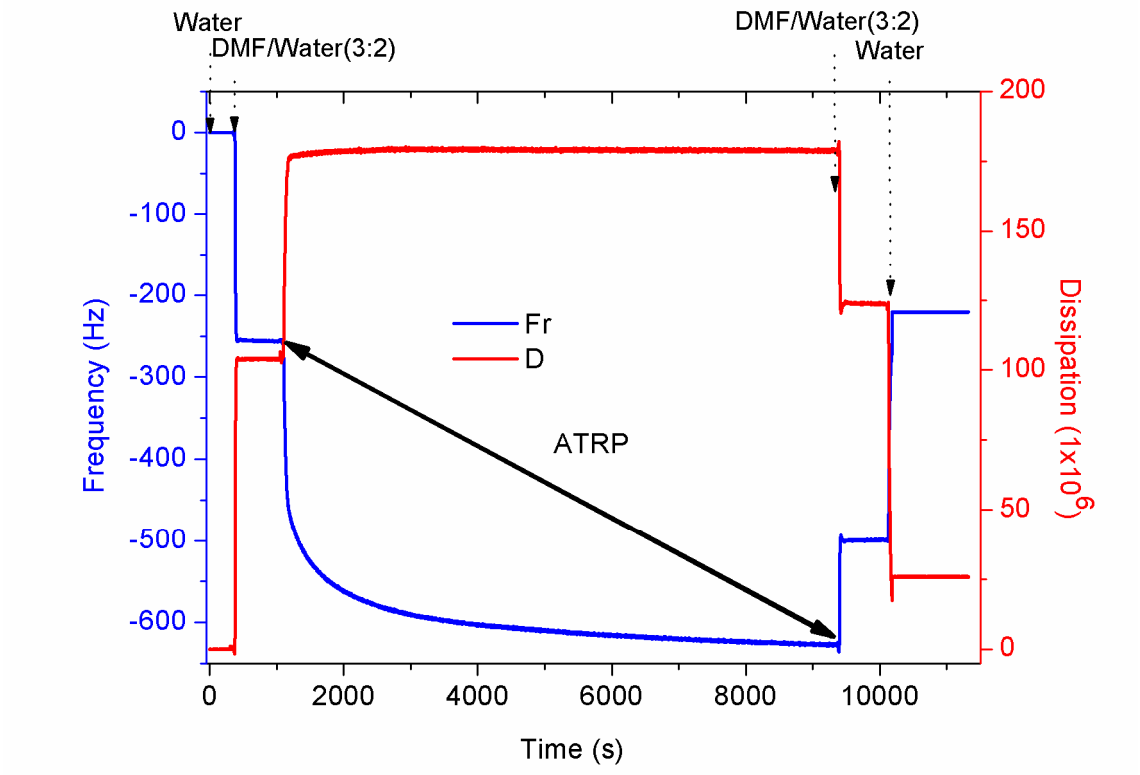

**Figure 6.1.** Synthesis of the PMETAC brush from a monolayer of w–mercaptoundecylbromobutyrate assembled on top of a gold surface. QCM–D response, i.e., Δ*f* and Δ*D* vs. time for a selected overtone ($3^{rd}$).

Figure 6.1 shows data recorded with the QCM-D technique as the $3^{rd}$ overtone evolution with time of the acoustic parameters frequency (blue line) and dissipation (red trace) related to the growth of a PMETAC brush grown from a monolayer of ω–mercaptoundecylbromobutyrate previously assembled on the gold-coated QCM-D substrate. Frequency follows a continuous decrease according to the polymerization process that is indicative of the progressive mass growth on top of the substrate. At the same time, values for the dissipation rise as the polymerization progresses, indicating the formation of a film with a viscoelastic character. After ATRP polymerization, a consecutive rinse with a DMF/water (3:2) mixture and pure water sweeps the polymerization solution away. This results in an increase in frequency and a corresponding decrease in dissipation. Considering the relationship between dissipation and frequency values and the Sauerbrey equation (see below) it is possible to estimate the increase in total film mass, $m_{QCM}$ as the brush grows according to the total measured change in frequency $\Delta f = -225$ Hz.

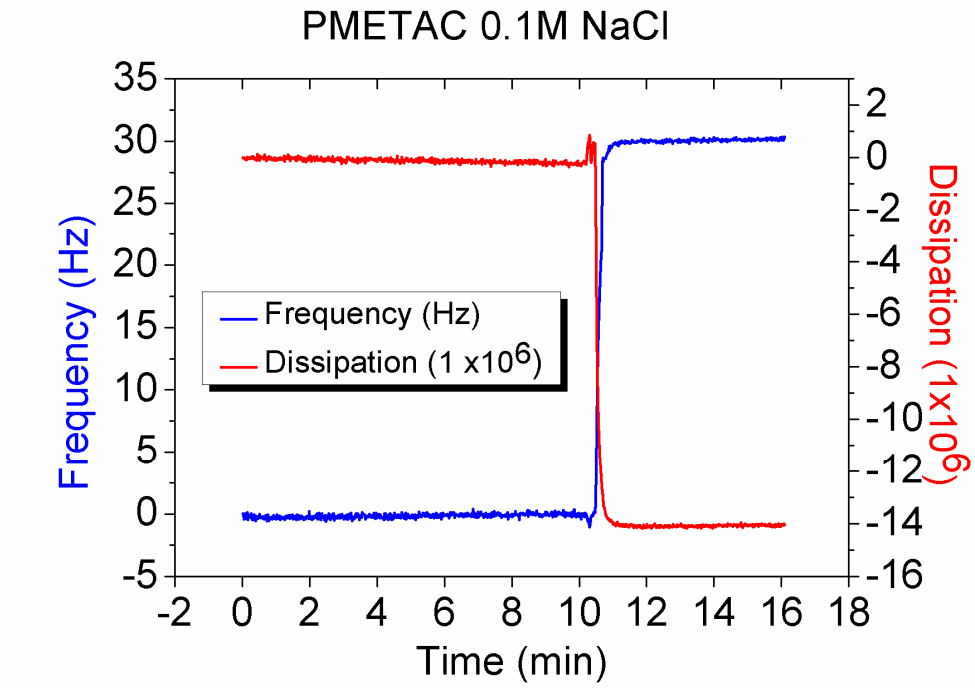


**Figure 6.2.** Temporal variation of the frequency (blue line) and dissipation (red trace) during the collapse of the PMETAC-brush in 0.1 M NaCl solution.

Figure 6.2 shows the time evolution of frequency and dissipation (3$^{rd}$ overtone) during a brush collapse in presence of 0.1 M NaCl. The salt solution was injected at minute 10 causing an increase in the frequency in 30 Hz and a decrease in dissipation in 14 relative units.

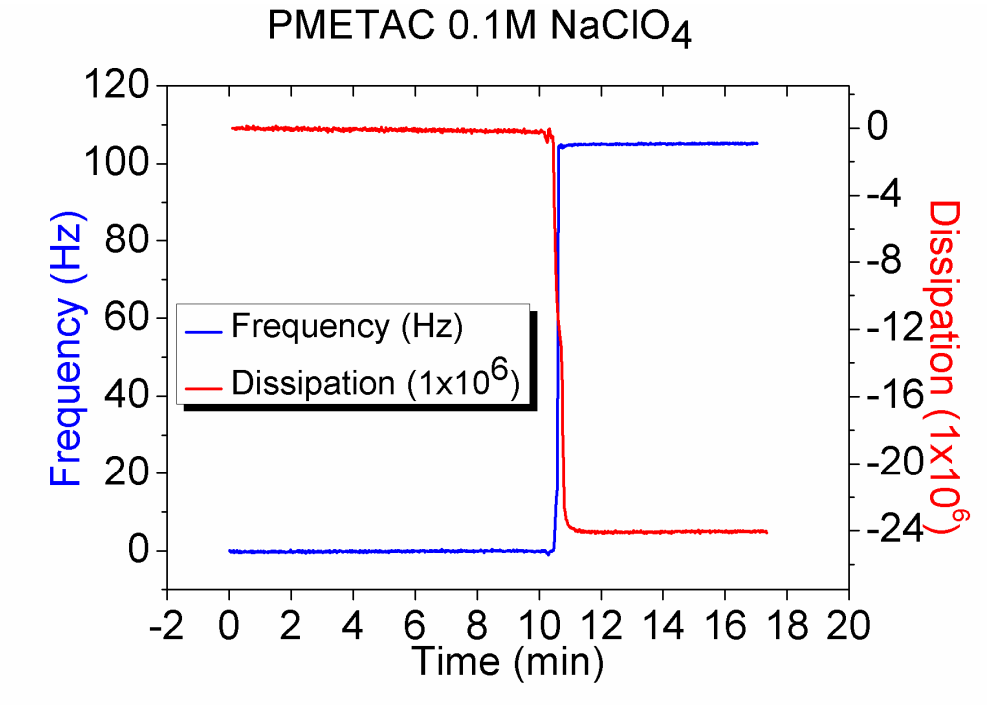


**Figure 6.3.** Temporal variation of frequency (blue line) and dissipation (red trace) related to a PMETAC-brush collapse in 0.1 M $NaClO_4$ solution.

Figure 6.3 depicts time-evolutions of frequency and dissipation (3$^{rd}$ overtone). Larger values for the changes in the acoustic parameters associated with a brush collapse due to the addition of 0.1M $NaClO_4$ indicate a stronger effect of perchlorate ion in comparison with chloride ion.

QCM-D data were evaluated quantitatively in terms of the Sauerbrey equation that links frequency shifts and adsorbed masses per unit area in the following simple way [10]:

$$m_{QCM} = -C\frac{\Delta f_i}{i} \qquad (6.1)$$

with the mass sensitivity constant, C = 18.06 ± 0.15 ng·cm$^{-2}$·Hz$^{-1}$ for sensors with a resonance frequency of 4.95 ± 0.02 MHz, and the overtone number *i*. The normalized frequency shifts, $\Delta f = \Delta f_i / i$, for the 3$^{rd}$ overtone were employed to

determine $m_{QCM}$. The applicability of Equation (6.1) is limited to sufficiently rigid films. For soft and dissipative films, more complex models would be required that account for their viscoelastic properties.[11,12]

For the PMETAC brushes investigated here, the ratio of dissipation and normalized frequency shifts, $\Delta D/(-\Delta f)$, indicates that Eq. (6.1) is a good approximation. The application of different viscoelastic models to selected data-sets (details of the modeling procedure are detailed elsewhere [13]) corroborated that the Sauerbrey equation is indeed a good approximation for our films, with an error below 5%. The experimental noise was typically below 2 ng/cm$^2$.

The brush thickness was further determined by

$$d_{QCM} = m_{QCM} / \rho_{Brush} \qquad (6.2)$$

where $\rho_{Brush}$ = 1.0 g/cm$^3$ is the density of the solvated polymer film. In the pure form, the employed polymer exhibits densities between 1.0 and 1.1 g/cm$^3$, while the density of water or salt solutions is also 1.0 g/cm$^3$. Hence, equation (6.2) could overestimate the thickness by at most 10%.

Combining equations (6.1) and (6.2) results in the following relationship: $d_{QCM}(nm) \cong -\frac{1}{5}\Delta f(Hz)$ that relates film thicknesses and the corresponding normalized frequency shifts at the end of the polymerization step (brush immersed in water) and after exposure of the brushes to the salt solutions (0.1 M NaCl and 0.1 M $NaClO_4$), respectively.

Owing to its acousto-mechanical transducer principle, the QCM-D technique is not only sensitive to the adsorbed molecules but also to the solvent retained within or hydrodynamically coupled to the surface-bound film. Therefore, from the QCM frequency response alone, it is difficult to discriminate between the adsorbed polymer mass and the contribution of the solvent coupled to the polymer. Polyelectrolytes are charged molecules with hydrated monomers. Besides that, water can be entrapped in cavities between neighboring chains. The QCM-D will thus sense the total mass of the brush, consisting of polyelectrolyte and water. Moreover, it can measure the amount of water that is reversibly lost during collapse with the ionic strength.

An evaluation of data in Figure 6.1 yields $\Delta f = -225$ Hz, corresponding to $d_{QCM} = 45$ nm. This value represents the total thickness in aqueous medium of the PMETAC brush.

From Figure 6.2 a change $\Delta f = 30$ Hz can be observed after adding 0.1 M NaCl corresponding to a reduction in film thickness of 6 nm, while the addition of 0.1 M $NaClO_4$ results in a $\Delta f$ change = 105 Hz, corresponding to a reduction in film thickness of 21 nm. Consequently, final thicknesses of collapsed PMETAC brushes are 39 nm in 0.1 M NaCl solution and 24 nm in 0.1 M $NaClO_4$ solution as shown in Figure 6.4.

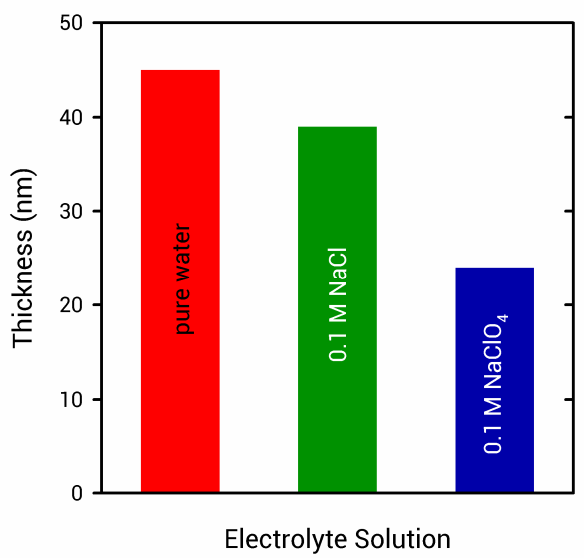


**Figure 6.4.** Calculated values for the acoustic thickness ($d_{QCM}$) as measured in pure water, chloride and perchlorate solutions.

Exposure of the brush to salt solutions yielded positive changes in frequency, indicative of brush collapse and water mass loss.[14] Data from the literature inform the hydration % of PMETAC brushes in water and after collapse transitions in $Cl^-$– and $ClO_4^-$–containing electrolytes.[4,15] The initial water content of the brushes, expressed as the percentage of solvent contributing to the total film mass, was informed to be ca. 67%. Comparing the percentages of water loss related to collapsed conditions it can be observed that while NaCl solution only removes 17 % of the entrapped water through the originated collapse, $NaClO_4$ solution provokes the release of 54 % of the water initially entrapped before collapse.

In Figure 6.5 we observe the effect of changing the electrolyte temperature T on the voltammetric response of an electrode modified with a PMETAC brush in 0.1 M $Cl^-$ solution containing 1 mM $K_3[Fe(CN)_6]$ / $K_4[Fe(CN)_6]$.

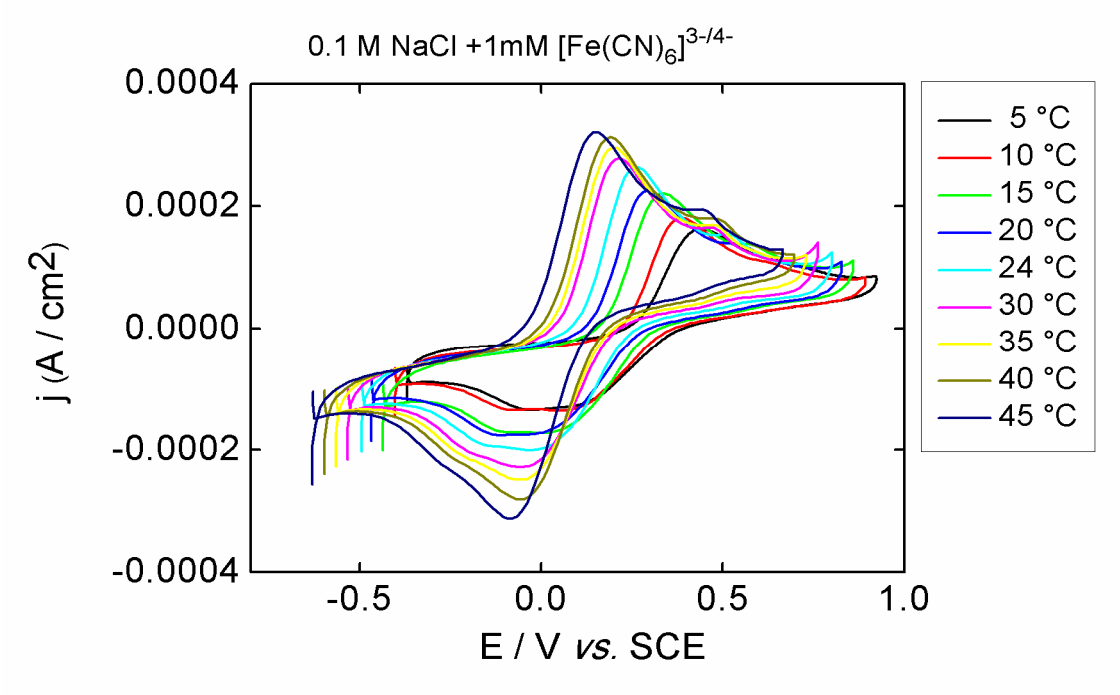


**Figure 6.5.** Voltammetric responses of a brush-modified Au electrode in 0.1 M NaCl + 1 mM $[Fe(CN)_6]^{3-/4-}$ for different electrolyte temperatures as indicated in the inset.

Comparable results are shown in Figure 6.6 for the same experimental conditions as in Figure 6.5 but in 0.1 M $ClO_4^-$ solution containing 1 mM $K_3[Fe(CN)_6]$ / $K_4[Fe(CN)_6]$.

Anodic and cathodic peak current densities $j_p$ become larger at higher temperature T in both electrolytic solutions.

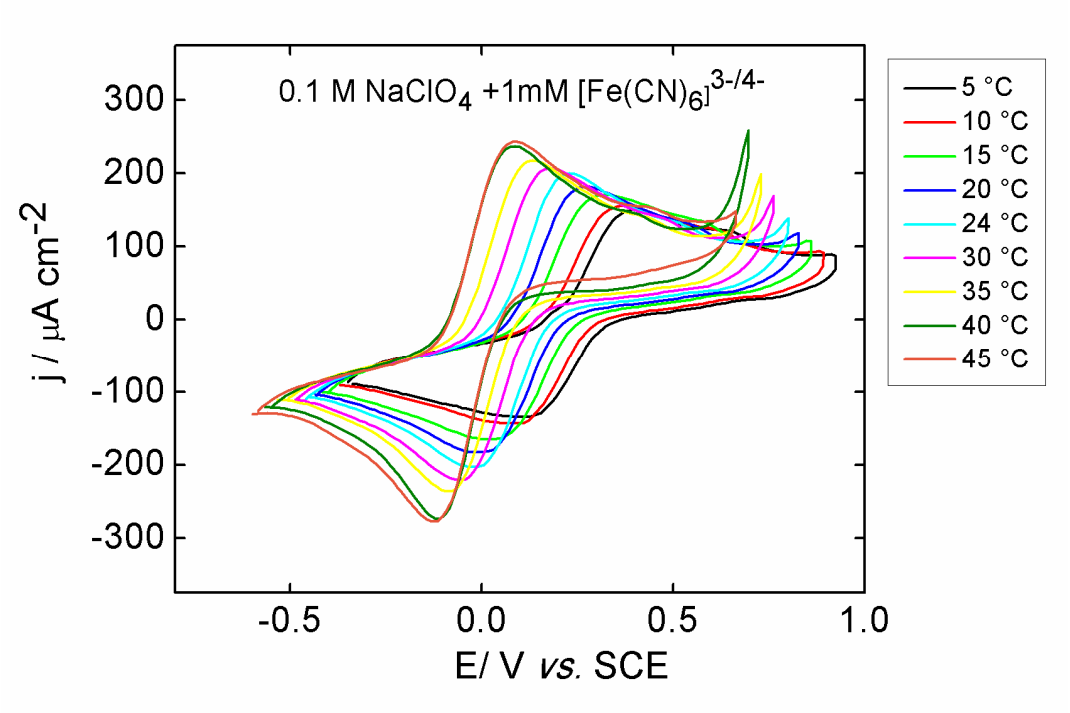


**Figure 6.6.** Voltammetric response of a Au electrode coated with a PMETAC brush in 0.1 M $NaClO_4$ + 1 mM $[Fe(CN)_6]^{3-/4-}$ at different electrolyte temperatures as indicated in the inset.

The separation of peak potentials ($\Delta E_p$) becomes smaller for higher T, in both electrolytes, as shown in Figure 6.7, although at each temperature, $\Delta E_p$ is larger than the value obtained for the same redox couple on bare gold surfaces that is characterized by a highly reversible electrochemical reaction. $\Delta E_p$ values measured in $NaClO_4$ solution are almost constant at the lowest studied temperatures; in principle, this indicates a singular behavior associated with the presence of the $ClO_4^-$ anion. Here, it is perhaps worth mentioning that voltammetric peaks in the low T range are less sharp while peak current values cover a somewhat extended potential window. It has been indicated in the literature that it is necessary to be cautious about interpreting these trends because of the difficulties in determining accurate redox potentials from voltammograms adopting a sigmoidal shape.[16]

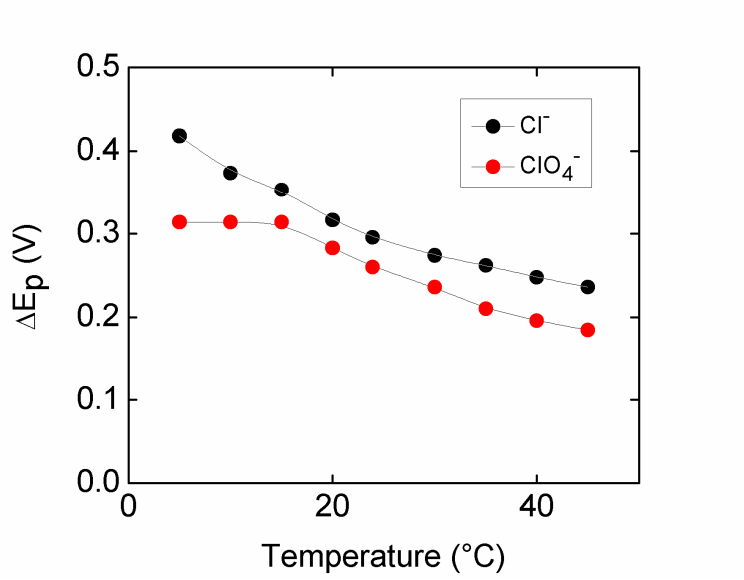


**Figure 6.7.** Variation of the separation of peak potentials ($\Delta E_p$) with the electrolyte temperature for chloride and perchlorate solutions. Values derived from data in Figures 6.5 and 6.6.

Data in Figures 6.5, 6.6 and 6.7 are consistent with a quasi-reversible electron transfer model. For a SAM-modified electrode a marked decrease in the peak currents is observed in the cyclic voltammogram as well as an increase in the splitting of the peak potentials, while the voltammogram tends to adopt a sigmoidal shape. These observations indicate that the electron transfer reaction might be occurring at pinhole sites. [17]

Higher peak current densities and smaller peak separations for increasing T can be interpreted in terms of faster electrochemical kinetics exhibited by the electron transfer reaction at the surface and higher diffusion coefficients D of the redox probe inside the brush. However, one cannot succeed in separating the individual effects of T on each reaction step from the voltammetric responses. Thus, slow interfacial charge transfer cannot be distinguished from hindered diffusion effects.

Therefore, to gain a deeper insight into this question we performed impedance experiments, where both effects can be separated.

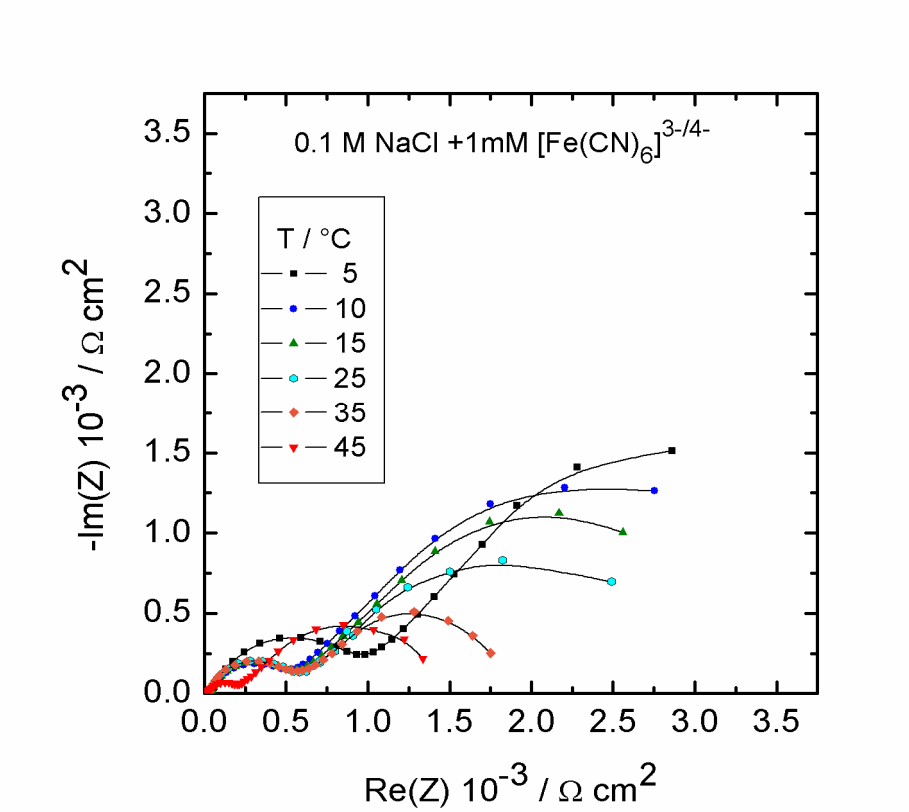


**Figure 6.8**. Nyquist plots of the experimental impedance measured with a Au electrode modified with a PMETAC brush at different temperatures in the presence of $1\times10^{-3}$ M $[Fe(CN)6]^{3-/4-}$ + 0.1 M NaCl.

Figure 6.8 shows impedance spectra for an electrode modified with the PMETAC brush immersed in NaCl solution at different temperatures within the 5 °C-45°C range. Nyquist diagrams in Figure 6.9 exhibit a semicircle in the high frequencies f region followed at low frequencies by impedance values containing diffusion effects corresponding with a finite-length diffusion-type impedance. Impedance values decrease according to T in the whole frequency range.

The same qualitative behavior was measured for an electrode modified with the polyelectrolyte brush immersed in $NaClO_4$ solution (Figure 6.9).

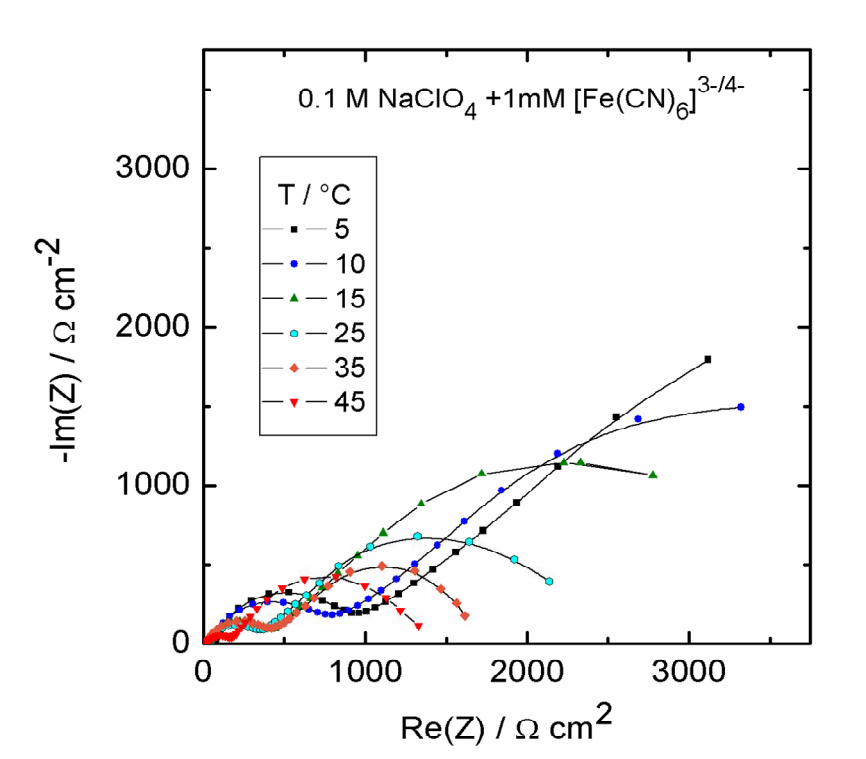


**Figure 6.9.** Nyquist plots of the experimental impedance measured with a Au electrode modified with a PMETAC brush at different temperatures in the presence of $1\times10^{-3}$ M $[Fe(CN)6]^{3-/4-}$ + 0.1 M $NaClO_4$.

The high-f semicircle is related to electron-transfer processes at the uncovered gold surface.[18] The semicircle diameter represents the charge-transfer resistance $R_{ct}$, whereas the intercept of the semicircle with the real part of the impedance Re(Z)-axis for $f \rightarrow \infty$ corresponds to the bulk solution resistance, $R_e$. $R_{ct}$ contains kinetic information according to the following expression.

$$\frac{1}{R_{ct}} = A_e F\left[C_O^{dc}\left(\frac{k_c \alpha_c F}{RT}\right) + C_R^{dc}\left(\frac{k_a \alpha_a F}{RT}\right)\right] \qquad (6.3)$$

where $\alpha_a$ and $\alpha_c$ are the transfer coefficients, $k_a$ and $k_c$ correspond to the rate constants for the anodic and cathodic reactions, respectively, $C_O$ and $C_R$ represent concentrations of the oxidized and reduced species at the surface for dc conditions, $A_e$ is the electrode area while R and F are the gas and Faraday constants, respectively.

Impedance values in the low-f region are related to the brush layer building a diffusion-limiting barrier of finite thickness $\delta$ for the electroactive molecular probes. In this way the electrode is uniformly accessible to mass transfer through a hydrated brush of finite thickness.

In the transition region between the semi-infinite and the true finite diffusion control, where the angular frequency $\omega \approx D / \delta^2$, the Nernst diffusion layer thickness $\delta$ corresponds to the distance travelled by the diffusion species for the low-frequency oscillating perturbations and is equivalent to the brush thickness d. Then, the diffusion impedance $Z_d$ is given by

$$Z_d = \frac{\sigma}{\sqrt{\omega}}\left[tanh\left(B\sqrt{i\omega}\right)\right](1-i) \qquad (6.4)$$

where $i = \sqrt{-1}$, $\omega = 2\,\pi\,f$, is the angular frequency of the potential perturbation and the so-called mass transfer coefficient $\sigma$ contains the contributions of the oxidized and reduced forms of the redox couple and $B = \delta/\sqrt{D}$. As already indicated above $\delta = d$, i.e., the thickness of the polymer brush and D is the diffusion coefficient. The

complete mathematical treatment used to derive equations (6.3) and (6.4) can be found elsewhere. [6,7]

Experimental impedance data were fitted to the following theoretical expression for the electrode impedance $Z_t$:

$$Z_t = R_e + \frac{1}{(i\omega)^n Y_o + \frac{1}{R_{ct} + Z_d}} \qquad (6.5)$$

resulting from the inclusion of a constant-phase-element of impedance that carries the non faradaic portion of the current and contains the parameter $Y_o$ that can be used to derive the interfacial capacitance $C_i$ with the consideration of a distribution of values on the surface. As usual, when the exponent n = 1, $Y_o$ is equal to $C_i$. Moreover, the sum ($R_{ct}$ + $Z_d$) corresponds to the faradaic or reaction impedance. The structure of this sum reflects the fact that the faradaic current, i.e., the overall rate of the electrode reaction, is controlled by two impedance elements in series connection, accounting for diffusion and reaction kinetics.[20]

The charge-transfer resistance is directly related to the electron-transfer reaction of the probe molecules at the gold surface. Both in presence of the PMETAC brush or in its absence (electrode covered only with the initial SAM) the electron-transfer reaction takes place at bare spots or pinhole sites, i.e. at the uncovered electrode surface. Consequently, the fractional coverage of the monolayer of thiol initiator is the main factor that determines the absolute value of the measured charge-transfer resistance, particularly in the absence of a strong brush collapse that could further decrease the rate constant, as indicated above. However, with the electrode

covered by the initial SAM alone the low frequency region of the impedance spectra corresponds to semi-infinite diffusion in the electrolyte, while in the presence of the brush this spectral region is related to a finite-length diffusion of the electroactive probe inside the brush. This shows again that impedance measurements can sense in a distinctive way the effect of thermally induced transitions on both electron transfer and diffusion processes occurring in the polymer brush. [6]

When the electron transfer rate of the redox couple is not markedly diminished by a collapse transition, the global reaction rate within the polymeric environment is generally controlled by ion transport or, at least, exhibits a mixed control. This might resemble the condition set by a polymer brush conformation described as a compressed state in contrast to a fully collapsed state.[21] On the other hand, when the electron transfer at the substrate is markedly inhibited due to a strong collapse of the brush, impedance data, may not be able to resolve both contributions separately. Indeed, the low frequency mass-transfer region may not be observed because the reaction is under kinetic control over the entire frequency range. In the literature, a strong conformational transition that collapses the structure was informed related to either the presence of a very high concentration of counterions exhibiting ion-pairing interactions with the polymer chain (e.g., 1 M $NaClO_4$) or for a polymer film relatively thick before collapsing. [5]

Typical results of the good agreement obtained between theory and experiment are shown in terms of both Nyquist and Bode plots in Figures 6.10 and 6.11 for a selected temperature T = 35 °C in the two electrolytic solutions.

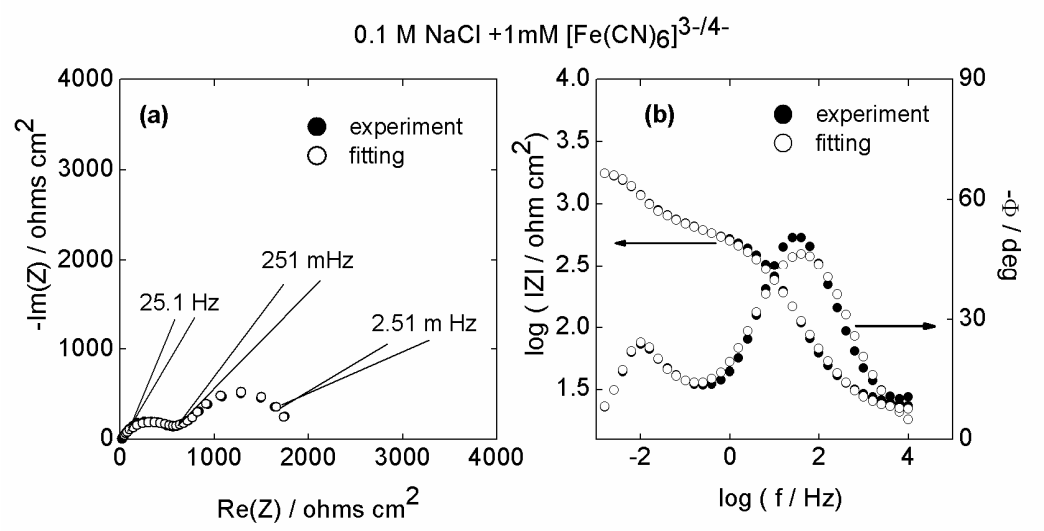


**Figure 6.10.** Nyquist (a) and Bode (b) plots of impedance data for Au electrodes coated with a PMETAC brush in 0.1 M NaCl containing 1 mM $K_3[Fe(CN)_6]$ / $K_4[Fe(CN)_6]$ (1:1) mixture at T = 35°C. Experimental data (●) and fit results (○) according to equation 6.5.

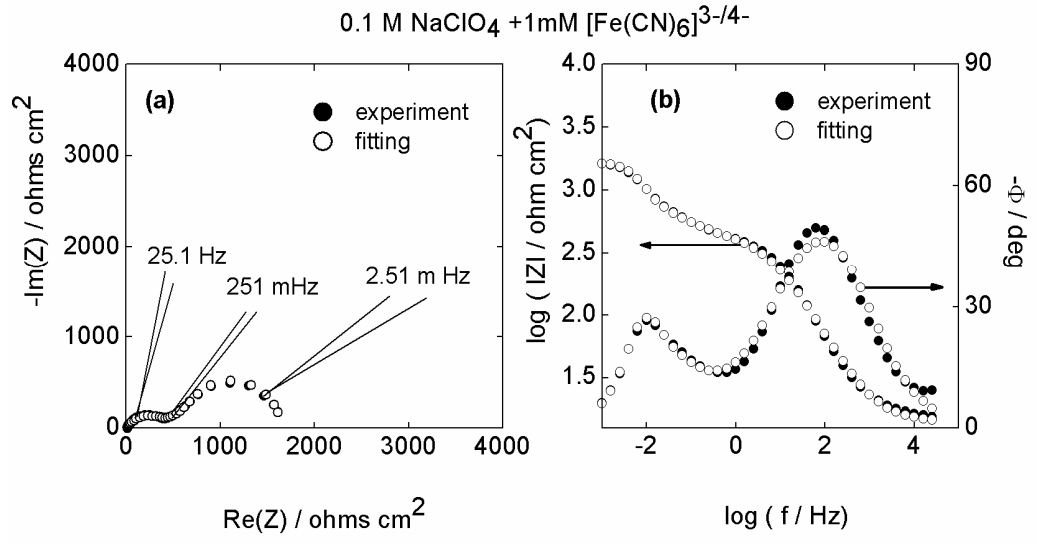


**Figure 6.11.** Nyquist (a) and Bode (b) plots of impedance data for Au electrodes coated with PMETAC in 0.1 M $NaClO_4$ containing 1 mM $K_3[Fe(CN)_6]$ / $K_4[Fe(CN)_6]$

(1:1) mixture at T = 35°C. Experimental data (●) and fit results (○) according to equation 6.5.

Interestingly, fit parameter $R_{ct}$ is inversely proportional to the real electrode area (equation 6.3) unlike fit parameter B which is independent of the electrode area. Since B is used together with the brush thickness d (previously measured) to calculate D (equation 6.4) variations in the latter cannot be ascribed to changes in the active area according to the working conditions. [16]

Assuming, as usual, that the transfer coefficients $\alpha_a = \alpha_c = 0.5$ for both anodic and cathodic reactions[22] and remembering that the applied dc potential corresponds to the formal potential of the redox couple ($C_O^{dc} = C_R^{dc} = C$) results in $k_c = k_a = k$ and equation (6.3) reduces to:

$$\frac{T}{R_{ct}} = \frac{A_e F^2 C}{R} k \qquad (6.6)$$

Since k obeys the Arrhenius equation from the slope of the linear plot $\ln\frac{T}{R_{ct}}$ vs. $\frac{1}{T}$ the activation energy can be calculated. [23]

T variations of k and D in terms of Arrhenius plots are shown in Figures 6.12 and 6.13 within the studied 5°C - 45°C temperature range in the two electrolytic solutions.

Activation energy for the diffusional process in $Cl^-$ solution (Figure 6.13a) is *ca.* 38 kJ $mol^{-1}$ while for the electron transfer is *ca*. 19 kJ $mol^{-1}$ (Figure 6.12b).

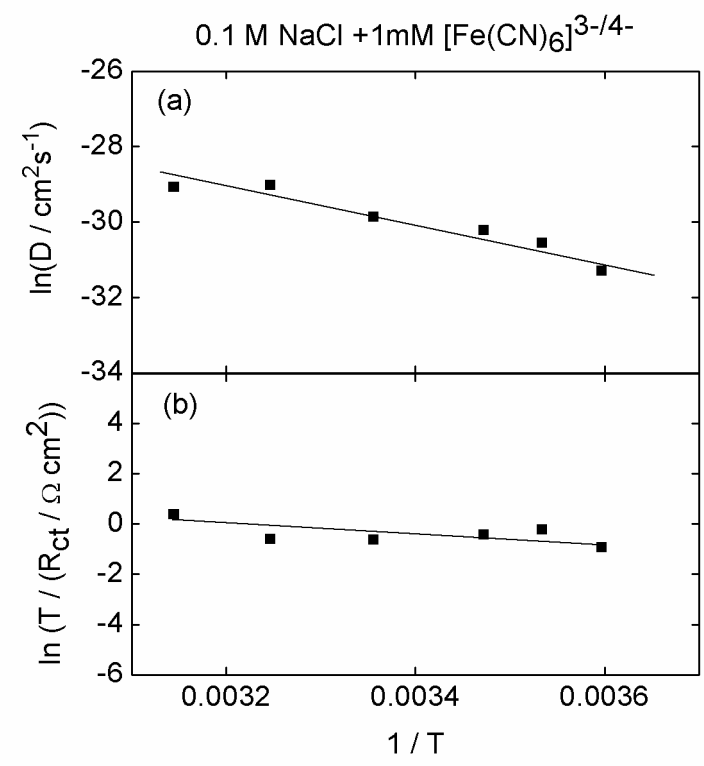


**Figure 6.12.** Arrhenius plots for the diffusion coefficient (a) and the kinetic constant (b) for Au electrodes coated with a PMETAC brush in 0.1 M NaCl containing 1 mM $K_3[Fe(CN)_6]$ / $K_4[Fe(CN)_6]$ (1:1) mixture. Data derived from impedance fit parameters ($R_{ct}$ and B) and the brush acoustic thickness ($d_{QCM}$).

In $NaClO_4$ solution (Figure 6.13b) it can be observed that the electron transfer requires different activation energies whether the process occurs below or above a certain threshold temperature that was interpreted as the glass transition temperature of the brush $T_g$; assuming a glassy state for the PMETAC brushes bearing $ClO_4^-$ counterions below this temperature. Activation energy values calculated from the experimental data are *ca*. 60 kJ/mol and 29 kJ/mol for

temperature values below and above this $T_g \cong 17°C$, respectively. These results indicate that the activation energy for the electron transfer taking place within the brush in a "*glassy*" state is twice the activation energy in the "*rubbery*" state. Moreover, around the $T_g$ the measured diffusion coefficient of the redox probe inside the brush decreases up to ca 3 times, from $4.12 \times 10^{-14}$ $cm^2$ $s^{-1}$ to $1.48 \times 10^{-14}$ $cm^2 s^{-1}$, associated with the thermal transition into the glassy region. The final value for D observed at 5 °C is $1.26 \times 10^{-14}$ $cm^2 s^{-1}$, being $2.56 \times 10^{-14}$ $cm^2 s^{-1}$ at the same temperature for the brushes in NaCl. The activation energy for the diffusional process in $ClO_4^-$ solution (Figure 6.13a) is *ca.* 24 kJ $mol^{-1}$ for temperatures above $T_g$ that result lower than the value obtained in $Cl^-$ solution. However, below $T_g$ the activation energy for the diffusional process in $ClO_4^-$ solution becomes much larger and close to 60 kJ $mol^{-1}$. Clearly, both reaction steps result independently inhibited by the thermal transition. Interestingly, polyelectrolyte multilayers modifying Au electrodes and in contact with a solution 0.5 M $NaClO_4$ and 1 mM $K_4Fe(CN)_6$ resulted in a diffusion coefficient for the redox probe inside the polymeric assembly that follows the Arrhenius law, and the activation energy was estimated as 61 kJ $mol^{-1}$.[24]

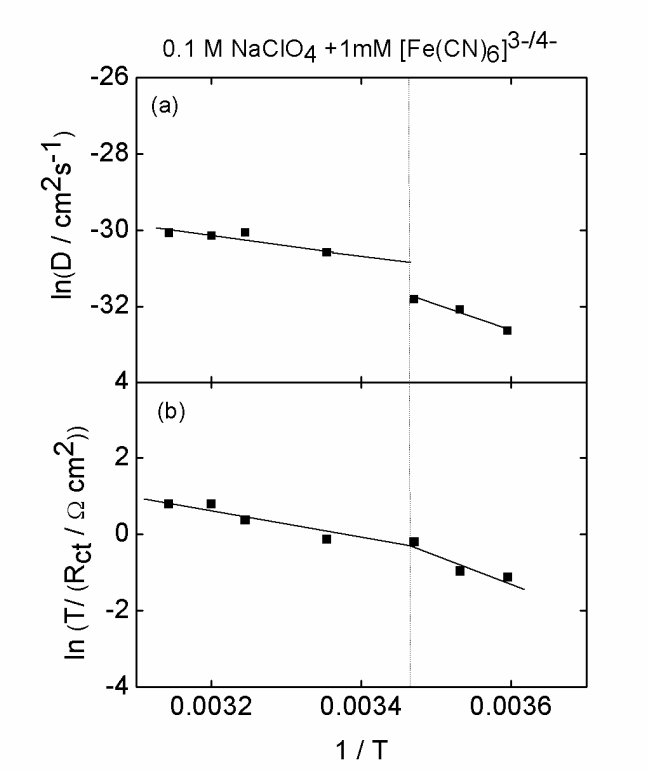


**Figure 6.13.** Arrhenius plots for the diffusion coefficient (a) and the kinetic constant (b) for PMETAP-modified electrodes in 0.1 M $NaClO_4$ containing 1 mM $K_3[Fe(CN)_6]$ / $K_4[Fe(CN)_6]$ (1:1) mixture. Data derived from impedance fit parameters ($R_{ct}$ and B) and the brush acoustic thickness ($d_{QCM}$).

When PMETAC brushes collapse by ion paring with $ClO_4^-$ ions, they show very compact stiff structures with less entrapped water and so markedly different from the same brushes whose collapse is driven by pure Coulombic screening. This has been quantitatively discussed above and confirmed by means of indentation experiments with AFM and also more qualitatively by QCM-D.[3¡Error! Marcador no definido.] Since water plays a role of plasticizer in the glassy state increasing the fluidity of the material and lowering the $T_g$, this could explain why in our measurements only the brushes in contact with a $ClO_4^-$ solution exhibit a detectable thermal transition in the

studied temperature range. [25] Moreover, this transition can be reversibly changed back to the original state reversing the medium temperature beyond $T_g$.

At this point it is perhaps worth mentioning that additional QCM-D experiments were performed that allowed to confirm that the brush thickness remained independent of the electrolyte temperature within the working temperature range. It is clear that a decrease in temperature below the glass transition limit does not lead to a further collapse of the structure, at least in the temperature range studied. Regardless of its precise origin, the thermal behavior of the PMETAC brush in $ClO_4^-$ solution is characterized by a morphological nanostructural transition at a well-defined temperature that has a direct impact on the mass transport through the brush and on the electron transfer at the substrate. Clearly, a switchable thermocontrolled electrode activity induced specific counterions represents an interesting case of thermally controlled electrode interface with surface states becoming less active or inactive for the electrochemical process of the redox species (i.e., $[Fe(CN)_6]^{3-/4-}$ anions). In a separate paper we reported recently [8] glass transition temperature measurements in PMETAC brushes in $ClO_4^-$ solutions using impedance spectroscopy as a novel method for the determination of $T_g$. Likewise, the highly restricted mass transport inside the brush below $T_g$ results in an adaptive surface selective for ionic species having catalytic or pharmaceutical activity.[26] The glass transition is associated with a change in the local degrees of freedom. At the Tg the spacing and free internal volume available for molecular motions achieve minimum values. Thus, it is reasonable to expect that a glass transition may lead to increased reorganization energy for the redox species during the electron jump [27] or, put it in other words, may lead to increased activation energy for the electron transfer.

Moreover, the usual model describing the influence of the solvent–polymer interaction on diffusion coefficients is the free volume model. This model proposes that mass transport is regulated by the redistribution of the polymer free volume within the solvent [28] and predicts a decrease in transport of a solute (+solvent) into a polymer matrix with a decrease in solvent–polymer (and solute–polymer) interactions.

Noteworthy, temperature effects are different according to the counterion in the supporting electrolyte. While the activation energies are markedly different for the diffusion and electron transfer steps in chloride solution, they are practically the same for these two steps in perchlorate solution, even when the thermal transition takes place.

## 6.4. CONCLUSIONS

We have shown that impedance spectroscopy (EIS), can be used to resolve separately the thermal effects of diffusion and electron-transfer steps of an electrochemical reaction taking place at a brush-modified electrode. Additionally, a link between these effects and the structural transitions of the polymer brush has been proposed. Results lead to the conclusion that the electron-transfer step exhibits lower activation energy when the grafted brush suffers a collapse transition resulting from purely electrostatic screening of charges, using NaCl to trigger collapse than when the collapse transition is promoted by ion-pairing interactions, induced by the counterion $ClO_4^-$. Charge screening collapse induced by NaCl, reduces water content only to a lesser degree and polymer chains remain more

viscous as we can interpret from the changes in dissipation. Increasing temperature inside the brush leads to increased chain mobility, what offers the probe more possibilities for diffusing through free space between the chains. However, in the case of the brushes collapsed with $ClO_4^-$ counterions the lower water content and restricted chain mobility hinder diffusion pathways for the probe. This causes the mobility of the probe to be significantly lower at temperatures below 17 °C than for the PMETAC brush in NaCl under equal conditions. Only when the temperature exceeds 17 °C chain mobility is largely increased and the probe can find a more favorable pathway for diffusion. This thermal transition of the polymer layer has a strong impact on the mass transport through the brush as well as the electron transfer at the substrate. The activation energy for the electron transfer in the "*glassy*" state is twice as large as the activation energy in the "*rubbery*" state. The experimental evidence presented in this work shows the full potential of a specific counterion to modify/tune the rates of electrochemical reactions taking place at electrode surfaces modified with polyelectrolyte brushes, something that is essential for improving technological applications that rely on molecule-surface interactions, such as designing new electrocatalysts for use in synthesis and power-generation/energy storage applications. For instance, stimulus-triggered ionic transport enhancements would greatly improve the versatility/adaptability of electrochemical functions within polymer brush layers, including electrochemiluminescence for light-emitting diodes, electrochromic thin films and impedance-based sensors. Another interesting example is the development of synthetic strategies for producing interfacial architectures based on polyelectrolyte brushes to facilitate proton transport. Extensive research conducted during last years revealed that polyelectrolyte brush films show great promise in that both

polyelectrolyte nanostructures and local solvation dynamics can be tuned and optimized to facilitate ion transport. [29–31] However, our understanding of solvent and ion dynamics in highly conductive and crowded polymeric environments is scarce.[32] These studies combining electrochemical impedance and QCM studies provide further insight into the delicate interplay between ion diffusion, electron transfer energy barriers, and polymer/ion hydration within the maromolecular environment. We consider that these results are important in unraveling the functional richness of polymer brushes and establishing new concepts of material design to attain functional polymer thin films with controllable interfacial transport properties.

## 6.5 REFERENCES


(1). Azzaroni, O*. J. Polym. Sci. Part A: Polym. Chem*.**2012**, 50, 3225–3258.

(2). Azzaroni, O.; Brown, A. A.; Cheng, N.; Wei, A.; Jonas, A. M.; Huck, W.T.S.. J. *Mater. Chem*. **2007**, 17, 3433-3439

(3). Azzaroni, O.; Moya, S; Farhan,T.; Brown, A.A.; Huck, W.T.S. *Macromolecules* **2005**, 38, 10192-10199.

(4). Iturri Ramos, J. J.; Moya, S. E., *Macromol. Rapid Commun*, **2011**, 32, 1972−1978.

(5). Zhou, F.; Hu, H. Y.; Yu, B.; Osborne, V. L.; Huck, W. T. S.; Liu, W. M., *Anal. Chem*. **2007**, 79, 176–182

(6). Azzaroni, O.; Gervasi, C.A. Characterization of Responsive Polymer Brushes at Solid/Liquid Interfaces by Electrochemical Impedance Spectroscopy In Functional Polymer Films, Characterization and Applications, First Edition; Knoll, W.; Advincula, R C. Eds; Wiley-VCH Verlag GmbH & Co. KgaA: Weinheim, Germany, **2011**; Vol. 2, Chapter 26, pp. 809-830.

(7). Rodríguez Presa, M. J.; Gassa, L. M.; Azzaroni, O.; Gervasi, C. A. *Anal. Chem*. **2009**, 81, 7936–7943.

(8). Alonso-García, T.; Rodríguez-Presa, M.J.; Gervasi, C.A.; Moya, S.; Azzaroni, O., *Anal. Chem*. **2013**, 85, 6561–6565.

(9). Choi, E.-Y.; Azzaroni, O.; Cheng, N.; Zhou, F.; Kelby, T.; Huck, T.S.H. *Langmuir* **2007**, 23, 10389-10394.

(10). Sauerbrey, G. Z. Phys. **1959**, 155, 206-222.

(11). Domack, A.; Prucker, O.; Rühe, J.; Johannsmann, D*. Phys Rev.* **1997**, 56, 680-689.

(12). Voinova, M. V.; Rodahl, M.; Jonson, M.; Kasemo, *B. Phys. Scripta*. **1999**, 59, 391-396.

(13). Daimon, M.; Masumura, A*. Appl. Opt.* **2007**, 46, 3811-3820.

(14). Moya, S.; Azzaroni, O.; Farhan, T.; Osborne, V.L.; Huck, W.T.S. *Angew. Chem. Int. Ed.* **2005**, 44, 4578 –4581.

(15). Ramos, J. J. I. PhD Thesis, Doctor Europeus, San Sebastián, Spain, **2011**.

(16). Seshadri, K.; Wilson, A.M.; Guiseppi-Elie, A.; Allara, D.L. *Langmuir* **1999,**15, 742-749.

(17). Finklea, H. O.; Snider, D. A.; Fedyk, J., Sabatani, E.; Gafni, Y.; Rubinstein, I. *Langmuir* **1993,** 9, 3660-3667.

(18). Alonso-García, T.; Gervasi, C.A.; Rodríguez-Presa, M.J.; Irigoyen-Otamendi, J.; Moya, S.E.; Azzaroni, O. *J. Phys. Chem. C* **2012,** 116, 13944-13953.

(19).Qu, D. Electrochimica Acta **2004**, 49, 657–665.

(20). Freger, V.; Bason, S. J. *Membr. Sci*. **2007**, 302, 1–9.

(21). Gao, X.; Kučerka, N.; Nieh, M-P.; Katsaras, J.; Zhu, S.; Brash, J.L.; Sheardown, H. *Langmuir* **2009**, 25, 10271–10278.

(22). Limat, M.; El Roustom, B.; Jotterand, H.; György Fóti, Comninellis, C. Electrochim. Acta **2009**, 54, 2410–2416.

(23). Imre, Á.W.; Schönhoff, M.; Cramer, C. A *J. Chem. Phys*. **2008**, 128, 134905-1/9.

(24) . Silva, T.H.; Garcia-Morales, V.; Moura, C.; Manzanares, J.A.; Silva, F. *Langmuir* **2005**, 21, 7461-7467.

(25) . Yeo, S.C.; Eisenberg, A.J. *Macromol. Sci., Part B: Physics*, **1977**, 13, 441-484.

(26). Spruijt, E.; Choi, E-Y.; Huck, W.T.S. *Langmuir*, **2008,** 24, 11253-11260.

(27). Eckermann, A.L.; Feld, D. J.; Shaw, J.A.; Meade, T.J. *Coord. Chem. Rev.* **2010**, 254, 1769–1802.

(28). Pickup, S.; Blum, F.D. *Macromolecules* **1989**, 22, 3961-3968

(29). Yameen, B.; Kaltbeitzel, A.; Langner, A.; Duran, H.; Müller, F.; Gösele, U.; Azzaroni, O.; Knoll, W.*J. Am. Chem. Soc*. **2008**, 130, 13140–13144.

(30). Yameen, B.; Kaltbeitzel, A.; Langer, A.; Müller, F.; Gösele, F.; Knoll, W.; Azzaroni, O. *Angew. Chem. Int. Ed*. **2009**, 48, 3124 –3128.

(31). Yameen, B.; Kaltbeitzel, A.; Glasser, G., Langer, A.; Müller, F.; Gösele, F.; Knoll, W.; Azzaroni, O. *ACS Appl. Mater. Interfaces*. **2010,** 2, 279-287.

(32). Wang, S.; Jing, B.; Zhu, Y.*J. Polym. Sci. Part B: Polym. Phys.* **2014** - DOI: 10.1002/polb.23414 .

# Chapter 7

## SEPARATE ASSESSMENT OF PERMEATION AND ELECTRON TRANSFER OF CHARGED REDOX PROBES AT GOLD ELECTRODES MODIFIED WITH CATIONIC POLYELECTROLYTE BRUSHES.

## ABSTRACT

The use in combination of Electrochemical Impedance and Cyclic Voltammetry (EIS and CV) with the Quartz Microbalance with Dissipation technique QCM-D allowed a quantitative characterization of charge transfer resistances and diffusion coefficients associated with electrochemical reactions of $Ru(NH_3)_6^{3+/2+}$ and $Fe(CN)_6^{3-/4-}$ redox couples on gold electrodes modified with cationic Poly(2-(methacryloyloxy) ethyl trimethylammonium chloride) (PMETAC) brushes. PMETAC brushes were grown with varying grafting density and tested in low ionic-strength solution of 50mM NaCl, in order to avoid strong charge-screening effects on the polymer chains by chloride counterions. Shifts in QCM-D parameters, frequency Δf and dissipation ΔD, related to changes in viscoelastic parameters of the brush after immersion in the salt solution can be correlated with decreased viscoelastic characteristics due to the release of water or reduction in viscosity (η) of the sample while increasing the brush grafting density. Charge transfer resistance ($R_{tc}$) is considerably larger for the Ru-probe reaction than for the Fe-probe discharge. More favorable adsorption of negatively charged $Fe(CN)_6^{3-/4-}$ due to the positive charge on the neighboring polymer chain units is expected to enhance electron transfer. On the other hand, this situation results in a hindered electron transfer for the positively charged $Ru(NH3)_6^{2+/3+}$ and a consequent increase in $R_{tc}$.

Similar values were obtained for the diffusion coefficients (*D*) independently of the probe charge sign. In these systems *D* is hardly affected by electrostatic interaction between charged moieties in the polyelectrolyte chains and the redox probes. However, changes in viscoelastic properties after immersion of the brush in the

electrolyte show that for both redox species decreasing the brush grafting density originates a drop in the diffusion coefficients. A large increase in $R_I$ values was measured in the presence of the cationic Ru-probe as compared to the anionic Fe-probe. It is believed that this results from compositional changes and/or change in ionic mobility of migrating ions.

## 7.1. INTRODUCTION

The structure of polyelectrolyte brushes anchored to surfaces, and how it is influenced by charge density, chain length and grafting density of the polyelectrolyte molecules has been theoretically investigated in detail. The effect of the ionic strength, multivalent ions, the nature of the charged groups, either weak or strong, and solvent quality have also been considered in a large number of publications over the last two decades [1] .

Among the main different factors that influence the structure of grafted polyelectrolyte brushes, the ionic strength of the electrolyte solution in which the brushes are immersed is particularly important since it will determine their responsive character. The ionic strength of the medium influences strongly the electrostatic interactions between the charged groups in a polyelectrolyte brush and the oppositely charged counterions. In solutions of low ionic-strength, highly charged polyelectrolyte brushes adopt extended conformations due to the strong repulsion between charged monomers. As the salt concentration is increased the repulsive interactions between the densely packed polymer chains diminish and chain compression (collapse) normal to the substrate surface occurs [2].

The swelling/collapse behavior of polyelectrolyte brushes can be used to modulate the reaction impedance of a redox probe getting through the brush via the conformational changes triggered by external electrolytes and solvent. There is a strong interest in developing polyelectrolyte brush-modified electrodes with switchable or tunable redox activity that can be used to selectively control the electrochemical reactions occurring at their surface. However, redox reactions are expected to be influenced by the charge sign of the redox probe relative to the charge sign of the polyelectrolyte brush. Indeed, it can be expected that redox couples of the same sign of the brush will experience an electrostatic repulsion from the brush chains and on the other hand probes oppositely charged to the polyelectrolyte chains will be attracted to the brush.

Recently, an ITO electrode was modified with a mixed polymer brush composed of poly(2-vinylpyridine) (P2VP) and Polyacrylic acid (PAA) to generate an electrode with switchable selectivity for cationic and anionic redox species in solution [3].In this work it was considered that the collapse of one or both polymers within different pH windows renders the film either with charged swelled domains that hinders penetration of the electroactive ions with the same charge sign or with both polymers in neutral hydrophobic or collapsed states that inhibit the electrode access for all ionic species. Electron transfer resistance $R_{ct}$ values related only to the kinetic rate constants of the interfacial reaction were derived at different pH values through the fitting of the impedance spectra to a Randle's type equivalent circuit. Then, the interfacial electrode resistances were correlated with the various states of the polymer brushes. Unfortunately, the exact degree in which mass transport of the

redox probes through the film is specifically inhibited in each state was not measured.

Transport of anionic and cationic species through a polyzwitterionic brush-modified mesoporous silica film deposited on an ITO electrode has also been studied. The polyzwitterionic brush-modified mesoporous silica was probed with cyclic voltammetry using $Ru(NH_3)_6^{3+}$ and $Fe(CN)_6^{3-}$ species diffusing across the film to reach the conductive ITO substrate. Depending on the solution pH either a permselective transport of cations or the exclusion of all ionic species was obtained[4]. Also here, the influence of the sign of the charge of the ionic species on each reaction step, namely mass transport through the film and electron transfer at the substrate could not be resolved separately.

A separate characterization of the influence of the charge sign of the redox probe in relation to the sign of the charge of the polyelectrolytes in the brush is highly desirable. Only after this has been achieved it will be possible to clearly understand the processes leading to the development of switchable selective electrode materials based on grafted polyelectrolyte brushes. Accordingly, we present in this work an individual and quantitative characterization of charge transfer resistances and diffusion coefficients for the electrochemical reactions of $Ru(NH_3)_6^{3+/2+}$ and $Fe(CN)_6^{3-/4-}$ redox couples on gold electrodes modified with cationic Poly(2 -(methacryloyloxy) ethyl trimethylammonium chloride) (PMETAC) grown with varying grafting densities.

## 7.2. EXPERIMENTAL

### 7.2.1 Synthesis of Polyelectrolyte Brushes

Au substrates were prepared by sputtering deposition and cleaned by sonication, followed by water rinsing. .In a final cleaning step substrates were exposed to UV radiation in a Bioforce Nanosciences chamber for 30 minutes just before thiol assembly. Au substrates were coated with a thiol monolayer by immersion in solutions containing a mixture with different proportions of w–mercaptoundecylbromobutyrate as initiator thiol and 1-undecanethiol as blank thiol. After 16 hours immersion the spontaneous formation of the initial assembled monolayer (SAM) takes place. In order to obtain brushes with four different grafting densities, four different thiol solutions were prepared mixing initiator and inhibitor thiols with the following content of the initiator: 100%; 50%; 25% and 5%.

Brushes were synthesized by Atom Transfer Radical Polymerization (ATRP). The polymerization solution was prepared as follows: 1 mL of commercially–available (Aldrich) METAC monomer (75 wt. % solution in water), 40 mmol, were dissolved in a mixture of 2 $cm^3$ of water and 3 $cm^3$ of dimethylformamide (DMF), 99.85%, at 20 ºC and degassed by passing a continuous stream of dry $N_2$ through the solution whilst being stirred, approximately for 15 minutes. 2,2'-bipyridyl (416 mg, 2.7 mmol), $Cu^{I}Cl$ (105 mg, 1.1 mmol) were added to this solution. The mixture was then further stirred and degassed with a stream of dry $N_2$ for another 15 minutes. Gold substrates coated with the initiator SAM were sealed in Schlenk tubes, degassed and left at 20 ºC under $N_2$. The polymerization solution was then syringed into each Schlenk tube, adding enough solution to submerge each sample completely. Once the polymerization step was accomplished, the samples were carefully removed

from the Schlenk tubes, washed with water, then with methanol, and finally dried under a stream of $N_2$.

### 7.2.2 Characterization Techniques

#### *7.2.2.1 In situ* QCM-D measurements

Growth of the polymer brush and brush thickness were measured by QCM-D (Q-Sense AB, Västra Frölunda, Sweden). Brushes were synthesized in situ in the QCM-D chamber from gold coated quartz crystals following the same conditions as in the schlenck tubes. $\Delta f$ and $\Delta D$, were acquired at 6 overtones ($i$ = 3, 5 … 13, corresponding to resonance frequencies of $f_i \approx$ 15, 25 … 65 MHz) simultaneously, with sub-second time resolution.

#### 7.2.2.2 Electrochemical techniques

Electrochemical measurements were carried out at 25°C in a conventional three-electrode cell. A platinum sheet with large area and a saturated calomel electrode (SCE) were used as counter and reference electrodes, respectively. All potentials are referred to the SCE. Au substrates modified with polyelectrolyte brushes served as working electrodes. 0.05 M NaCl solutions were used as supporting electrolytes and prepared from analytical grade (Merck) reagents and Milli-Q water. Before performing each measurement the working electrode was thoroughly rinsed with Milli-Q water and immersed in the supporting electrolyte solution 10 minutes. Experiments were performed under purified $N_2$ gas saturation in the presence of a 1 mM $K_3[Fe(CN)_6]$ / $K_4[Fe(CN)_6]$ (1:1) and 1mM $Cl_2[Ru(NH_3)_6]$ / $Cl_3[Ru(NH_3)_6]$ mixtures as a redox probes in the supporting electrolyte.

Cyclic voltammetry (CV) measurements were performed by scanning the potential at a scan rate of 0.05 $Vs^{-1}$. Impedance spectra were obtained with a Zahner IM6d electrochemical workstation. The dc potential of the working electrodes was held at the open circuit potential while a 10 mV amplitude ac potential was applied. The voltage signal frequencies used for EIS measurements ranged from 100 kHz to 1 mHz. Impedance data analysis was performed according to proper procedures for transfer function derivation and identification by using complex non-linear least squares (CNLS) fitting based on the Marquardt-Levenberg algorithm.

## 7.3. RESULTS AND DISCUSSION

The time evolution of frequency Δf and dissipation ΔD for PMETAC-grafted QCM-D crystals at the four considered grafting densities were measured adding initially 0.05 M chloride solution and later washing out the brush with water. Δf an ΔD curves for a polymer brush grown from an initial SAM with 100% initiator thiol are shown in Figure 7.1.

QCM-D data were evaluated quantitatively in terms of the Sauerbrey equation that links frequency shifts and adsorbed masses per unit area in the following simple way [5] :

$$m_{QCM} = -C\frac{\Delta f_i}{i} \qquad (7.1)$$

with the mass sensitivity constant, C = 18.06 ± 0.15 $ng \cdot cm^{-2} \cdot Hz^{-1}$ for sensors with a resonance frequency of 4.95 ± 0.02 MHz, and the overtone number *i*. The

normalized frequency shifts, $\Delta f = \Delta f_i / i$, for the 3rd overtone were employed to determine $m_{QCM}$.

The brush thickness was further determined by

$$d_{QCM} = m_{QCM} / \rho_{Brush} \qquad (7.2)$$

where $\rho_{Brush}$ = 1.0 g/cm$^3$ is the density of the solvated polymer film. This value was assumed taking into account that polyelectrolytes exhibit densities between 1.0 and 1.1 g/cm$^3$, while the density of water or salt solutions is also 1.0 g/cm$^3$.

Combining equations (7.1) and (7.2) results the following relationship: $d_{QCM}(nm) \cong -\frac{1}{5}\Delta f(Hz)$ that relates film thicknesses and the corresponding normalized frequency shifts at the end of the polymerization step (brushes immersed in water) and after exposure of the brushes to the salt solution (0.05 M NaCl.), respectively.

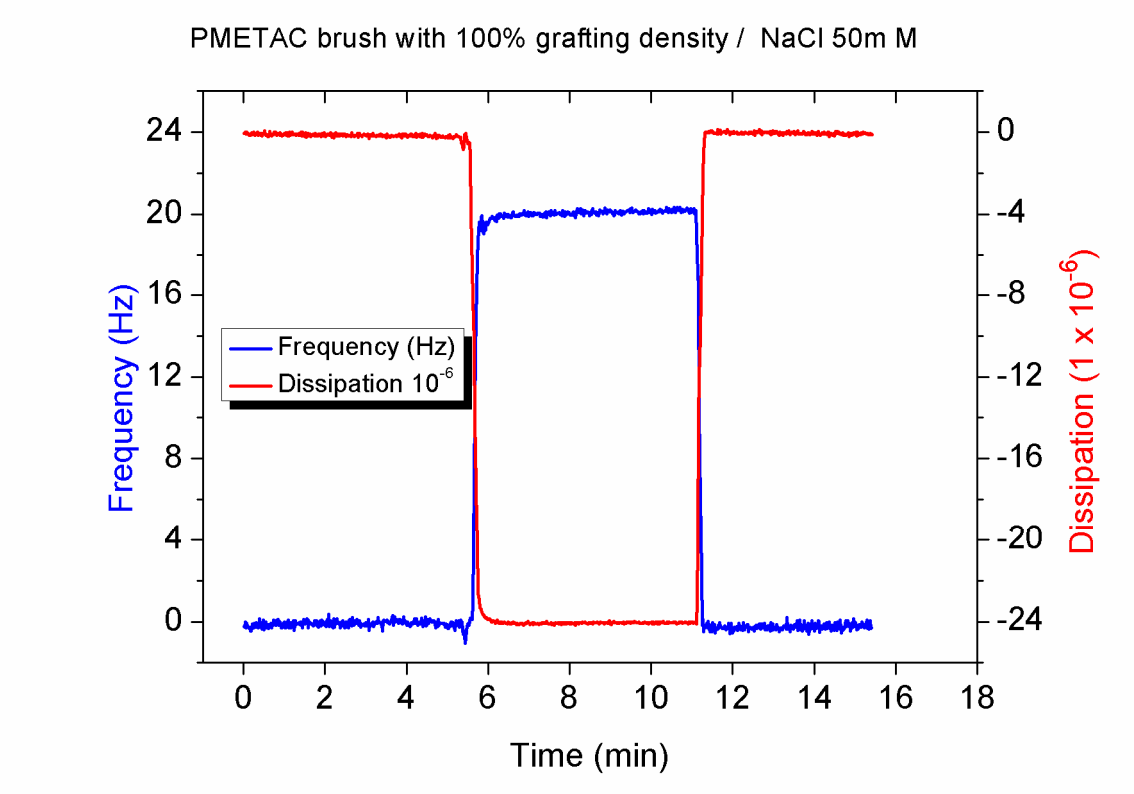


**Figure 7.1.** Temporal variation of the frequency (blue line) and dissipation (red trace) of a PMETAC-brush having 100% grafting density when the ionic strength is increased to 50 mM NaCl and then decreased again to water.

Acoustic thickness values calculated at the end of the polymerization step $d_{QCM}^{initial}$ for PMETAC brushes assembled from monolayers with different initiator–blank thiol ratios confirmed previous results [6] and correspond to the initial conditions of the QCM-D experiments shown in this work, namely samples immersed in water as reference states. Exposure of the brushes to the salt solution yielded positive changes in frequency and negative changes in dissipation as it can be seen in Fig. 7.1. These data show weak brush collapse and water mass loss while the polymer chains still retain a net charge and hydrophilic character [7]. Table 7.1 provides: $d_{QCM}^{initial}$ values together with shifts in frequency Δf and dissipation ΔD upon addition of 0.05

M NaCl solution, the corresponding reductions in film thickness and resulting final values for the PMETAC brush thickness $d_{QCM}^{final}$ for each brush grafting density.

Noteworthy, dissipation shifts are commonly used to follow changes in viscosity of the sample. As discussed in the literature [8] for polymer chains grafted at a solid-liquid interface, dehydration/hydration can be described by the frequency shift (Δf), whereas viscoelastic changes driven by the collapse/swelling transition are related to the dissipation change (ΔD). The observed behavior of Δf vs. ΔD indicates cooperativity between both phenomena resulting from exposure of the brushes to the salt solution. Thus, Δf and ΔD variations, as observed in this work, can be correlated with a reduction in viscosity of the sample after immersion in the salt solution [9]. The lower the grafting density the smaller the frequency change during collapse and the smaller the change in dissipation. As the density of chains in the brush decreases chains are able of occupying more lateral space and are not as extended in water as in the case of the brushes synthesized from a monolayer of 100 % initiators. Consequently the viscoelastic character of the brush diminishes as well as the change in dissipation during collapse. The water content decreases with brush density as the less extended chains reduce the volume available for free water. Frequency and dissipation values return to their initial levels after rinsing with water proving a reversible behavior.

**Table 7.1.** Values for $d_{QCM}^{initial}$ (nm), shifts in frequency $\Delta f_{collapse}$ (Hz), variation in thickness due to collapse $d_{QCM}$(nm), final brush thickness $d_{QCM}^{final}$ (nm) and dissipation ΔD x $10^6$ upon addition of 0.05 M NaCl solution for PMETAC brushes with different grafting density (%).

| Grafting density (%) | $d_{QCM}^{initial}$ (nm) | $\Delta f_{collapse}$ (Hz) | Collapsed $d_{QCM}$ (nm) | Final thickness $d_{QCM}^{final}$ (nm) | $\Delta D \times 10^6$ |
|---|---|---|---|---|---|
| 100 | 50 | +20 | -4 | 46 | -24 |
| 50 | 30 | +15 | -3 | 27 | -11 |
| 25 | 24 | +10 | -2 | 22 | -5 |
| 5 | 6 | +5 | -1 | 5 | -4 |

For the electrochemical characterization of the PMETAC-coated electrodes the voltammetric response was measure for both the couples $K_3[Fe(CN)_6]$ / $K_4[Fe(CN)_6]$ and $Cl_2[Ru(NH_3)_6]$ / $Cl_3[Ru(NH_3)_6]$

Figure 7.2 shows the voltammetric response of a Au electrode modified with a PMETAC brush grown from an initial SAM with 100 % grafting density and recorded at a scan rate v of 50 mV $s^{-1}$ in 0.05 M NaCl solutions containing 1 mM $K_3[Fe(CN)_6]$ / $K_4[Fe(CN)_6]$ (1:1).

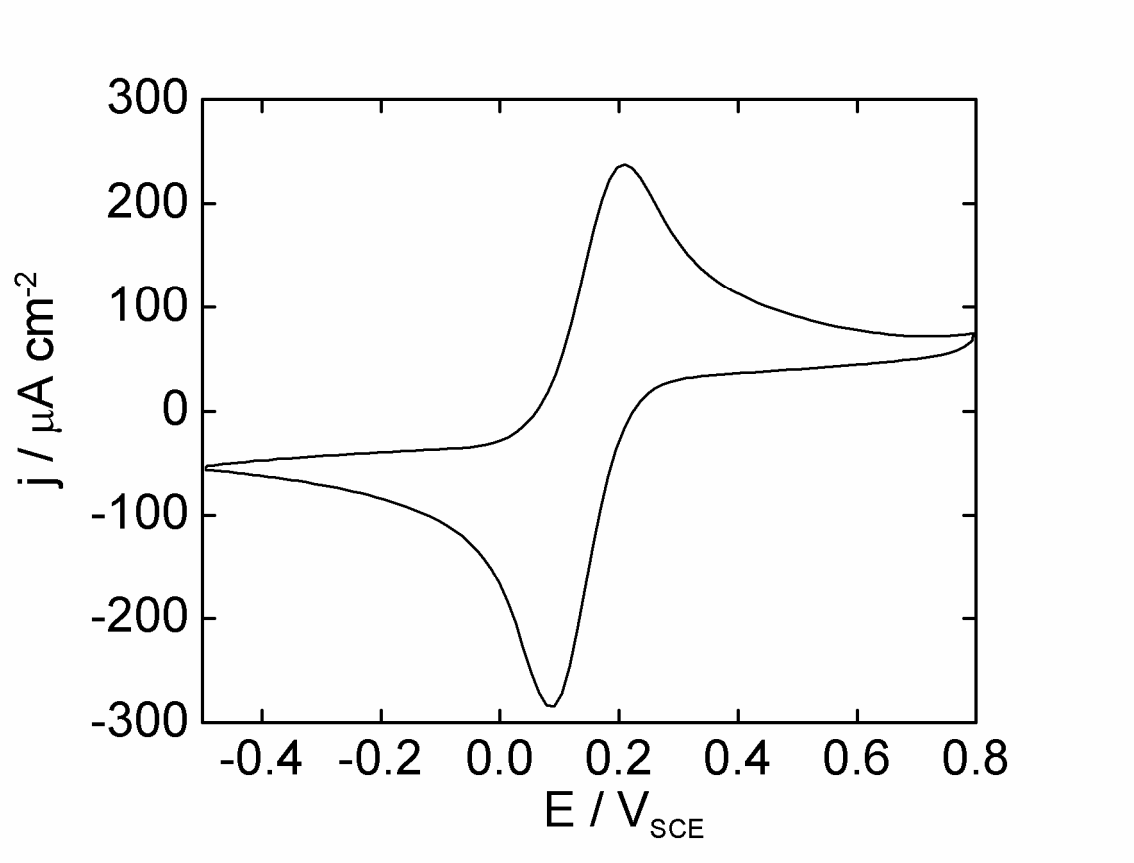


**Figure 7.2.** Voltammogram of a PMETAC brush-modified electrode grown from an initiator SAM with 100 % grafting density and recorded at 50 mV $s^{-1}$ in 0.05 M NaCl solution containing 1 mM $K_3[Fe(CN)_6]$ / $K_4[Fe(CN)_6]$ (1:1)

Figure 7.3 shows the voltammetric response of the Au electrode modified with a PMETAC brush grown from an initial SAM with 100 % grafting density and recorded at a scan rate v of 50 mV $s^{-1}$ in 0.05 M $Cl^-$ solutions containing 1 mM $Cl_2[Ru(NH_3)_6]$ / $Cl_3[Ru(NH_3)_6]$ (1:1).

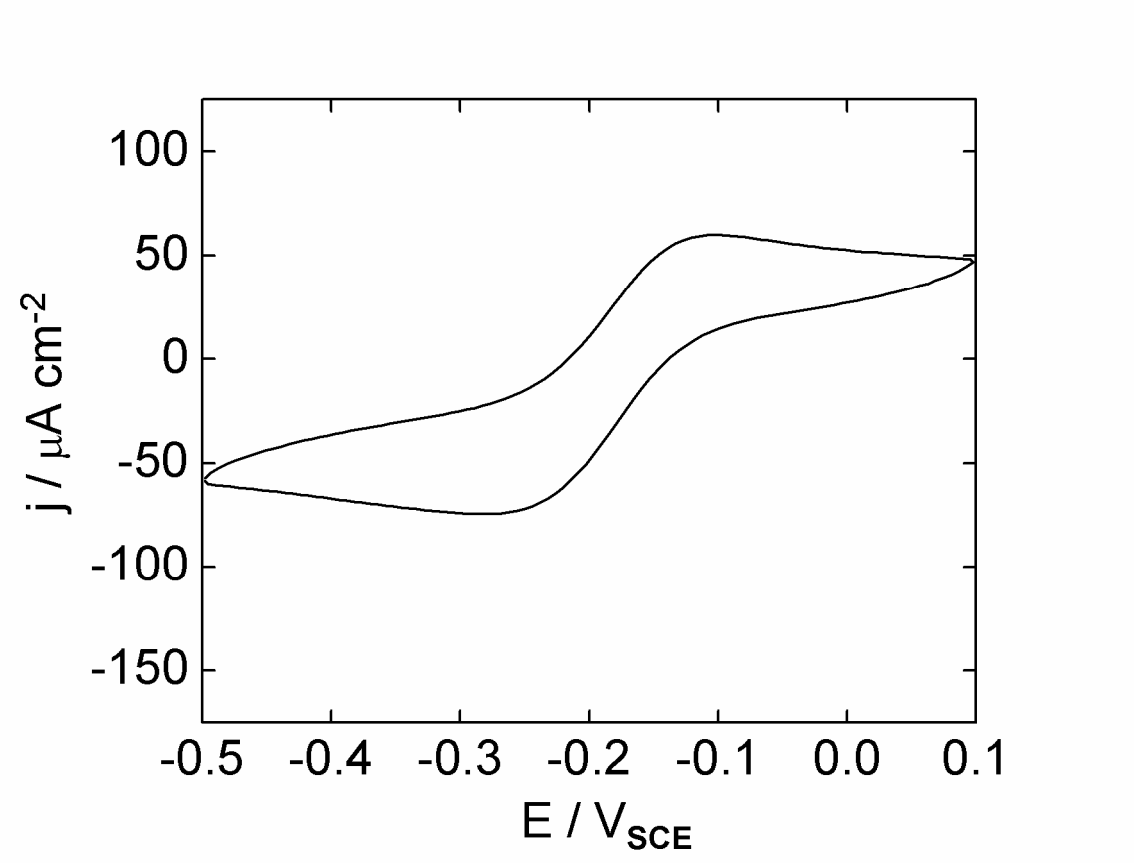


**Figure 7.3.** Voltammogram of a PMETAC brush-modified electrode grown from an initiator SAM with 100 % grafting density and recorded at 50 mV $s^{-1}$ in 0.05 M NaCl solution containing 1 mM $Cl_2[Ru(NH_3)_6]$ / $Cl_3[Ru(NH_3)_6]$ (1:1).

It has already been discussed in the literature that for initial SAMs of the type [–SH $–(CH_2)_k – CH_3$] with a large number of methylene units ($k \geq 9$) charge transfer takes place at pinholes and other defects in the monolayer [10] . Consequently, the electrochemically active area of the substrate modified with the polymer brush corresponds to the fractional area determined solely by pinhole sites in the initial SAM [11]. This is particularly true under our experimental conditions, where the concentration of the $Cl^-$ counterion in solution was kept relatively low, in order to avoid the formation of an uncharged polymer brush that after collapsing could

change the active electrode area [12]. Clearly, as indicated above, uncharged brushes are inadequate to assess the effect of the redox probe charge. Moreover, electrochemical transformations of the redox couples on gold electrodes modified with polymer brushes grown from the initial SAMs, as tested in this work, are quasi-reversible processes [13,14]. For quasi-reversible systems (with a standard rate constant k° in the range $10^{-1} > k° > 10^{-5}$ cm $s^{-1}$) the current is controlled by both charge transfer and mass transport. The shape of the cyclic voltammogram is a function of the following ratio (7.3)

$$k° / (\pi v n F D / R T)^{1/2} \qquad (7.3)$$

where v is the potential scan rate and *D* the diffusion coefficient for a *n*-electron transfer reaction [15]. As the ratio (7.3) increases, the process approaches the reversible case, with a separation between anodic and cathodic peaks given by $\Delta E_p = E_{pa} - E_{pc} = 59/n$ mV. For small values of this ratio, the system would exhibit an irreversible behavior. Overall, the voltammograms of a quasi-reversible system are more drawn out and exhibit a larger separation in peak potentials compared to a reversible system. According to data presented in Figures 7.2 and 7.3 the Ru-probe exhibits, under comparable working conditions, a voltammetric response characterized by peaks that are less sharp and with a larger separation in peak potentials ($\Delta E_p$ = 180 mV), characteristic of a less reversible behavior than the observed response for the Fe-probe ($\Delta E_p$ = 105 mV). Considering the terms in ratio (7.3) it can be understood why the voltammetric experiment is unable to resolve independently the influence of mass transport through the film and electron transfer at the substrate.

Consequently, we performed impedance experiments to uncouple the effects of mass transport and electron transfer steps on a charged redox probe reacting at the active area of a substrate modified with PMETAC brushes.

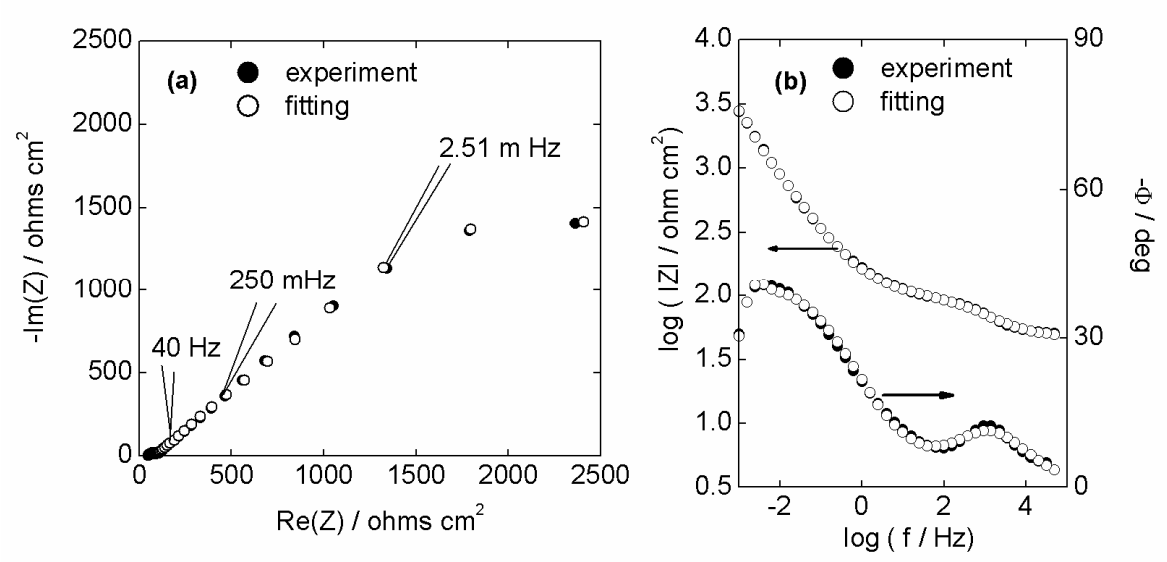


**Figure 7.4.** Impedance spectra recorded in 0.05 M NaCl solution containing 1 mM $K_3[Fe(CN)_6]$ / $K_4[Fe(CN)_6]$ (1:1) for an electrode modified with an initial SAM with 100 % thiol initiator from which the PMETAC brush was grown. Experimental data (●) and fit results (○) according to the theoretical impedance of equivalent circuit in Fig. 7.6) and the reaction impedance $Z_f$ from Equation (7.4).

Figure 7.4 shows impedance spectra for an electrode modified with a PMETAC brush grown from an initial SAM containing 100% thiol initiator. The impedance spectra were recorded in a solution containing the negatively charged $Fe(CN)_6^{3-/4-}$ probe. Nyquist diagrams in Figure 7.4a exhibit a semicircle in the high frequencies f region (f > 100 Hz) followed by a the low frequency region containing diffusion effects that are compatible with finite-length diffusion-type impedances. The

semicircle is related to electron transfer-limited processes at the uncovered gold surface, whereas the finite-length diffusion of the redox probe takes place within the brush structure. Hence, the electron transfer kinetics and the diffusional characteristics can be evaluated independently from the EIS data. The semicircle diameter represents the charge transfer resistance $R_{ct}$ whereas the intercept of the semicircle with the real part of the impedance Re(Z)-axis for $f \rightarrow \infty$ corresponds to the electrolyte resistance, $R_e$. Measured impedance data were corrected by the apparent electrode area. Data representation in terms of Bode plots is also included in Figure 7.4b since these plots show the frequency response characteristic of the system over the entire measured frequency range, with points equally spaced in the frequency axis.

The same qualitative behavior was observed for each electrode modified with an initial SAM containing a percentage of thiol initiator in the 5 % - 100% range and from which the PMETAC bruses were grown.

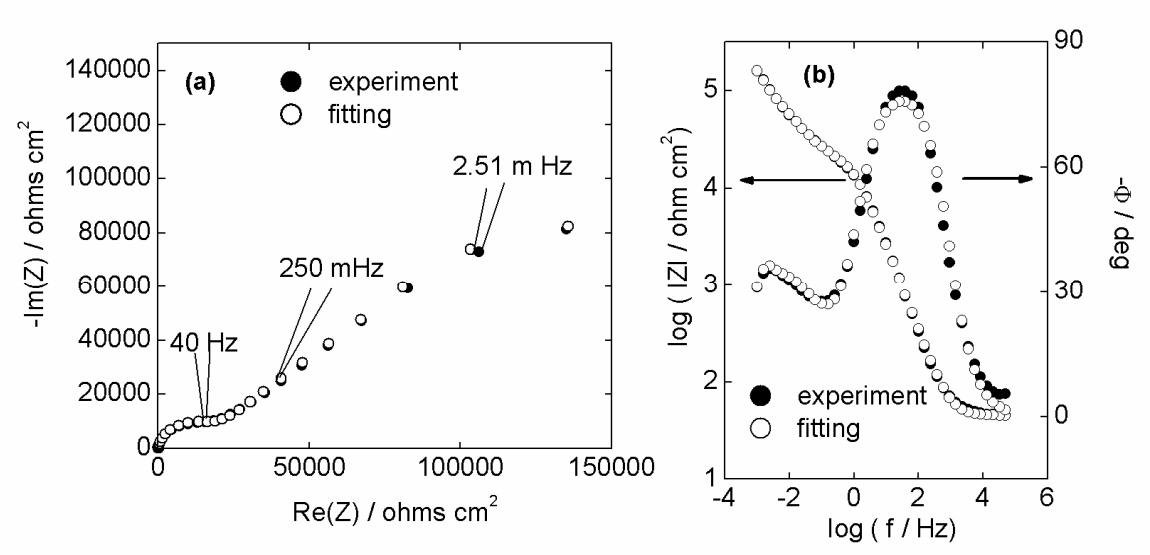


**Figure 7.5.** Impedance spectra recorded in 0.05 M NaCl solution containing 1 mM $Cl_2[Ru(NH_3)_6]$ / $Cl_3[Ru(NH_3)_6]$ (1:1) for an electrode modified with an initial SAM with

100 % thiol initiator from which the PMETAC brush was grown. Experimental data (●) and fit results (○) according to the theoretical impedance of equivalent circuit in Fig. 7.6) and the reaction impedance $Z_f$ from Equation (7.4).

Figure 7.5 shows impedance spectra for an electrode modified with a PMETAC brush grown from an initial SAM containing 100% thiol initiator but this time spectra were recorded in a solution containing the positively charged $[Ru(NH_3)_6]^{2+/3+}$ probe. Nyquist diagrams are presented in Figure 7.5a, while Figure 7.5b contains the corresponding Bode plots. The same dynamic behaviour can be observed for data in both Figures 7.4 and 7.5. However, the magnitude of the impedance increased in the spectra obtained with the Ru-probe when compared with the Fe-probe. Additionally, the frequency region related to the charge transfer step of the electrochemical reaction of the Ru-probe extends to lower frequencies (in the order of 10 Hz) and so covers a much wider range. Thus, regarding the global process, electron transfer becomes comparatively more sluggish and participates more markedly in the control of the reaction. Impedance data obtained with the Ru-probe exhibit all the same qualitative behavior, independently of the percentage of thiol initiator in the initial SAM (from 5 % to 100%) from which the PMETAC brushes were grown (data not shown).

A quantitative analysis of impedance data was performed considering that the impedance response of the system can be described in terms of a partially blocked electrode surface determined by the initial SAM. Then, the main influence of the polymer brush on mass transport and electron transfer steps would be related to the sign of the charge of the monomers in the polymer chains relative to the charge

sign of the redox probe. A physical model of the interface of the modified electrode is given on the basis of the equivalent circuit for the impedance in Figure 7.6, with $R_e$ the electrolyte resistance, $C_{dl}$ the double layer capacitance, $R_l$ the resistance of the ionic path within the brush, $C_l$ the capacitance of the intact SAM, and $Z_f$ the Faradaic impedance associated with the electrochemical reactions of the redox probe at the fraction of area of the electrode that is not blocked, i.e. at the defect sites of the initial SAM.

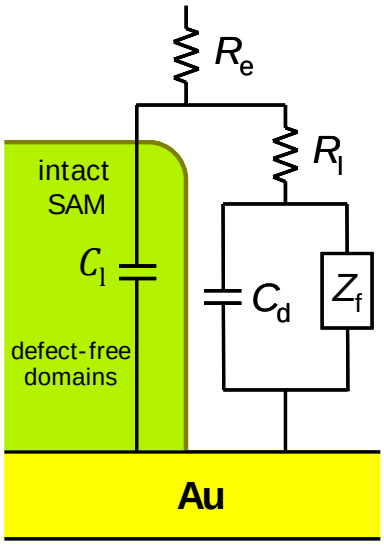


**Figure 7.6.** Schematic representation of an electrode modified with a PMETAC brush grown from an initial SAM. The initial SAM contained defects exposing the bare Au surface.

A theoretical derivation of the interfacial impedance $Z_f$ together with an explanation of the assumptions made, are given in detail elsewhere [12,16] . The resulting expression for $Z_f$ is

$$Z_f = R_{ct} + \frac{\sigma}{\sqrt{\omega}}\left[\tanh\left(B\sqrt{j\omega}\right)\right](1-j) \qquad (7.4)$$

where $j = \sqrt{-1}$, $\omega = 2\,\pi\,f$, is the angular frequency of the potential perturbation and the so-called mass transfer coefficient $\sigma$ contains the contributions of both forms O (oxidized) and R (reduced) of the redox couple and $B = \delta/\sqrt{D}$. Finite diffusion length $\delta$ is equal to the brush thickness, since diffusion outside the brush in the bulk electrolyte is not hindered and consequently, a non-null concentration gradient is only present inside the brush.

$R_{ct}$ contains kinetic information according to the following expression:

$$\frac{1}{R_{ct}} = A_e F\left[C_O^{dc}\left(\frac{k_c \alpha_c F}{RT}\right) + C_R^{dc}\left(\frac{k_a \alpha_a F}{RT}\right)\right] \qquad (7.5)$$

where $\alpha_a$ and $\alpha_c$ are the transfer coefficients, $k_a$ and $k_c$ correspond to the rate constants for the anodic and cathodic reactions, respectively, $C_O$ and $C_R$ represent concentrations of the oxidized and reduced species at the surface for dc conditions, $A_e$ is the electrode area while R and F are the gas and Faraday constants, respectively.

Typical results of the good agreement obtained between theory and experiment are shown in terms of both Nyquist and Bode plots in Figures 7.4 and 7.5. Data shown correspond to selected brushes grown from SAMs with 100% initiator thiol and measured in the two electrolytic solutions. Best-fit parameters assembled in Tables 7.2 and 7.3 correspond to both electrolytic solutions, i.e. one containing the Fe-probe and the other the Ru-probe, respectively.

**Table 7.2.** Calculated diffusion coefficient and best-fit parameters obtained for the experimental spectra recorded in 0.05 M NaCl solution containing 1 mM $K_3[Fe(CN)_6]$ / $K_4[Fe(CN)_6]$ (1:1) (Figure 7.4). Data were fitted to the theoretical impedance resulting from the equivalent circuit (Figure 7.6) and the reaction impedance $Z_f$ according to Equation (7.4).

| Grafting density (%) | $R_l$ ($\Omega cm^2$) | B ($s^{1/2}$) | D x $10^{14}$ ($cm^2 s^{-1}$) | $R_{ct}$ ($\Omega cm^2$) |
|---|---|---|---|---|
| 100 | 1.6x10 $^4$ | 20.3 | 5.1 | 47 |
| 50 | 3.8 x10 $^3$ | 18.7 | 2.1 | 68 |
| 25 | 1.2 x10 $^4$ | 23.6 | 0.87 | 86 |
| 5 | 7.4x 10 $^4$ | 24.5 | 0.042 | 97 |

As already discussed in previous [17] it is worth observing that fit parameter $R_{ct}$ is inversely proportional to the active electrode area (equation 7.5) in contrast with fit parameter B which is independent of the electrode area. Since B is used together with the brush thickness $d_{QCM}^{final}$ (previously measured) to calculate *D* (equation 7.4) variations in the latter cannot be ascribed to changes in the active area according to the working conditions.

**Table 3.** Calculated diffusion coefficient and best-fit parameters obtained for the experimental spectra recorded in 0.05 M NaCl solution containing 1 mM $[Ru(NH_3)_6]Cl_2$/$[Ru(NH_3)_6]Cl_3$ (1:1) (Figure 7.5). Data were fitted to the theoretical

impedance resulting from the equivalent circuit (Figure 7.6) and the reaction impedance $Z_f$ according to Equation (7.4).

| Grafting density (%) | $R_l$ ($\Omega cm^2$) | B ($s^{1/2}$) | $D \times 10^{14}$ ($cm^2 s^{-1}$) | $R_{ct}$ ($\Omega cm^2$) |
|---|---|---|---|---|
| 100 | $6.0 \times 10^5$ | 23.4 | 3.86 | $1.77 \times 10^4$ |
| 50 | $7.7 \times 10^5$ | 30.9 | 0.76 | $2.77 \times 10^4$ |
| 25 | $1.1 \times 10^6$ | 64.6 | 0.12 | $3.38 \times 10^4$ |
| 5 | $1.7 \times 10^6$ | 20.3 | 0.06 | $4.24 \times 10^4$ |

Comparison of data shown in tables 7.2 and 7.3 discloses some interesting aspects. Firstly, charge transfer resistance is considerably larger for the Ru-probe reaction than for the Fe-probe discharge. This can be understood in terms of the effect of the charge sign of each redox couple on the electrostatic interaction with the charged environment at the region where adsorption/desorption steps take place before/after the electron jump [14,18] . More favorable adsorption of negatively charged $Fe(CN)_6^{3-/4-}$due to the positive charge on the neighboring polymer chain units is expected to enhance electron transfer. On the other hand, this situation may result in a hindered electron transfer for the positively charged $Ru(NH_3)_6^{2+/3+}$ [19]. It must be taken into account that both redox probes have comparable ionic sizes ,0.64 nm for the ruthenium hexamine complex vs. 0.60 nm for the potassium ferrocyanide complex, and consequently, both species have similar access to the active area of the electrode surface, i.e. we can rule out size-exclusion-based molecular discrimination [20]. Regardless of the evident difference in charge sign, the

two redox active metal complexes also differ in their inherent kinetics of heterogeneous electron transfer reactions. Since on bare gold the $Ru(NH_3)_6^{2+/3+}$ redox couple exhibits much faster electrochemical kinetics than $Fe(CN)_6^{3-/4-}$ [21], the observed effect of selective hindering of electron transfer for the Ru-couple on the modified electrode, as compared to the Fe-couple, results still more noticeable.

Secondly, a remarkable aspect is the fact that similar values were obtained for the diffusion coefficients independently of the probe charge sign. This agrees with previously derived diffusion coefficients of the same redox probe inside neutral PNIPAM brushes exhibiting values with the same order of magnitude [13] . However, for the present system although a brush-to-mushroom transition of the polymer chains is expected upon reduction of the grafting density, there is no evidence for semi-infinite diffusion conditions, as obtained with PNIPAM brushes.

Thirdly, a large increase in the values of $R_I$ were measured in the presence of the Ru-probe as compared to the Fe-probe. Clearly $R_I$ depends basically on the thickness of the film and content and mobility of ions in the film [18] .The thickness of the brush is invariant, and $Na^+$ is the ion with the highest transport number, due to simultaneous high concentration and high mobility [22].

However, it is believed that incorporation of highly mobile $K^+$ ions at a concentration of 7mM together with the negatively charged redox couple into the structure increases markedly the conductivity of the solution in comparison with that of the positively charged redox couple incorporating only chloride ions that are associated

with a lower transport number in this system. This situation results in larger resistance of the ionic path within the brush for the Ru-probe solution.

Finally, for both redox species decreasing the brush grafting density originates a drop in the diffusion coefficients D. As discussed above, QCM-D data show that lower brush grafting densities result in smaller reductions in dissipation shift ($\Delta$D) upon addition of NaCl 0.05 M solution what may render a fluid media with larger final values of viscosity $\eta$. To explain these findings it is perhaps worth considering the inverse dependence of diffusion coefficients of ions D (considered as spherical particles) on viscosity $\eta$ in a viscous media with low Reynolds number, when the well-known Stokes-Einstein relationship holds [23]:

$$D = \frac{kT}{Br\eta} \qquad (7.6)$$

where k is the Boltzmann's constant, r is the radius of the spherical particle and the numerical coefficient value of B = 6$\pi$ according to the Stokes formula.

The grafting density influences electron transfer of the Ruthenium-probe during the electrochemical reaction, as can be observed when considering data from Table 7.3. Thus, decreasing the brush grafting density originates a drop in the kinetic constant or an equivalent increase in $R_{tc}$. In a comparable system, a viscosity-imposed drop of the heterogeneous rate constant for the Ru-probe was already [10]. This was ascribed to the manifestation of the solvent-friction mechanism under a condition where the redox species penetrates the internal region of a surface film marked by much higher local viscosity (slower dielectric relaxation) compared to the electrolyte solution.

## 7.4. CONCLUSIONS

For PMETAC brushes synthesized on gold electrodes an increase in the electron transfer rate at the substrate/electrolyte interface is not due, as postulated previously, to the formation of ion channels or facilitated mass transport through the brush but is closely related to the sign of the charge of the polymer units in the brush chains near the electrode surface being opposite to the sign of the charge of the electroactive ions. Moreover, mass transport in these systems is hardly affected by electrostatic interaction between both charged moieties. However, changes in viscoelastic properties after immersion of the brush in the electrolyte depend on the grafting density, what in turn, modifies mass transport within the brush.

The analysis performed with a successful combination of electrochemical and acoustic measuring techniques clearly shows that in order to arrive at the above mentioned conclusions a separate assessment of both contributions to the reaction rate (electron transfer and mass transport) must be carried out.

## 7.5 REFERENCES


(1). Claesson, P. M.; Poptoshev, E.; Blomberg, E.; Dedinaite, A. *Adv. Colloid Interface Sci.* **2005,** *114–115*, 173–187.

(2). Chen, T.; Ferris, R.; Zhang, J.; Ducker, R.; Zauscher, S. *Prog. Polym. Sci.* **2010,** *35*, 94–112.

(3). Tam, T. K.; Pita, M.; Motornov, M.; Tokarev, I.; Minko, S.; Katz, E. *Electroanalysis* **2010,** *22,* 35–40.

(4). Calvo, A.; Yameen, A. B.; Williams, F. J.; Soler-Illia, G. J. A. A.; Azzaroni, O. *J. Am. Chem. Soc.* **2009,** *131,* 10866–10868.

(5). Sauerbrey, G. *Z. Phys.* **1959,** *155,* 206-222.

(6). Iturri-Ramos, J., Moya, S. E. *Macromol. Chem. Phys.* **2012**, *213,* 549−556.

(7). Moya, S.; Azzaroni, O.; Farhan, T.; Osborne, V. L.; Huck, W. T. S. *Angew. Chem. Int. Ed.* **2005,** *44,* 4578–4581.

(8). Zhang, G.; Wu, C. *Macromol. Rapid Commun.* **2009,** *30,* 328–335

(9). Voinova, M. V.; Rodahl, M.; Jonson, M.; Kasemo, B. *Physica Scripta* **1999,** *59*, 391-396.

(10). Dolidze,T. D.; Rondinini, S.; Vertova, A.; Longhi, M.;.Khoshtariya, D. E. *The Open Physical Chemistry Journal* **2008,** *2,* 17-21.

(11). Alonso-García, T.; Rodríguez-Presa, M. J.; Gervasi, C. A.; Moya, S. E.; Azzaroni, O. *Anal. Chem.* **2013,** *85,* 6561–6565.

(12). Rodríguez Presa, M. J.; Gassa, L. M.; Azzaroni, O; Gervasi, C. A. *Anal. Chem.* **2009,** *81,* 7936–7943.

(13). Alonso García, T.; Gervasi, C. A.; Rodríguez Presa, M. J.; Irigoyen Otamendi, J.; Moya, S. E.; Azzaroni, O. *J. Phys. Chem. C* **2012,** *116,* 13944-13953.

(14). Hwang, S. B.; Lee, S.; Chi, Y. S.; Kwak, J.; Choi, I. S.; Lee, S. *Electrochim. Acta* **2008,** *53*, 2630–2636.

(15). Wang, J. *Analytical Electrochemistry,* 3rd Edition, J. Wang Editor, John Wiley & Sons, Inc., Hoboken, New Jersey, 2006; pp 35-36.

(16). Azzaroni, O.; Gervasi, C. A. Characterization of Responsive Polymer Brushes at Solid/Liquid Interfaces by Electrochemical Impedance Spectroscopy In *Functional Polymer Films, Characterization and Applications,* 1st ed.; Knoll, W., Advincula, R. C., Eds.; Wiley-VCH Verlag: Weinheim, Germany, 2011; Vol. 2, Chapter 26, pp 809−830.

(17). Alonso-García, T.; Gervasi, C. A.; Rodríguez-Presa, M. J.; Gutiérrez-Pineda, E.; Moya, S. E.; Azzaroni, O. *J. Phys. Chem. C* **2013,** *117,* 26680–26688.

(18). Gu, N.; Wei, D.; Niu, L.; Ivaska (Grotthuss-018). *Electrochim. Acta* **2006,** *51,* 6038–6044.

(19). Raghu, S.; Berchmans, S.; Phani, K. L. N.; Yegnaraman, V. *Chem. Asian J.* **2007,** *2,* 775–781.

(20). Chailapakul, O.; Crooks, R. M. *Langmuir* **1995,** *11,* 1329-1340.

(21). Ganesh, V. Electrochemical studies and molecular self-assembly on surfaces in surfactant based systems. Ph.D. Thesis, Jawaharlal Nehru University, New Delhi, India, 2006.

(22). Wu, J.; Gerstandt, K.; Zhang, H.; Liu, J.; Hinds, B. J. *Nat. Nanotechnol.* **2012,** *7,* 133-139

(23). Einstein, A. *Annalen der Physik* **1905,** *17,* 549-560.

# Chapter 8

# CONCLUDING REMARKS AND PERSPECTIVES

## 8.1. CONCLUSIONS

The electrochemical approach developed for the present Thesis work to characterize grafted polymer brushes, in particular what regards the way impedance spectroscopy (EIS) was used, has recently gained recognition for its novelty as well as for being the single established alternative to fluorescence-based techniques when studying critical aspects, like diffusion of molecules inside the brushes [1]. Moreover, the combination of impedance, voltammetry and QCM-D studies to follow diffusion of ions, electron transfer energy barriers, and hydration of the brushes all in one represents a major achievement and provides an unprecedented level of insight.

Some previously considered aspects were revisited here but using the novel approach described above and for example the studies performed succeeded in addressing measurements of the thermal effects of diffusion and electron transfer steps of an electrochemical reaction taking place at a polymer brush-modified electrode. The results have linked these effects to the structural transitions of a polymer brush in the presence of different types of counterions. Overall, this research demonstrated the important role of ion-pairing interactions in determining the properties of the surface-grafted brushes, and the knowledge obtained will be useful in designing new smart surfaces.

When the electron transfer rate of a redox couple on the Au substrate is not markedly diminished by the brush collapse transition, the global reaction rate within the polymeric environment is generally controlled by ion transport or, at least,

exhibits a mixed control. One major contribution of this work is to succeed in explaining mass transport in terms of linear diffusion with a finite-length path equal to the brush thickness, that can be characterized by EIS independently of the electron transfer step.

A second significant contribution is related to the measurement of a limiting grafting density below which the brush does not build a diffusion barrier. When the electron transfer at the substrate is markedly inhibited due to a strong collapse of the brush, impedance data, for example, cannot resolve both contributions separately.
A strong conformational transition that collapses the structure was detected related to either the presence of a high concentration of counterions capable of forming ion-pairs with moeties in the polymer chain or for a polymer film relatively thick before collapsing. Recognition that the conformational collapse may not lead to changes in the charge transport resistance is a third original aspect regarding the characterization of the system in this work, that was not previously reported in the literature.

Despite the evolving perception of the importance of measuring the glass transition temperature $T_g$ under aqueous conditions in thin film configurations, its straightforward measurement poses a challenging situation that has proved elusive in polymer and materials science. In this regard the fourth main contribution is the development of a strategy to measure $T_g$ in grafted polymer brushes under certain experimental conditions using impedance measurements as a simple convenient tool.

## 8.2. FUTURE TRENDS

From a characterization point of view and bearing in mind that the presence of an initial SAM determines the electroactive area of the modified electrode and that the grafted polymer brush builds a mass transport barrier according to finite diffusion with a permeable boundary on the electrolyte side of the film, the following aspects appear as some of the ones needing renewed research effort in future electrochemically-oriented studies:

i) derivation of an explicit expression relating the film capacitance $C_f$ and the water content inside the polymer film that takes into account structural macromolecular features;

ii) deepening the understanding of the influence of size and charge of the redox probe molecule on molecular transport through polyelectrolyte brushes;

iii) getting a more detailed insight into the effect of varying brush grafting density on molecular transport with focus on the variation of the viscoelastic properties of the sample upon immersion in a salt solution;

iv) characterization of the particular degree of impact on surface blocking of hydrophobic collapse and electrostatic–driven collapse of polyelectrolyte brushes;

v) development of the theoretical treatment describing the voltammetric response under conditions of finite diffusion with a transmissive boundary located at a distance $\delta$ from the electrode.

From an applied point of view, it must be recognized that the studies presented in this work combining electrochemical impedance and QCM-D characterizations provide further insight into the delicate interplay between ion diffusion, electron

transfer energy barriers, and polymer/ion hydration within the maromolecular environment. We consider that these results are important in unraveling the functional richness of polymer brushes and establishing new concepts of material design to attain functional polymer thin films with controllable interfacial transport properties.

Moreover, the experimental evidence presented shows the full potential of a specific counterion to modify/tune the rates of electrochemical reactions taking place at electrode surfaces modified with polyelectrolyte brushes, something that is essential for improving technological applications that rely on molecule-surface interactions, such as designing new electrocatalysts for use in synthesis and power-generation/energy storage applications. For instance, stimulus-triggered ionic transport enhancements would greatly improve the versatility/adaptability of electrochemical functions within polymer brush layers, including electrochemiluminescence for light-emitting diodes, electrochromic thin films and impedance-based sensors. Another interesting example is the development of synthetic strategies for producing interfacial architectures based on polyelectrolyte brushes to facilitate proton transport. Extensive research conducted during last years revealed that polyelectrolyte brush films show great promise in that both polyelectrolyte nanostructures and local solvation dynamics can be tuned and optimized to facilitate ion transport [2-4]. However, implementing our understanding of solvent and ion dynamics in highly conductive and crowded polymeric environments still requires further applied research effort

## 8.3. REFERENCES

(1). Wang, S.; Jing, B.; Zhu, Y., *J. Polym. Sci. Part B: Polym. Phys*. **2014** - DOI: 10.1002/polb.23414.].

(2). Yameen, B.; Kaltbeitzel, A.; Langner, A.; Duran, H.; Müller, F.; Gösele, U.; Azzaroni, O.; Knoll, W., *J. Am. Chem. Soc*. **2008**, 130, 13140–13144.

(3). Yameen, B.; Kaltbeitzel, A.; Langer, A.; Müller, F.; Gösele, F.; Knoll, W.; Azzaroni, O. *Angew. Chem. Int. Ed*. **2009**, 48, 3124 –3128.

(4). Yameen, B.; Kaltbeitzel, A.; Glasser, G., Langer, A.; Müller, F.; Gösele, F.; Knoll, W.; Azzaroni, O. *ACS Appl. Mater. Interfaces*. **2010**, 2, 279-287.